UNIVERSITY OF SOUTHAMPTON

MAGNETIC RESONANCE AND LIGHT SCATTERING STUDIES OF NEMATICS

by

Noboru Kunimatsu

A dissertation submitted in partial
fulfilment of the requirements for
the degree of Doctor of Philosophy
at the University of Southampton

Department of Chemistry

September 2000

UNIVERSITY OF SOUTHAMPTON

ABSTRACT

FACULTY OF SCIENCE

CHEMISTRY

Doctor of Philosophy

MAGNETIC RESONANCE AND LIGHT SCATTERING STUDIES OF NEMATICS

by Noboru Kunimatsu

This Thesis reports the results of investigations into the effect of dopants on the physical properties of nematic liquid crystals, mainly the rotational viscosity coefficient, γ_1, and the twist elastic constant K_2, which play important roles in the response times and threshold voltages of liquid crystal displays. The measurement techniques chosen are the magnetic resonance method based on ESR spectroscopy to determine γ_1, and the dynamic light scattering method to determine K_2 and γ_1. Chapter 1 gives an introduction to the physical properties of liquid crystals, including visco-elastic properties, liquid crystal displays and physical properties of nematic mixtures. In Chapter 2, we discuss the measurement of the rotational viscosity coefficient for nematic liquid crystals by ESR spectroscopy; the advantage of this method is that we can monitor the distribution as well as the orientation of the director of a nematic. Here, theory and the methodology of this measurement are mainly discussed and γ_1 values obtained from the relaxation times are found to be in good agreement with the literature values for γ_1. In Chapter 3, using this technique, the effect of dopants on γ_1 was examined. The temperature dependence of these properties are significantly different depending on the temperature scales used for their comparison, here we consider the absolute and the reduced temperature scales. However, the absolute value of γ_1 is not available by the ESR method without a knowledge of the value of the diamagnetic anisotropy, $\Delta\tilde{\chi}$. Therefore, $\Delta\tilde{\chi}$ was determined by ESR spectroscopy and the results described in Chapter 4, they are found to be in good agreement with the literature values. In Chapter 5, the effect of dopants on K_2 is investigated using dynamic light scattering. By this method, γ_1 can also be obtained and is seen to be in good agreement with the values determined by the ESR method.

CONTENTS

Acknowledgements

Page

CHAPTER 1 **Introduction to the Physical Properties of Nematic Liquid Crystals**

1.1 Introduction 1
1.2 Elastic Properties and the Continuum Theory of Nematic Liquid Crystals 2
1.2.1 The Continuum Theory of Nematics 2
1.2.2 Freedericksz Transitions 4
1.2.3 Dependence of the Elastic Constants on the Molecular Structure of Liquid Crystals 6
1.3 Visco-elastic Properties of Liquid Crystals 10
1.3.1 Viscosity Coefficients 11
1.3.2 Dependence of the Rotational Viscosity on the Molecular Structure of Liquid Crystals 16
1.4 Liquid Crystal Displays 18
1.4.1 Display Modes 18
1.4.2 Threshold Voltages 20
1.4.3 Switching Times 20
1.5 Mixtures 21
1.6 Overview of the Thesis 23
1.7 References 24

CHAPTER 2 **Measurement of the Rotational Viscosity Coefficient for Nematic Liquid Crystals by ESR Spectroscopy**

2.1 Introduction 27
2.2 Director Dynamics of Nematic Liquid Crystals 28
2.3 Investigation of the Relaxation Process by ESR Spectroscopy 31
2.4 Experimental 34
2.4.1 Sample Preparation 34

2.4.2 Nematic-Isotropic Transition Temperature 36
2.4.3 The Rotation-relaxation Experiment using ESR Spectroscopy 37
2.5 Analysis of Results 41
2.6 Rotational Dynamics of Liquid Crystals 46
2.6.1 ESR Spectra Immediately after the Step Rotation 46
2.7 Results and Discussion 52
2.7.1 Accuracy of the Measurement of the Relaxation Time 52
2.7.2 Test of the Methodology for Determining the Rotational Viscosity γ_1 53
2.8 Summary 55
2.9 References 56
2.10 Appendix (A Qualitative Analysis of the ESR Spectra after the Step Rotation) 57

CHAPTER 3 **The Effect of Dopants on the Rotational Viscosity Coefficient for Nematic Liquid Crystals**

3.1 Introduction 64
3.2 Experimental 65
3.2.1 The Base Mixture and Dopants 65
3.3 Results and Discussion 67
3.3.1 The Effect of Dopants on the Nematic-Isotropic Transition Temperature 67
3.3.2 The Effect of Dopants on the Temperature Dependence of the Relaxation Time 70
3.3.3 The Effect of Dopants on the Temperature Dependence of the Rotational Viscosity 72
3.3.4 Analysis of the Temperature Dependence of the Relaxation Time 76
3.4 Summary 81
3.5 References 81

CHAPTER 4 **Determination of the Diamagnetic Anisotropy for Nematic Liquid Crystals by ESR Spectroscopy**

4.1 Introduction 83
4.2 Theory 84
4.3 Experimental 91

4.3.1 Sample Cell Preparation 91
4.3.2 The Field-Balance Experiment 93
4.4 Results and Discussion 96
4.4.1 Results of the Field Balance Measurements 96
4.4.2 Results for a Selection of the Angles between the Two Fields 101
4.5 Summary 106
4.6 References 107

CHAPTER 5 **The Effect of Dopants on the Twist Elastic Constant and the Rotational Viscosity Coefficient for Nematics Studied by Dynamic Light Scattering**

5.1 Introduction 109
5.2 Theory 110
5.3 Experimental 113
5.3.1 Sample Preparation 113
5.3.2 Sample Cell Preparation 114
5.3.3 Dielectric Anisotropy Measurement 117
5.3.4 Dynamic Light Scattering Measurement 119
5.3.5 The Rotational Viscosity Coefficient and the Twist Elastic Constant for 5CB 121
5.4 Results and Discussion 123
5.4.1 The Effect of Dopants on the Nematic-Isotropic Transition Temperature 123
5.4.2 Temperature Dependence of the Dielectric Anisotropy 124
5.4.3 Temperature Dependence of the Rotational Viscosity Coefficient 130
5.4.4 Temperature Dependence of the Twist Elastic Constant 136
5.5 Summary 138
5.6 References 140

CHAPTER 6 **Conclusions and Future Work**

1 Conclusions 142
2 Future Work 143

To Miyuki

Acknowledgements

I would like to express my gratitude to the following people who have contributed to the work described in this Thesis:
First of all, my supervisor Professor Geoffrey Luckhurst for his support and guidance, above all his strong encouragement and patience which I believe made me complete this Thesis.
Prof. David Dunmur for introducing me to this project and a lot of useful suggestions as my Adviser.
Prof. Harry Coles for allowing me to use the dynamic light scattering apparatus and valuable instruction in this technique.
Prof. Jim Emsley for useful suggestions.
Drs. Doina Ionescu and Chris Dunn for introducing me to ESR spectrometer and much kind help.
Dr. Fiona Farrand for the synthesis of 5(O)PCP.
Ms. Cecile Schott for the technical instruction in using the dynamic light scattering apparatus.

I am also grateful to all of the past and present members of the Liquid Crystal group: thank you Tim (Timimi), Katsuhiko (Sato), Andrew, Steven for your useful suggestions. Thanks also to Amir, Sean, Marco, Rao, Tim (Payne), Jochen, Fred and Stephan for your friendship.
Miguel and Kathy for your best friendship.

I would also thank Hitachi, Ltd. Japan for allowing me to have this precious opportunity and financial support, especially my managers Mr. Kinugawa, Mr. Matsuyama and Mr. Setsu Kobayashi. Thank you to my colleagues in the office in Mobara and in Hitachi Research Laboratory: I wish to thank Mr. Hasegawa, Dr. Kondo, Mr. Kagawa, Mr. Hanawa, Mr. Hanada and Mr. Kikuchi for your useful suggestions in science and engineering.

Finally thanks to my parents for their understanding and support.

Chapter 1

Introduction to the Physical Properties of Nematic Liquid Crystals

1.1 Introduction

The nematic phase is the simplest and most disordered liquid crystal phase. The constituent rod-like molecules in the nematic have no positional order (that is order of the centre of the mass) but have long range orientational order of the effective symmetry axes. To describe the local direction of alignment of the nematogenic molecules, we use a unit vector $\hat{n}$, called the director, which gives at each point in a sample the preferred direction of the symmetry axis of the molecule (see Fig.1). The extent of the molecular fluctuations with respect to the director in the nematic phase changes with temperature. This is commonly described by the orientational order parameter, $\overline{P}_2$, and is defined by

$$\overline{P}_2 = \frac{\overline{3\cos^2\beta - 1}}{2}, \tag{1}$$

where β is the angle between the director and the molecular symmetry axis, and the bar indicates a time or ensemble average. This order parameter, $\overline{P}_2$, has particularly convenient limiting forms varying from 0 (for the isotropic phase) to 1 (for complete orientational order of the molecular long axis in a crystal).

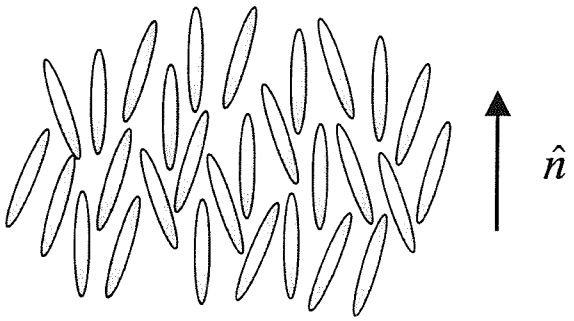

Fig.1 A schematic diagram of rod-like liquid crystal molecules in the nematic phase and the director $\hat{n}$

1.2 Elastic Properties and the Continuum Theory of Nematic Liquid Crystals

1.2.1 The Continuum Theory of Nematics

The long range orientational order of the constituent molecules of a nematic confers on it anisotropic properties including an elastic behaviour. In a thin nematic layer, the orientations of $\hat{n}$ imposed at the boundaries is not necessarily parallel, which means that orientation changes from one to the other. A curvature of $\hat{n}$ is also introduced if the orienting effect of an external field competes with that imposed by the boundaries. In this case, the director is not uniform across the sample. However, we can still take a nematic to be locally uniaxial, then $\overline{P_2}$ is the degree of order with respect to the local director and, to a good approximation, does not change with the director curvature. This is the basis of the continuum theory of liquid crystals. From a theoretical point of view, the curvature of $\hat{n}$ can be described in terms of continuum theory which gives the elastic energy as a function of the curvature. The fundamental equation of the continuum theory for nematics is given by [1]

$$F_{\text{dist}} = \frac{1}{2}K_1\left[\nabla\cdot\hat{n}\right]^2 + \frac{1}{2}K_2\left[\hat{n}\cdot\left(\nabla\times\hat{n}\right)\right]^2 + \frac{1}{2}K_3\left|\hat{n}\times\left(\nabla\times\hat{n}\right)\right|^2, \tag{2}$$

where F_{dist} is the distortion free energy per unit volume, K_1, K_2 and K_3 are the Oseen-Zocher-Frank constants. The derivatives in each term at a point in a liquid crystal where the director at the origin is along the z-axis (see Fig.2) are given by

$$\left[\nabla\cdot\hat{n}\right] = \left(\frac{\partial n_x}{\partial x}\right)_{y,z} + \left(\frac{\partial n_y}{\partial y}\right)_{x,z}, \tag{3}$$

$$\left[\hat{n}\cdot\left(\nabla\times\hat{n}\right)\right] = \left(\frac{\partial n_y}{\partial x}\right)_{y,z} - \left(\frac{\partial n_x}{\partial y}\right)_{x,z}, \tag{4}$$

$$\left|\hat{n}\times\left(\nabla\times\hat{n}\right)\right|^2 = \left(\frac{\partial n_x}{\partial z}\right)_{x,y}^2 + \left(\frac{\partial n_y}{\partial z}\right)_{x,y}^2. \tag{5}$$

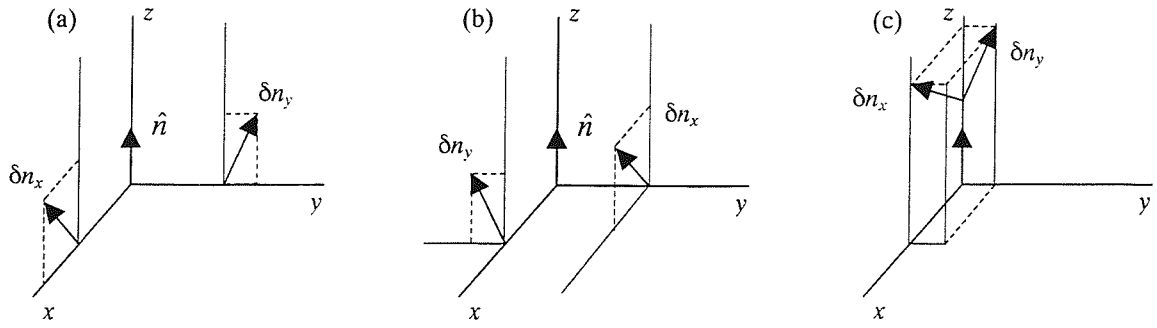

Fig.2 The director deformation, (a) splay, (b) twist and (c) bend

Fig.2 shows the three principal distortions of the director, namely splay, twist and bend distortion. Thus K_1, K_2 and K_3 are called the splay, twist and bend elastic constants, respectively.

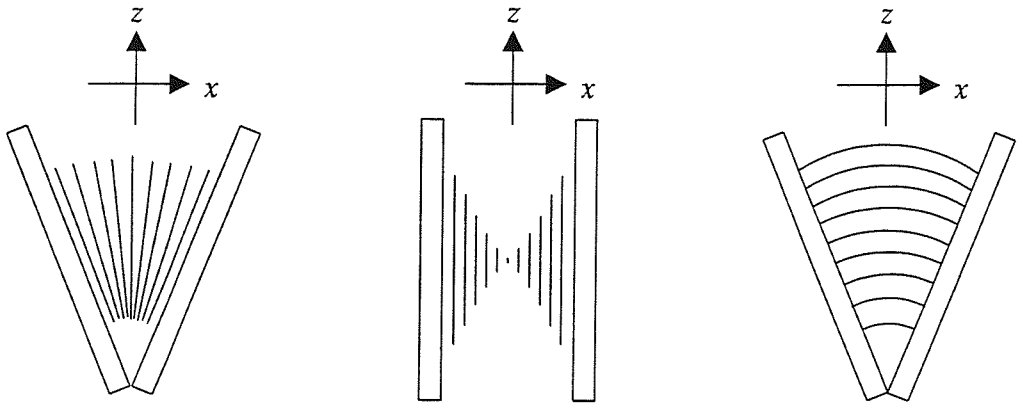

Fig.3 Three principal distortions of the director, (a) splay, (b) twist and (c) bend

To obtain the condition for equilibrium in the bulk of a nematic, the total elastic energy associated with the distortion must be a minimum. In the presence of a magnetic field or electric field, the total free energy is the sum of the magnetic or the electric free energy density and the elastic free energy density (equation (2)).

1.2.2 Freedericksz Transitions

A Freedericksz transition is a threshold phenomena of the director distortion caused by the competition between an external field and the surface effect for the director orientation, and this provides a way to determine the elastic constants. The Freedericksz transition for the three pincipal director distortions is obtained in three separate geometries for the director in a thin slab at the interfaces and the direction of an external field. Fig.4 shows the geometries of splay, twist and bend distortion modes for a Freedericksz transition in a static magnetic field. The director is indicated by the lines between the two substrates which are separated by a distance d and the director is strongly anchored by the substrates. When the applied magnetic field, B, is less than the threshold field, B_c, the director aligns as shown in Fig.4. If B is larger than B_c, the director moves away from this suface induced alignment.

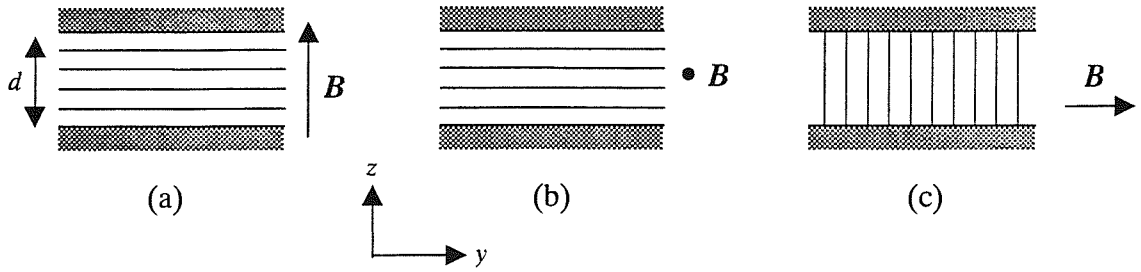

Fig.4 Splay (a), twist (b) and bend (c) modes for a Freedericksz transition used in the determination of the elastic constants

Fig.5 shows the dependence of the director deformation on the applied magnetic field for the splay deformation (see Fig.4 (a)). In Fig.5, θ_m is the angle of the director in the middle of the cell (two substrates) and the director starts to move at a critical point of the field, which is the threshold field B_c.

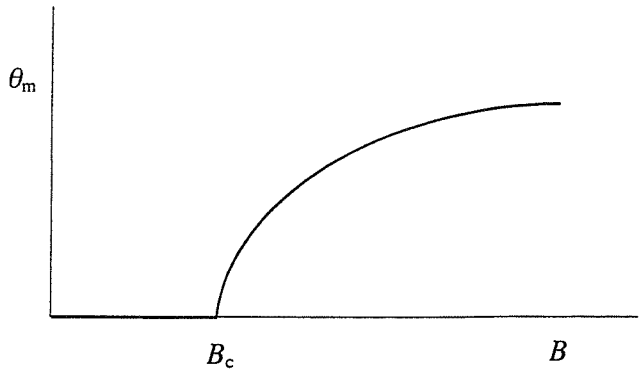

Fig.5 The dependence of the angle of the director in the middle of the cell

The threshold fields for the three distortion modes are given by [2]

$$B_c = \frac{\pi}{d}\left(\mu_0 \frac{K_i}{\Delta\tilde{\chi}}\right)^{\frac{1}{2}} \qquad i=1, 2, 3 \qquad (6)$$

where μ_0 is the vacuum permeability and $\Delta\tilde{\chi}$ is the diamagnetic anisotopy, that is $\tilde{\chi}_{\parallel} - \tilde{\chi}_{\perp}$ where $\tilde{\chi}_{\parallel}$ is the diamagnetic susceptibility parallel to the director and $\tilde{\chi}_{\perp}$ is that perpendicular to the director.

Thus three elastic constants can be obtained by measuring the threshold fields of the Freedericksz transitions for the three distortion modes shown in Fig.4. For the splay and bend modes, the same measurement is possible using an electric field applied perpendicular to the substrates by applying a voltage to electrodes coated on the two substrates. However, the measurement for the twist mode is not so simple for K_2; the electric field parallel to the plates is available using interdigitated electrodes on one of the two substrates but the intensity of the field is not uniform from one side of the substrate to the other. This clearly complicates the analysis of the director response to the non-uniform fields.

The elastic constants clearly vary with the extent of the orientational order and according to theory, the elastic constants depend on the order parameter according to [3]

$$K_1 = K_3 = 2\overline{P}_2^2(L_1 + \tfrac{1}{2}L_2), \tag{7}$$

$$K_2 = 2\overline{P}_2^2 L_1, \tag{8}$$

where L_1 and L_2 are elastic constants which do not depend on the orientational order parameter. Thus, the relationship between elastic constants and the order parameter is

$$K_i \propto \overline{P}_2^2. \tag{9}$$

However, in general the three elastic constants are different but nonetheless they are still predicted and usually found to be quadratic in the order parameter.

1.2.3 Dependence of the Elastic Constants on the Molecular Structure of Liquid Crystals

The elastic constants are determined not only by the orientational order but also by the molecular structure and we consider this dependence here. Fig.6 shows the typical model of a liquid crystal molecule; A and B are the core units which are normally ring systems (aromatic and/or alicyclic). These are sometimes linked by a group (Y), such as dimethylene (-CH_2-CH_2-) and ester (-COO-), however usually a direct link is used. R denotes the terminal chain which is usually an alkyl or an alkoxy; X is another terminal group. If it is a polar group, such as cyano (-CN), fluoro (-F) and trifluoro methyl (-CF_3), the mesogenic molecule has a strong dipole moment parallel to the long axis and so the nematic has a positive dielectric anisotropy, $\Delta\tilde{\varepsilon}$, that is $\tilde{\varepsilon}_{\parallel} - \tilde{\varepsilon}_{\perp}$ where $\tilde{\varepsilon}_{\parallel}$ is the dielectric permittivity parallel to the director and $\tilde{\varepsilon}_{\perp}$ is that perpendicular to the director, according to [4]

$$\Delta\tilde{\varepsilon} = \frac{NhF}{\varepsilon_0}\left[\Delta\alpha - \frac{F\mu^2}{2k_B T}\left(1 - 3\cos^2\beta\right)\right]\overline{P}_2, \tag{10}$$

where $\Delta\alpha$ is the polarisability anisotropy for a single molecule, μ is the permanent dipole moment, k_B is the Boltzmann constant, T is the absolute temperature, β is the angle

between the long axis of the molecule and the dipole moment, N is the number of the molecules per unit volume, and h and F are constants.

On the other hand, if it is a non-polar group, such as another alkyl and alkoxy chain (that is X is exactly the same as R), then the mesogenic molecule has a small dipole moment and the nematic a small dielectric anisotropy. The polar group may link to the core group in the lateral direction and in this case, the liquid crystal is more likely to have a negative dielectric anisotropy.

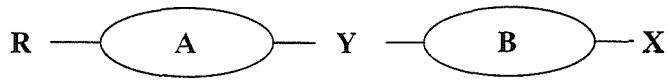

Fig.6 A typical structure of a liquid crystal molecule

The dependence of the elastic constants on the molecular structure of liquid crystals has been investigated by several authors [5-8]. One example is the dependence of the ratio of the two elastic constants, K_3/K_1 on the molecular length (L) and width (D) [9]. Because it is found that longer mesogenic molecules increase K_3/K_1 and wider molecules decrease K_3/K_1, it is suggested that the ratio K_3/K_1 depends on L/D. This relationship does not always hold. The structures of the core units (A, B) and the structures of the terminal chains (R) have different effects on the elastic constants.

For example, the materials shown in Fig.7, 7CB (4-heptyl-4'-cyanobiphenyl) [10,11], PCH7 (4-heptyl-4'-cyanophenylcyclohexane) [12] and CCH7 (4-heptyl-4'-cyanobicyclohexane) [12], have different elastic constants although their length to breadth ratios are similar.

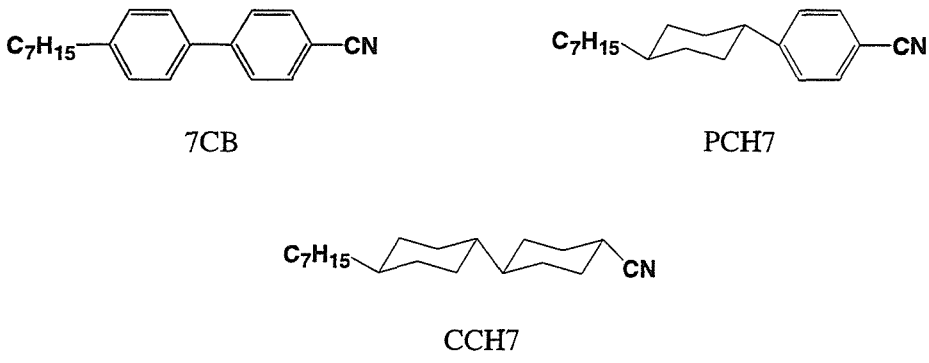

Fig.7 Molecular structures of the 7CB, PCH7 and CCH7

Figs. 8 (a), (b) and (c) show the dependence of K_1, K_2 and K_3, respectively on the structure of the core units. Here, the increasing order is found to be CCH7, PCH7 and 7CB for K_1 and K_2. Therefore, it would seem that the larger the number of phenyl rings the larger K_1 and K_2. On the other hand, the increasing order for K_3 is different from the other elastic constants, however the extent of the variation is relatively small. From the results in Fig.8, we can infer that a higher number of phenyl rings gives a smaller value for the ratio K_3/K_1. This tendency for K_3/K_1 is also reported for other liquid crystals [7,13,14].

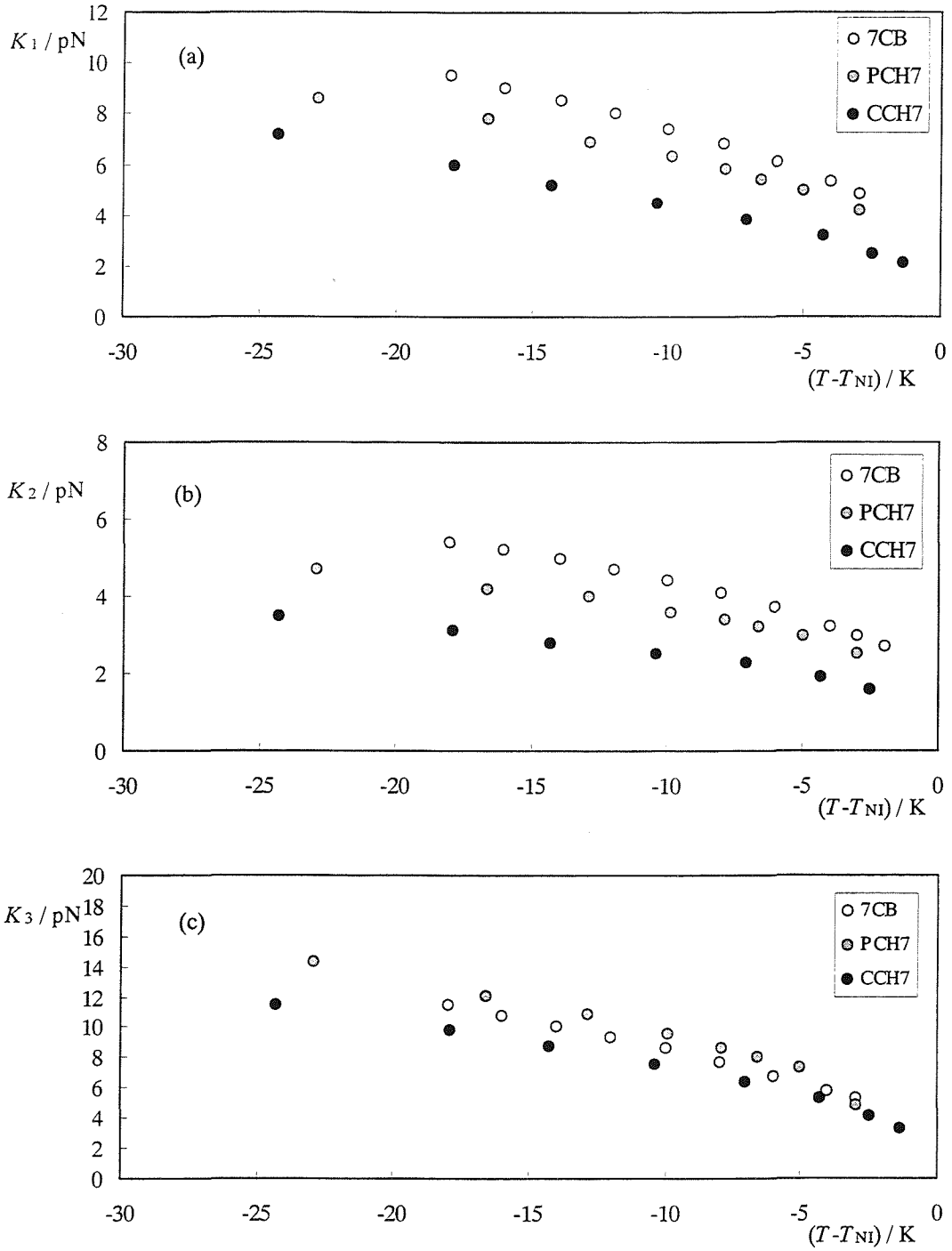

Fig.8 Dependence of the elastic constants; (a) K_1, (b) K_2 and (c) K_3 on the structure of the core unit of mesogenic molecules (see Fig.7)

Another example is the dependence of K_3/K_1 on the length of the terminal group (R). Fig.9 shows the dependence of K_3/K_1 on the number of carbon atoms in the alkyl chain for 5CB, 6CB and 7CB [10,11]; the structure of 7CB is shown in Fig.7. From Fig.9, we can see the dependence on the length of the alkyl chain; the longer the chain length, the smaller K_3/K_1 becomes. The same behaviour is also reported for other materials [15] and the reason for this behaviour is that the longer alkyl chain increases K_1 but K_3 is almost unchanged.

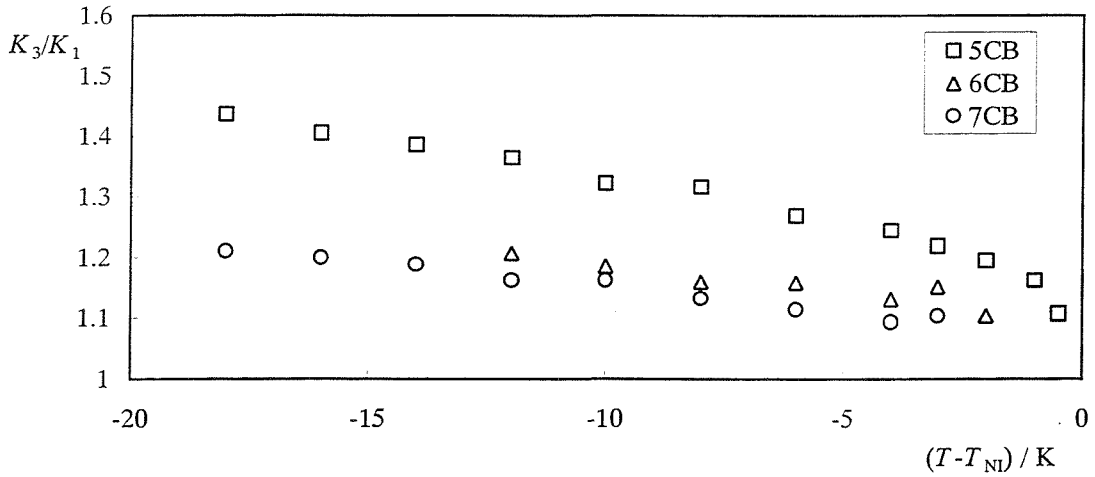

Fig.9 Dependence of K_3/K_1 on the length of the terminal group

1.3 Visco-elastic Properties of Liquid Crystals

A nematic liquid crystal flows like a conventional organic liquid. However, because a liquid crystal is anisotropic, the flow depends on the orientation of the director makes with the flow direction and with the velocity gradient, and the translational motions are coupled to inner, orientational motions of molecules. Consequently, the flow will disturb the alignment and cause the director to rotate. The description of the flow is based on the hydrodynamics of isotropic liquids and the extension will be made to simple shear flow of a nematic in which the orientation of the director is well controlled by an external field. In

this section, we discuss first a basic idea of the viscosity coefficients for a simple shear flow and the theory of the measurement of the rotational viscosity coefficient through the field-induced relaxation time. Then we will discuss the dependence of the rotational viscosity on the molecular structure of liquid crystals.

1.3.1 Viscosity Coefficients

Consider simple shear flow in a nematic liquid crystal. When the liquid crystal is situated between parallel plates and the orientation of the director is fixed by external forces, for example by a strong magnetic field), there are three values of viscosity coefficient;
η_1 which corresponds to the geometry where the director is parallel to velocity gradient,
η_2 which corresponds to the geometry where the director is parallel to flow direction, and
η_3 which corresponds to the geometry where the director is nomal to shear plane. These are called the Miesowicz viscosity coefficients, for the shear experiment which are associated with the three limiting orientations of the pinned director with respect to the shear direction and the velocity gradient that can be envisaged. These three geometries are pictured in Fig.10. If the experiment is not conducted with the sample lying between parallel plates then a further stretch type of distortion may occur and this is pictured in Fig.10 (d).

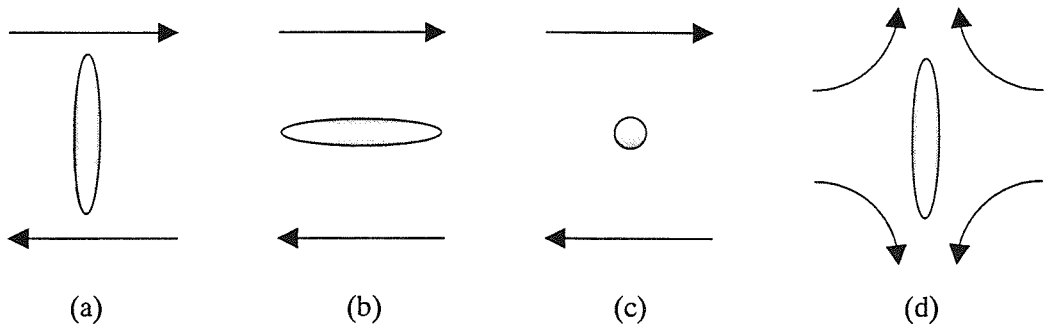

Fig.10 Miesowicz viscosity coefficients of a nematic liquid crystal, (a) η_1, (b) η_2, (c) η_3 and (d) η_{12}

At any temperature η_1 has the largest value reflecting the fact that in this geometry the neighbouring lamellae are effectively interlocked because of the average molecular orientation and are prevented from sliding easily over each other. η_2 has a lowest value, in this geometry the director is closest to the orientation seen when shear-induced alignment lowers the effective viscosity of isotropic fluids composed of rod-like molecules, and so η_2 is decreased for the same reasons. η_3 behaves like a continuation of the single isotropic viscosity coefficient η. As is shown in Fig.10 (c), there is no anisotropy in the place defined by the shear and velocity gradient direction as the anisotropy that characterises the nematic phase is only apparent outside of the shear plane.

We have been concerned the motion of a nematic when the director is fixed. Then we will consider a case in which the hydrodynamic behaviour of the liquid crystal has no isotropic counterpart. According to de Jeu [16], the rotation of the director of a nematic liquid crystal in an applied field is described by an equation of motion, or torque balance equation [16];

$$I\frac{d\Omega}{dt} = \Gamma_{\text{mag}} + \Gamma_{\text{elast}} + \Gamma_{\text{visc}} \tag{11}$$

The left-hand side represents the inertial term; I is the moment of inertia per unit volume and Ω is the local angular velocity of the director, given by

$$\Omega = \hat{n} \times d\hat{n} / dt \,. \tag{12}$$

The terms on the right-hand side are the torque per unit volume on the director due to the magnetic forces (magnetic torque), due to the elastic forces (elastic torque) and due to the frictional forces (viscous torque), respectively. At low angular velocity, the inertial term in equation (11) is much smaller than the elastic and the viscous torque. The elastic torque originally comes from the boundary effects. However, if we consider a bulk sample at a low angular velocity, the boundary effects are found, experimentally, to be rather

unimportant [17]. Therefore, the elastic torque can be ignored provided the director orientation is uniform which is the principle condition for this discussion. Thus, the torque equation (11) reduces to

$$\Gamma_{\text{mag}} + \Gamma_{\text{visc}} = 0 . \tag{13}$$

If there is no hydrodynamic flow, in other words, the director rotates without any translational motion of the molecules, the viscous torque is given by

$$\Gamma_{\text{visc}} = -\gamma_1 \frac{d\phi}{dt}, \tag{14}$$

where ϕ is the angle between the director and the field. Because the magnetic torque is given by [3]

$$\Gamma_{\text{mag}} = -\frac{1}{2}\mu_0^{-1}\Delta\tilde{\chi}B^2 \sin 2\phi , \tag{15}$$

equation (13) can be rewritten as

$$\gamma_1 \frac{d\phi}{dt} = -\frac{1}{2}\mu_0^{-1}\Delta\tilde{\chi}B^2 \sin 2\phi . \tag{16}$$

the solution of equation (16) is

$$\tan\phi(t) = \tan\phi_0 \exp(-t/\tau), \tag{17}$$

with a relaxation time

$$\tau = \frac{\gamma_1}{\Delta\tilde{\chi}B^2/\mu_0}. \tag{18}$$

The elastic torque becomes important when the anchoring at the boundary is strong. We consider the case when the nematic is contained between two substrates and the anchoring energy is large. In this case, it is not possible to ignore the elastic torque in equation (11). When the director deforms in the twist mode, the condition in Fig.3 (b) for example, with

a magnetic field larger than the threshold field of the Freedericksz transition, equation (11) is described by

$$\gamma_1 \frac{\partial \phi}{\partial t} = \frac{1}{2} \mu_0^{-1} \Delta\tilde{\chi} B^2 \sin 2\phi + K_2 \frac{\partial^2 \phi}{\partial z^2}. \tag{19}$$

This is a torque balance equation when the magnetic field is on. If the magnetic field is not much stronger than the threshold field, the twist angle is small. With the substrates at $z = \pm(1/2)d$ where necessarily $\phi = 0$, ϕ can be given, to a good approximation [16], by

$$\phi_0(z) = \phi_m \cos(\pi z / d), \tag{20}$$

where ϕ_m is the maximum distortion at z=0. If we assume a further approximation, ϕ is small where $\sin 2\phi \cong 2\phi$, the solution of equation (19) is

$$\phi(z,t) = \phi_0(z) \exp(-t/\tau_R), \tag{21}$$

with a relaxation time, τ_R,

$$\tau_{ON} = \frac{\gamma_1}{\pi^2 (K_2 / d^2) - \Delta\tilde{\chi} B^2 / \mu_0}. \tag{22}$$

When the magnetic field is suddenly removed, equation (19) reduces to

$$\gamma_1 \frac{\partial \phi}{\partial t} = K_2 \frac{\partial^2 \phi}{\partial z^2}. \tag{23}$$

This is the torque balance equation when the magnetic field is off and the director is aligned by surface forces. The solution of equation (23) is the same as equation (21) but with a different relaxation time, τ_R,

$$\tau_{OFF} = \frac{\gamma_1 d^2}{\pi^2 K_2}. \tag{24}$$

The situation for the splay geometry and the bend geometry is more complicated because rotation of the director causes hydrodynamic flow: the gradient of the angular velocity of $\hat{n}$ produces a backflow motion of the fluid, giving a frictional torque. The splay viscosity

coefficient, η_{splay}, and the bend viscosity coefficient, η_{bend} are given, in the case $B/B_c \rightarrow \infty$, by [16]

$$\eta_{\text{splay}} = \gamma_1 - \alpha_3^2/\eta_2, \tag{25}$$

$$\eta_{\text{bend}} = \gamma_1 - \alpha_2^2/\eta_1. \tag{26}$$

Here η_i (i=1, 2) are the Miesowicz viscosity coefficients which are defined by

$$\eta_1 = \frac{1}{2}(-\alpha_2 + \alpha_4 + \alpha_5), \tag{27}$$

$$\eta_2 = \frac{1}{2}(\alpha_3 + \alpha_4 + \alpha_6), \tag{28}$$

in which α_i (i=1~6) are the Leslie-Eriksen viscosity coefficients.

The viscosity coefficients, like that for a normal liquid, depend strongly on temperature. The viscosity of an isotropic liquid varies approximately as

$$\eta_{\text{iso}} = \eta_0 \exp(E/k_B T), \tag{29}$$

where $E > 0$ is an activation energy for diffusion, η_0 is a constant and k_B is the Boltzmann constant. In the case of liquid crystals, the order parameter, $\overline{P}_2$, should be taken into account because this parameter represents the anisotropy of liquid crystals which influences the viscosity coefficients. For γ_1, experimental results suggest that the temperature dependence can be written as [16]

$$\gamma_1 \propto \overline{P}_2 \exp(E'/k_B T). \tag{30}$$

1.3.2 Dependence of the Rotational Viscosity on the Molecular Structure of Liquid Crystals

There is little information about the relationship between the rotational viscosity coefficient and the molecular structure of the nematic liquid crystal. However, there are some empirical rules for the relationship between the molecular structure and the viscosity in general [18]. For example,

(1) Molecules with a higher number of rings or longer alkyl chains are characterised by an increased viscosity.

(2) Liquid crystals exhibiting high values of the dielectric anisotropy usually exhibit higher viscosities than those with low dielectric anisotropy. A plausible explanation for this behaviour might be the stronger polar interaction between the molecules.

(3) Liquid crystals with lateral functional groups usually have higher viscosities than molecules with the same substituent in a terminal position.

These rules are often superseded by a combination of a variety of other effects, such as the structural rigidity of the molecules, specific intermolecular attractions or repulsions and pretransitional phenomena, i.e. a growth in orientational / positional correlations as the transition is approached.

The rotational viscosity coefficient may also obey these empirical rules. Fig.11 shows the rotational viscosity coefficients for three different molecules; 5CB [19], 8CB [19] and PCH-5 [20]. The difference in the chemical structure between 5CB and 8CB is simply the length of the terminal chain. On the other hand, 5CB and PCH-5 have different core units; 5CB has two phenyl rings linked directly and PCH-5 has a phenyl ring and a cyclohexane ring linked directly. In Fig.11, two different temperature scales are used to compare the rotational viscosity coefficient. One is the absolute temperature (a) and the other is the reduced temperature, T/T_{NI} (b). This is because γ_1 depends on the absolute temperature and the order parameter which is often found to be a universal function of the reduced temperature [21] (see equation (30)).

For 5CB and 8CB, this dependence on both of the temperature scales indicate that the molecule with a longer alkyl chain has a higher γ_1. However, for 5CB and PCH-5, the behaviour is different depending on the temperature scale used for the comparison. PCH-5 has a larger γ_1 than 5CB on the absolute temperature while we can see the opposite phenomenon on the reduced temperature.

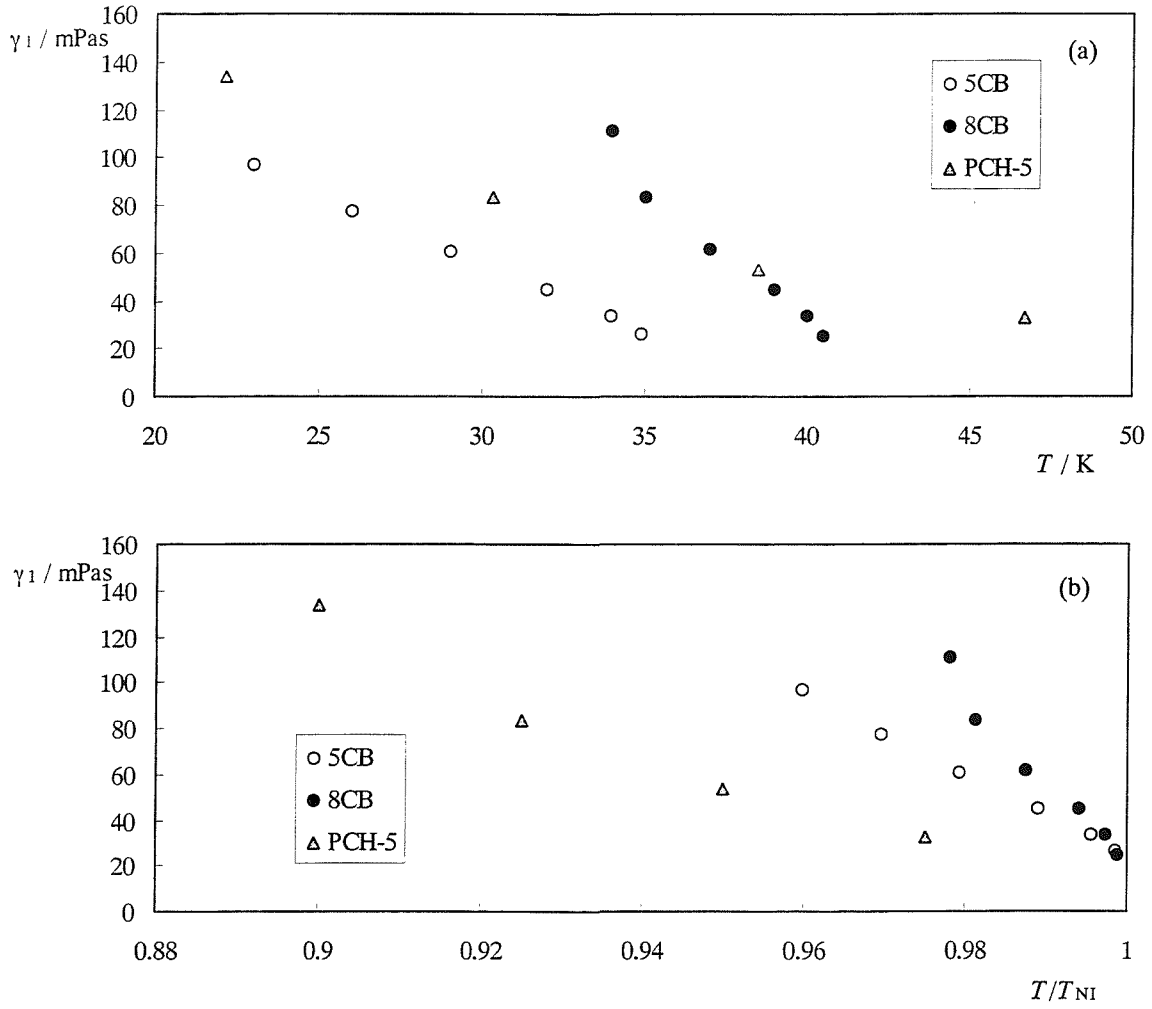

Fig.11 The dependence of the rotational viscosity coefficient for 5CB, 8CB and PCH-5 on the absolute temperature (a) and on the reduced temperature, T/T_{NI} (b)

1.4 Liquid Crystal Displays

1.4.1 Display Modes

Liquid crystal displays (LCD) have some major advantages over the conventional cathode ray tube (CRT); thus they are thin, light and have a low power consumption, which enables them to play an important role as display devices in notebook type personal computers (PC). Several types of LCD mode have been developed and improved. For example, the dynamic scattering (DS) mode, the twisted nematic (TN) mode [22] and the super twisted nematic (STN) mode [23]. Fig.12 shows the schematic diagram of TN mode, for example. These modes are controlled by an electric field applied perpendicular to two glass substrates. The development of thin film transistor (TFT) technology has made the TN-LCD an even more powerful display device [24]. This TN-TFT-LCD have the best quality and occupies the main position in the whole LCD market. However, even TN-TFT-LCD have several disadvantages, such as a narrow viewing angle and a relatively slow response time. The narrow viewing angle will be a disadvantage when the whole area of the device is so large that the viewing angle depends on the location of the picture. The relatively slow response times of LCD are one of the most critical problems if we use this device for moving pictures. Recently, new switching modes have been developed to solve these problems, such as the in-plane switching (IPS) mode. TFT-LCD using the in-plane switching (IPS) mode (IPS-TFT-LCD) has an extremely wide viewing angle and is expected to replace the CRT as the screen for desk top PCs [25,26]. Fig.13 shows the schematic diagram of IPS mode. This mode requires an applied electric field parallel to the glass substrate and this is achieved by interdigital electrodes on one side of the substrate. However, since the liquid crystal director moves in a totally different way, this mode needs a new range of nematic liquid crystal materials in order to possess the same levels of switching times and threshold voltages as in the TN mode.

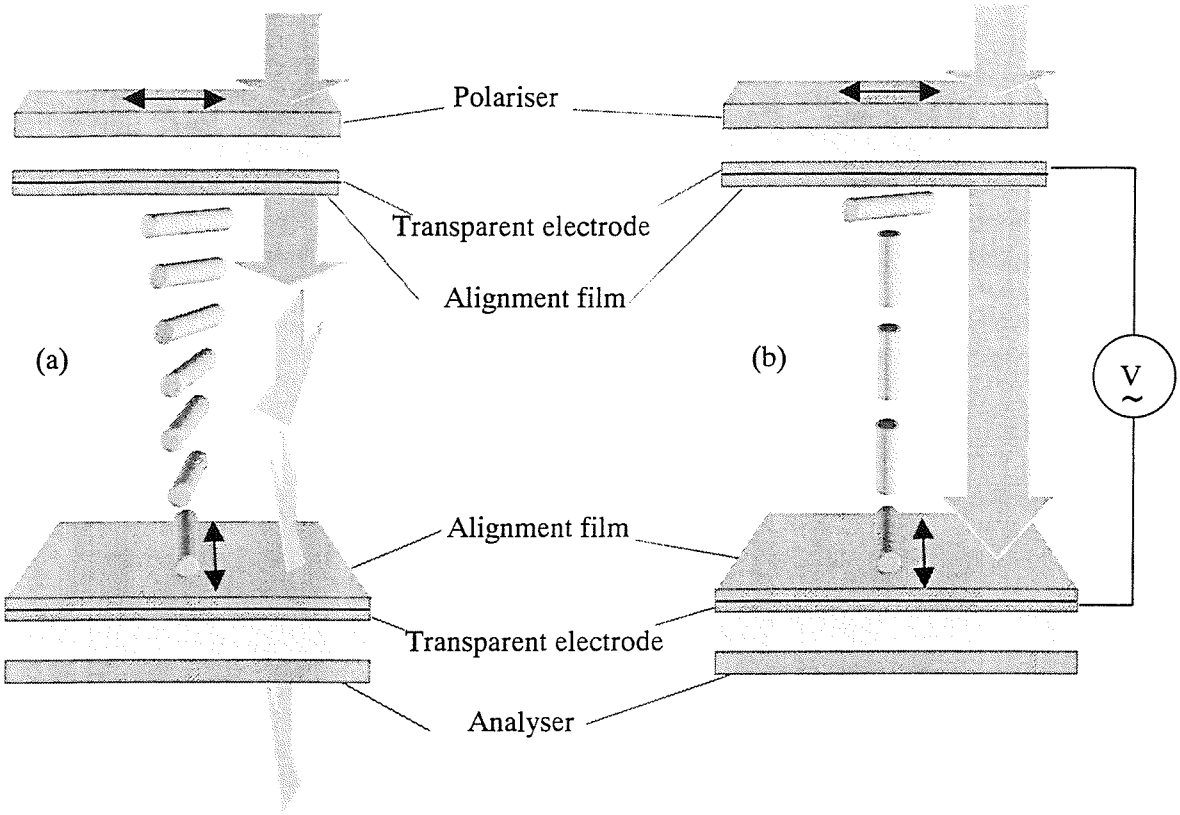

Fig.12 Schematic diagram of a liquid crystal display (TN mode),

(a) off-state and (b) on-state

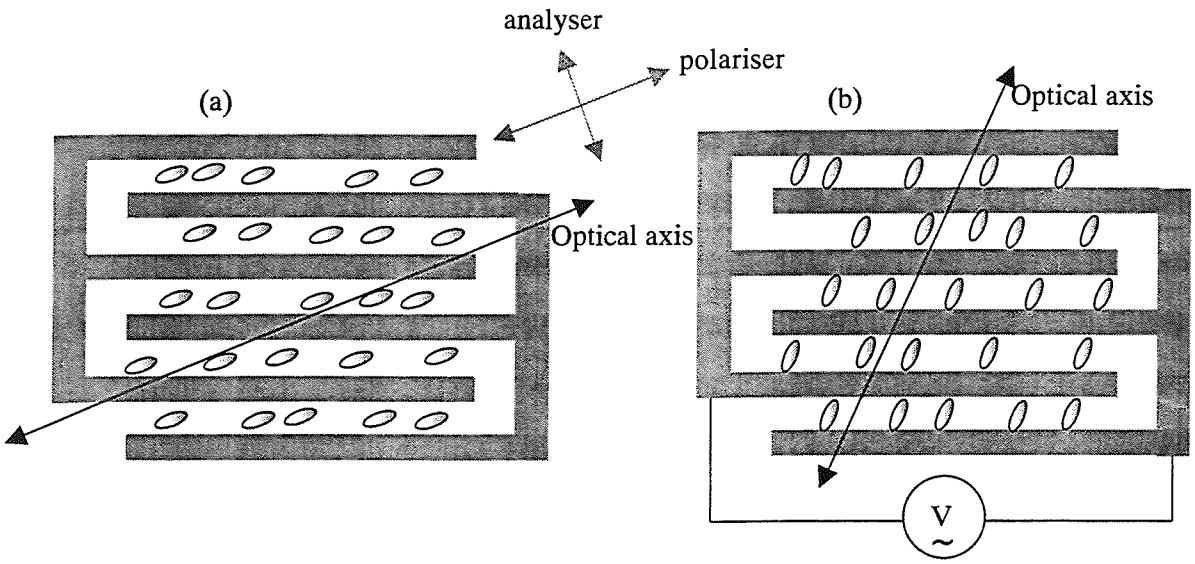

Fig. 13 Schematic diagram of the IPS mode, (a) off state and (b) on state

1.4.2 Threshold Voltages

Threshold voltages of LCD determine the range of applied electric field required to operate LCD and so it determines the cost of the driving devices. The threshold voltage in the TN mode is given by [22,27,28]

$$V_{th} = \pi \sqrt{\frac{K_1 + (K_3 - 2K_2)/4}{\varepsilon_0 \Delta\tilde{\varepsilon}}}, \tag{31}$$

where ε_0 is the dielectric permittivity of free space and $\Delta\tilde{\varepsilon}$ is the dielectric anisotropy of the liquid crystal used. This is the expression of the threshold voltage obtained from the Freedericksz transition experiment for the twisted planar layer, which can be obtained by rotating the upper boundary of a uniform planar layer through an angle 90°. For the IPS mode, the twist elastic constant is the dominant elastic constant since the director of a nematic simply twists in the plane parallel to the substrate. Therefore the threshold voltage in the IPS mode is given by [25]

$$V_{th} = \frac{\pi l}{d} \sqrt{\frac{K_2}{\varepsilon_0 \Delta\tilde{\varepsilon}}}, \tag{32}$$

where d is the gap of the LCD cell and l is the distance between a pair of interdigital electrodes. One of the main differences from the TN-mode is that V_{th} depends only on the single elastic constant K_2 but depends on the cell thickness.

1.4.3 Switching Times

The switching time is one of the most important characteristics of the LCD because it is clearly related to the quality of the image of moving pictures. The switching time in the TN mode when an electric field is applied, τ_{ON}, and the switching time when the electric field is removed, τ_{OFF}, are given by [22,27,28]

$$\tau_{ON} = \frac{\gamma_1 d^2}{\varepsilon_0 \Delta\tilde{\varepsilon} V^2 - \pi^2 \{K_1 + (K_3 - 2K_2)/4\}}, \tag{33}$$

$$\tau_{OFF} = \frac{\gamma_1 d^2}{\pi^2 \{K_1 + (K_3 - 2K_2)/4\}}, \tag{34}$$

where V is the applied voltage. According to these equations, the response times depend on γ_1 and the three elastic constants. In contrast, the response times in the IPS mode are given by [26]

$$\tau_{ON} = \frac{\gamma_1 d^2}{\varepsilon_0 \Delta\tilde{\varepsilon} V^2 - \pi^2 K_2}, \tag{35}$$

$$\tau_{OFF} = \frac{\gamma_1 d^2}{\pi^2 K_2}. \tag{36}$$

The same as for V_{th}, one of the main differences from the TN-mode is that the response times depend only on the single elastic constant K_2. In order to improve the switching times, a smaller γ_1 and a larger $\Delta\tilde{\varepsilon}$ are needed. For K_2, a compromised value would be required because this elastic constant affects the two response times in different ways.
To develop new nematic materials especially for IPS-TFT-LCD, the relationship between their molecular structure and physical properties (γ_1, $\Delta\tilde{\varepsilon}$ and K_2) must be examined and understood.

1.5 Mixtures

So far we have considered the physical properties for pure nematic liquid crystals. However, the nematic materials used in applications are mixtures because they require a very wide nematic range, appropriate physical properties, such as $\Delta\tilde{n}$, $\Delta\tilde{\varepsilon}$, K_i (i=1, 2, 3) and γ_1, and it is impossible to design a single nematogen to achieve these. Consequently we should consider the relationship between the single component system and the mixture system when we discuss the physical properties for a nematic mixture.
We begin with the nematic-isotropic transition temperature T_{NI}. For a two component mixture this is predicted by the Humphries-James-Luckhurst theory [29] to be

$$T_{\mathrm{NI}}^{\mathrm{mixture}} = xT_{\mathrm{NI}}^{A} + (1-x)T_{\mathrm{NI}}^{B}, \tag{37}$$

where T_{NI}^{A}, T_{NI}^{B} and $T_{\mathrm{NI}}^{\mathrm{mixture}}$ are the nematic-isotropic transition temperatures for component A, component B and the resulting mixture, respectively and x is the mole fraction of component A. According to equation (37) the dependence of T_{NI} on the mole fraction of component A should be a straight line. This ideal case occurs when the three intermolecular energy parameters, ε_{AA}, ε_{BB} and ε_{AB}, occurring in the potential of mean torque for the molecules, are related by the geometric mean

$$\varepsilon_{AB} = (\varepsilon_{AA}\varepsilon_{BB})^{\frac{1}{2}}. \tag{38}$$

The potential of mean torque for a molecule in a pure nematogen is given

$$U(\beta) = -\varepsilon\overline{P}_2\frac{3\cos^2\beta - 1}{2}, \tag{39}$$

where ε is the intermolecular energy parameter and β is the angle between the molecular long axis and the director. For a binary mixture, equation (39) will be extended for component A to

$$U_A(\beta) = -\left\{x\varepsilon_{AA}\overline{P}_2^{A} + (1-x)\varepsilon_{AB}\overline{P}_2^{B}\right\}\frac{3\cos^2\beta - 1}{2}, \tag{40}$$

where ε_{AA} is the intermolecular energy parameter for component A and ε_{AB} is the mixed intermolecular energy parameter, and $\overline{P}_2^{A}$ and $\overline{P}_2^{B}$ are the orientational order parameters for components A and B, respectively. There is an analogous expression for $U_B(\beta)$.

The plots of T_{NI} versus x can show both positive and negative deviations when the mixed interaction parameter ε_{AB} deviates from the geometric mean.

It is well-known that the diamagnetic anisotropy, $\Delta\tilde{\chi}$, is proportional to the orientational order parameter, $\overline{P}_2$ [30], so $\Delta\tilde{\chi}$ for a binary mixture is predicted to be

$$\Delta\tilde{\chi}_{\mathrm{mixture}} = x\Delta\chi_A\overline{P}_2^{A} + (1-x)\Delta\chi_B\overline{P}_2^{B}, \tag{41}$$

where $\Delta\chi_A$ and $\Delta\chi_B$ are the diamagnetic anisotropies of component A and component B in the limit of complete order, respectively, $\overline{P}_2^A$ and $\overline{P}_2^B$ are the order parameters of component A and component B, respectively. Other physical properties, such as $\Delta\tilde{\varepsilon}$ may be given by similar expressions as equation (41), for example

$$\Delta\tilde{\varepsilon}_{\text{mixture}} = x\Delta\varepsilon_A\overline{P}_2^A + (1-x)\Delta\varepsilon_B\overline{P}_2^B, \tag{42}$$

where $\Delta\varepsilon_A$ and $\Delta\varepsilon_B$ are diamagnetic anisotropies of component A and component B in the limit that the order parameters $\overline{P}_2^A$ and $\overline{P}_2^B$ are unity, respectively. For the elastic constants, K_i (i=1, 2, 3), because they are expected to be approximately proportional to the square of $\overline{P}_2$ (see equation (9)) the values for a binary mixture may be predicted to be

$$K_i^{\text{mixture}} = \left(x\sqrt{K_i^A}\overline{P}_2^A + (1-x)\sqrt{K_i^B}\overline{P}_2^B\right)^2, \tag{43}$$

where K_i^A and K_i^B are the elastic constants of component A and component B again in the limit that the order parameters are 1, respectively. K_1 and K_2 for binary mixtures of liquid crystals with similar T_{NI} measured at the same reduced temperature are reported to obey this equation [8].

1.6 Overview of the Thesis

The research described in this Thesis is concerned with the physical properties of liquid crystals, mainly the rotational viscosity coefficient, γ_1, and the twist elastic constant, K_2. These two physical properties play important roles in the performance of liquid crystal displays based on the in-plane switching mode, especially the switching times and the threshold voltages. From an industrial point of view, to develop liquid crystals to give an LCD with a better performance is of special interest. In order to do this, the effect of chemical structures of the component liquid crystals on these physical properties needs to be understood. The first step for the development of liquid crystal materials with the

desired physical properties could be to design or discover the dopants to be added to existing liquid crystals. However, the appropriate temperature scale to be used when comparing the results for different mixtures can be different depending on the particular physical properties chosen. What will be discussed in this Thesis is how the dopants added to a nematic liquid crystal mixture change, for example, γ_1 and K_2, and the appropriate temperature scale for their comparison. In order to study this, we need the appropriate measurement techniques for these particular physical properties. We have chosen to use the magnetic resonance method based on ESR spectroscopy to determine γ_1, and the dynamic light scattering method to determine K_2 and γ_1.

In Chapter 2, we will discuss the measurement of the rotational viscosity coefficient for nematic liquid crystals by ESR spectroscopy. Here, theory and the methodology of this measurement are mainly discussed. Next in Chapter 3, we examine the effect of dopants on γ_1 using this technique to measure the rotational viscosity. The temperature dependence of these properties and the suitable temperature scales for their comparison is the main point of Chapter 3. However, the absolute value of γ_1 is not available by this method without a knowledge of the value of the diamagnetic anisotropy, $\Delta\tilde{\chi}$. Therefore, we discuss the determination of $\Delta\tilde{\chi}$ by ESR spectroscopy in Chapter 4. In Chapter 5, the effect of dopants on K_2 will be studied by a different technique, namely dynamic light scattering. By this method, γ_1 can also be obtained, allowing us to compare the results between two methods. In the final chapter, Chapter 6, we present our conclusions and suggestions for future work.

1.7 References

[1] F.C. Frank; Disc. Faraday Soc., **59**, 1958, 958.

[2] A. Saupe; Z. Naturforsch, **15a**, 1960, 815.

[3] W.H. de Jeu; Physical Properties of Liquid Crystalline Materials, Chapter 6, 1980, Gordon and Breach, London.

[4] W.H. de Jeu; Physical Properties of Liquid Crystalline Materials, Chapter 5, 1980, Gordon and Breach, London.

[5] M. Schadt and F.Muller; Revue Phys. Appl., **14**, 1979, 265.

[6] F. Leenhouts, A.J. Dekker and W.H. de Jeu; Phys. Lett., **72A**, 1979, 155.

[7] Hp. Schad and M.A. Osman; J. Chem. Phys., **75**, 1981, 880.

[8] Hp. Schad and M.A. Osman; J. Chem. Phys., **79**, 1983, 5710.

[9] F. Leenhouts, H.J. Roebers, A.J. Dekker and J.J. Jonker; J. Phys. (Paris), **40-C3**, 1979, C3-291

[10] M.J. Bradshaw, E.P. Raynes, J.D. Bunning and T.E. Faber; J. Phys. (Paris), **46**, 1985, 1513.

[11] H.J. Coles; in The Optics of Thermotropic Liquid Crystals, Ed. S. Elston and R. Sambles, Chapter 4, 1998, Taylor&Francis, London.

[12] Hp. Schad, G. Baur and G. Meier; J. Chem. Phys., **70**, 1979, 2770.

[13] M.J. Bradshaw, E.P. Raynes; Mol. Cryst. Liq. Cryst., **91**, 1983, 145.

[14] B.S. Scheuble, G. Baur and G. Meier; Mol. Cryst. Liq. Cryst., **68**, 1981, 57.

[15] W.H. de Jeu and W.A. Claassen; J. Chem. Phys., **68**, 1978, 102.

[16] W.H. de Jeu; Physical Properties of Liquid Crystalline Materials, Chapter 7, 1980, Gordon and Breach, London.

[17] P.G. de Gennes and J. Prost; The Physics of Liquid Crystals (Second Edition), Chapter 5, 1993, Clarendon Press, Oxford.

[18] L. Pohl and U. Finkenzeller; Physical Properties of Liquid Crystals, Liquid Crystals-Application and Uses, Vol.1, Chapter 4, 1990, World Scientific.

[19] H. Kneppe, F. Schneider and N.K. Sharma; J. Chem. Phys., **77**, 1982, 3203.

[20] U. Finkenzeller, T. Geelhaar, G.Weber and L. Pohl; Liq. Cryst., **5**, 1989, 313.

[21] W.H. de Jeu; Physical Properties of Liquid Crystalline Materials, Chapter 1, 1980, Gordon and Breach, London.

[22] M. Schadt and W. Helfrich; Appl. Phys. Lett., **18**, 1971, 127.

[23] M. Schadt; Mol. Cryst. Liq. Cryst., **165**, 1988, 405.

[24] T.F. Brody, F.C. Luo, D.H. Davies and E.W. Greeneich; SID Digest (New York), 1981, 132.

[25] M. Oh-e and K. Kondo; Appl. Phys. Lett., **67**, 1995, 3895.

[26] M. Oh-e and K. Kondo; Appl. Phys. Lett., **69**, 1996, 623.

[27] H.Koelmans and A.M. van Boxlel; Mol. Cryst. Liq. Cryst., **12**, 1971, 185.

[28] E. Jakeman and E.P. Raynes; Phys. Lett., **39A**, 1972, 69.

[29] R.L. Humphries, P.G. James and G.R. Luckhurst; Symposia of the Faraday Society, **5**, 1971, 107.

[30] W.H. de Jeu; Physical Properties of Liquid Crystalline Materials, Chapter 3, 1980, Gordon and Breach, Lond

Chapter 2

Measurement of the Rotational Viscosity Coefficient for Nematic Liquid Crystals by ESR Spectroscopy

2.1 Introduction

The rotational viscosity coefficient, γ_1, is very important when we consider the response times of LCD as we saw in Chapter 1. γ_1 for a nematic liquid crystal with positive diamagnetic anisotropy, $\Delta\tilde{\chi}$, is often measured by the rotating magnetic field method. In this method, the torque exerted on the nematic, such as the frictional torque and the magnetic torque, is assumed to be fully transmitted to the sample container, and the torque on the container is directly measured [1,2]. However, this method does not monitor whether the director is uniform or not and, in addition, it requires a relatively large amount of material to obtain a better accuracy of the measurement. From this point of view, a magnetic resonance method is very effective because this can monitor the uniformity of the director. Moreover, the amount of sample required for this method is smaller than for the rotating field method. The basic idea of this method is to monitor the field-induced alignment of the director of the nematic as a function of time. The role of magnetic resonance is to determine the director orientation and its distribution.

There are two representative methods; one is ESR (electron spin resonance) spectroscopy and the other is NMR (nuclear magnetic resonance) spectroscopy. The principle for measuring γ_1 with both methods is basically the same. There are, however, two major differences between them. First, the magnitude of the magnetic field used is different. This affects the scale of the field-induced relaxation time. Since the magnetic field for ESR is much less than that for NMR, the time dependence of the director orientation is much slower than in NMR. The relaxation time estimated for ESR is the order of seconds whereas the order of less than one hundredth of a second for NMR. This means that errors

for the measurement of γ_1 are likely to be smaller in ESR than in NMR, and it also means that the ESR experiment is easier than NMR. Secondly, the magnetic properties of the samples required in order to obtain a spectrum should be different for these methods. The samples for ESR should be paramagnetic. Because liquid crystals are not normally paramagnetic, a paramagnetic solute must be added to a liquid crystal. Although the field-induced relaxation behaviour is of the paramagnetic material, it can be treated as that of the liquid crystal host since the paramagnetic solute is orientationally ordered by its anisotropic interaction with the liquid crystal. On the other hand, the samples for NMR do not have to be paramagnetic, so the liquid crystal sample can normally be used without adding any dopants. However, in order to obtain a simple and strong signal, deuterium NMR is usually used for the measurement of γ_1. That is why some of the hydrogen atoms of the liquid crystal sample should be replaced by deuterium atoms or a deuteriated solute should be added to a normal (protonated) liquid crystal sample. Therefore, generally the preparation of the sample is easier in the ESR experiment than in the NMR experiment. When we measure γ_1 using magnetic resonance spectroscopy, ESR spectroscopy is experimentally easier and may be more accurate than NMR spectroscopy. From this point of view, this Chapter focuses on the measurement of γ_1 using ESR spectroscopy. First, the director dynamics of nematic liquid crystals will be described. Secondly, the measurement of the relaxation process by ESR will be explained. Next, the materials and the experiment will be described. Then the analysis of the results will be presented. After this, the rotation dynamics of the director will be examined. Finally, the accuracy of this method, and a comparison with other methods will be discussed.

2.2 Director Dynamics of Nematic Liquid Crystals

Consider a nematic liquid crystal in a cylindrical tube whose axis is perpendicular to the magnetic field (see Fig1). In a static magnetic field, the nematic director aligns along the

field, provided the diamagnetic anisotropy, $\Delta\tilde{\chi}$, is positive.

In this method, the sample tube is rotated relatively suddenly, rather than rotate the magnet itself. To rotate the magnet of the spectrometer is not possible because it is too large and heavy to rotate in a short time for low molar mass nematics where the relaxation time is of the order of just a few seconds. In addition, an ESR spectrometer with a rotating magnet is not available for us. When the sample tube rotates suddenly typically within a few ms, the angle, θ, between the director and the magnetic field changes. Then, it gradually relaxes back to the initial alignment parallel to the magnetic field; this director reorientation is illustrated in Fig.2.

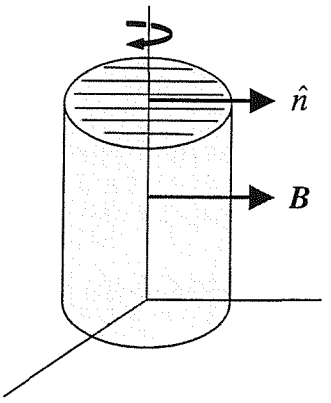

Fig.1 Geometry of the sample tube, magnetic field and the director of the nematic

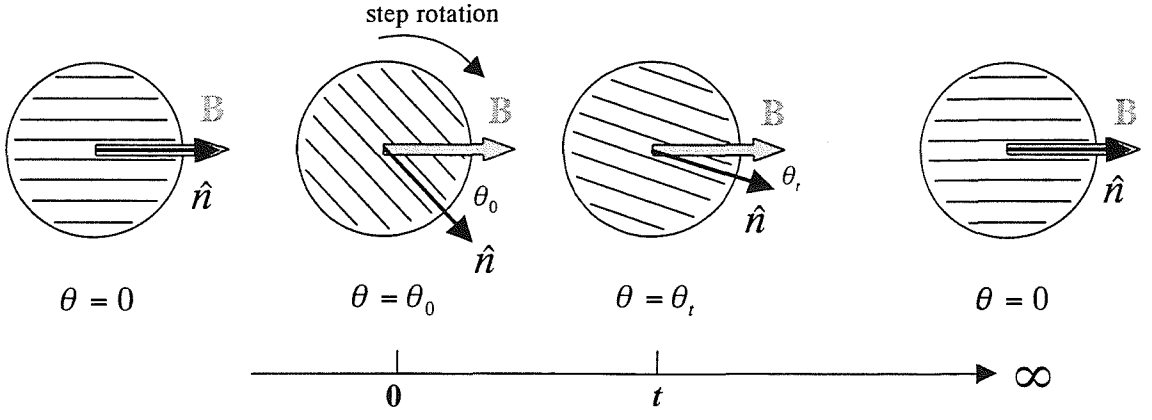

Fig.2 Director reorientation in a static magnetic field

The movement of the director is described by the torque-balance equation [3,4];

$$I\frac{d^2\theta}{dt^2} = -\gamma_1\frac{d\theta}{dt} - \frac{dF}{d\theta} - \frac{\Delta\tilde{\chi}}{2\mu_0}B^2\sin 2\theta\,. \tag{1}$$

In this equation, the left hand side term is the inertial term where I has the units of moment of inertia per unit volume. The first term of the right hand side is the viscous torque where γ_1 is the rotational viscosity coefficient. The second term of the right hand side is the elastic torque where F is the elastic free energy density and the third term is the magnetic torque in which μ_0 is the magnetic constant and B is the magnetic flux density. Surface effects are neglected. Since the inertial term is negligibly smaller than the elastic torque and the viscous torque in a relatively low frequency region [3] and in addition the elastic term is identically zero for a uniformly aligned director,

$$\gamma_1\frac{d\theta}{dt} = -\frac{\Delta\tilde{\chi}}{2\mu_0}B^2\sin 2\theta\,. \tag{2}$$

Integration of this equation gives

$$\tan\theta_t = \tan\theta_0\exp(-t/\tau), \tag{3}$$

where the field-induced relaxation time τ is

$$\tau = \frac{\mu_0\gamma_1}{\Delta\tilde{\chi}B^2} \tag{4}$$

while θ_t and θ_0 are the angles between the director and the magnetic field at time t and 0, respectively. γ_1 can be calculated from the equation (4) if the relaxation time τ has been measured and if the value of $\Delta\tilde{\chi}$ is known.

2.3 Investigation of the Relaxation Process by ESR Spectroscopy

The ESR experiment allows the director orientation to be determined as a function of time. However, liquid crystals do not give an ESR spectrum because they are not usually paramagnetic. Consequently, paramagnetic spin probes need to be added to the nematic liquid crystal in order to study it using ESR spectroscopy. Thus, the information we can obtain in this experiment is directly from the spin probe which is orientationally ordered by its anisotropic interaction with the nematic host. The ESR spectrum of a nitroxide spin probe in a liquid crystal normally contains three nitrogen hyperfine lines resulting from the interaction between the spin of the electron and that of the nitrogen atom of the oxazolidine ring of the spin probe. Fig.3 shows the spin energy levels and the hyperfine interaction of the spin probe.

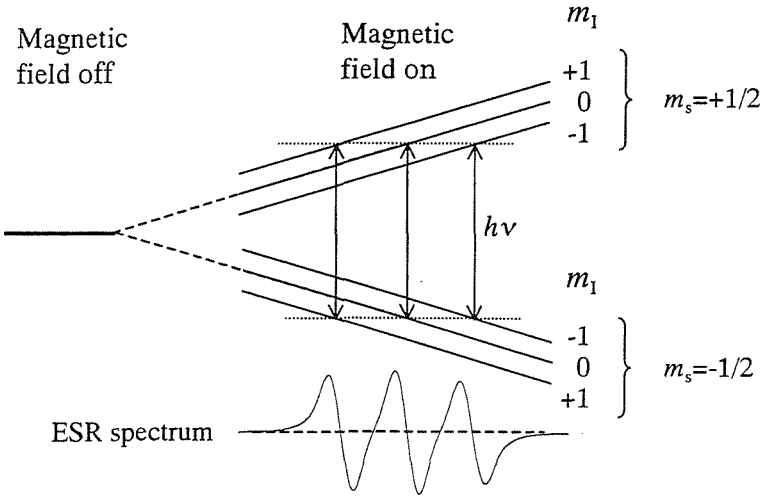

Fig.3 The hyperfine interaction between the spin of the electron and that of the nitrogen atom

In Fig.3, m_s is the electron spin quantum number and m_I is the nuclear spin quantum number for the nitrogen atom. The ESR spectrum is normally recorded as the first derivative of the absorption curve as a result of the detection technique. This is because

phase sensitive detection is used to improve the sensitivity of the technique and in this the magnetic field is modulated resulting in the first derivative.

The spacing between these spectral lines varies with the angle between the director and the magnetic field. Half of the spacing between the outer lines is defined as the hyperfine splitting. Fig.4 shows the ESR spectrum of a cholestane nitroxide spin probe (see Fig.5) dissolved in a nematic liquid crystal. The orientation of the spin probe dissolved in a nematogen may adopt many values due to Brownian motion. To take an average over this motion of the spin probe which results in simple ESR signals, the reorientation of the spin probe molecules dissolved in a nematogen must be fast enough to be in the fast motion limit which is given by [5]

$$\left(A_{\parallel} - A_{\perp}\right)^2 \tau_{RC}{}^2 << 1, \tag{5}$$

where $A_{\parallel}$ and $A_{\perp}$ are the principal components of the total hyperfine tensor and τ_{RC} is the rotational correlation time which is the average time for the spin probe to rotate through 1 radian. In the fast motion limit for spin probes, τ_{RC} needs to be much smaller than 10^{-8}s. Practically, the spectral linewidths contain information about this. If the system is not in the fast motion limit, the lineshape of the spectrum is not anti-symmetric. Fig.4 shows the anti-symmetric lineshapes of the spectra which tells us that the system is in the fast motion limit. While the director of the liquid crystal is relaxing, the hyperfine splitting changes as the angle, θ_t, varies. The hyperfine splitting depends on the angle, θ_t, according to [5];

$$\bar{a}(t) = \left(\frac{\tilde{A}_{\parallel}{}^2 \tilde{g}_{\parallel}{}^2 \cos^2\theta_t + \tilde{A}_{\perp}{}^2 \tilde{g}_{\perp}{}^2 \sin^2\theta_t}{\tilde{g}_{\parallel}{}^2 \cos^2\theta_t + \tilde{g}_{\perp}{}^2 \sin^2\theta_t} \right)^{1/2}, \tag{6}$$

where $\bar{a}(t)$ is the nitrogen hyperfine splitting of the nitroxide spin probe at time t, $\tilde{A}_{\parallel}$ and $\tilde{A}_{\perp}$ are the partially averaged principal components of the hyperfine tensor, that is

when the director and the magnetic field are parallel and perpendicular, respectively, and $\tilde{g}_{\parallel}$ and $\tilde{g}_{\perp}$ are the principal components of the g tensor that is parallel and perpendicular to the director, respectively. Because $\tilde{g}_{\parallel}$ and $\tilde{g}_{\perp}$ are almost equal, equation (6) can be simplified to

$$\bar{a}(t) = \left(\tilde{A}_{\parallel}^{\,2}\cos^2\theta_t + \tilde{A}_{\perp}^{\,2}\sin^2\theta_t\right)^{1/2}. \tag{7}$$

As Fig.4 shows, the hyperfine splitting before the step rotation is identical to $\tilde{A}_{\parallel}$. After the step rotation, the splitting becomes larger because the splitting is contains a contribution from $\tilde{A}_{\perp}$ which is larger than $\tilde{A}_{\parallel}$ for the cholestane spin probe. Combining equations (3) and (7) gives the hyperfine splitting $\bar{a}(t)$ as

$$\bar{a}(t) = \left\{\tilde{A}_{\perp}^{\,2} - \frac{\tilde{A}_{\perp}^{\,2} - \tilde{A}_{\parallel}^{\,2}}{\frac{\tilde{A}_{\parallel}^{\,2} - \bar{a}(0)^2}{\bar{a}(0)^2 - \tilde{A}_{\perp}^{\,2}} \cdot \exp\left(-\frac{2t}{\tau}\right) + 1}\right\}^{1/2} \tag{8}$$

in which $\bar{a}(0)$ is the hyperfine splitting when t=0 namely $\bar{a}(\theta_0)$. Thus, the field-induced relaxation time τ can be calculated from the measured time dependence of the hyperfine splitting $\bar{a}(t)$ using known values of $\tilde{A}_{\parallel}$, $\tilde{A}_{\perp}$, $\bar{a}(0)$ and a non-linear least squares fit where the function

$$\sum_t \left[(\bar{a}(t))_{\text{experiment}} - (\bar{a}(t))_{\text{theory}}\right]^2$$

is minimised.

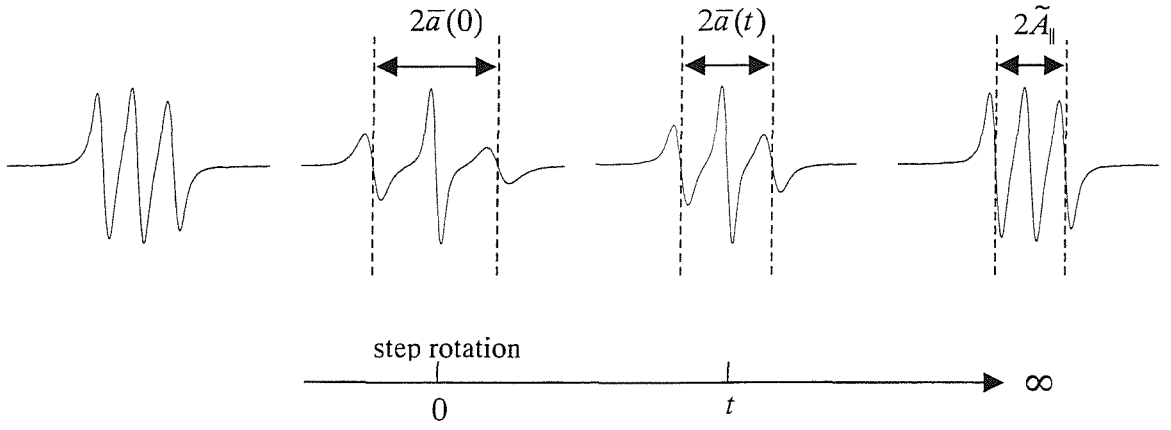

Fig.4 The ESR spectrum of a cholestane nitroxide dissolved in a nematic liquid crystal and its time dependence measured after a step rotation

2.4 Experimental

2.4.1 Sample Preparation

The nematogens used were 4-pentyl 4'-cyanobiphenyl (5CB), pentyl cyanophenylcyclohexane (PCH5) and ZLI-4792 (Merck). ZLI-4792 is a mixture of fluorinated compounds. This will be used as the base liquid crystal when we examine the effect of dopants in Chapter 3. The reason why we used this mixture is that it is one of the standard liquid crystals for TFT-LCD and has a wide nematic range (from -40°C to 92°C [6]) and positive $\Delta\tilde{\chi}$ which is necessary to align the nematic director parallel to the applied magnetic field [7]. More details of this mixture will be given in Chapter 3. Its relatively high nematic-isotropic transition temperature allows measurement to be made at a relatively low reduced temperature, where the orientational order is high. Consequently the ESR spectrum exhibits a strong dependence on the orientation of the director. This mixture has a relatively large biphasic region and we shall discuss this further in the next section. γ_1 values for 5CB and PCH5 were already measured by the rotating field method [8, 9] and their $\Delta\tilde{\chi}$ values are also known [7] which is necessary to obtain γ_1

values from this work. The paramagnetic solute (spin probe) added to the sample mixtures in this experiment was approximately 1×10^{-2}wt% of 4,4'-dimethylspiro(5-α-cholestane-3,2'oxazolidin)-3'-yloxy (cholestane) or 2,2,6,6-tetramethyl-4piperidone-N-oxide (tempone). Fig.5 shows the chemical structures of the nematogens and the nitroxide spin probes. Because the chemical structures of these two spin probes are different, their orientational order parameters should be different but their ability to give the director orientation is the same. Cholestane is more rod-like and is well-ordered by the nematic host [10] in comparison with tempone. We shall discuss the effect of the chemical structure on the rotational viscosity coefficient later in this Chapter. All of the compounds were purchased and were used without further purification.

The preparation of an ESR sample was carried out in the following manner. First, 2mg of a spin probe was dissolved in 20g of dichloromethane (the concentration of this solution was about 1×10^{-2}wt% or 1×10^{-4}M). Next, the same amount of sample mixture and the spin probe solution were mixed together and the volatile solvent was removed by evaporation. The ESR sample can also be made in another way, i.e. the spin probe solution was put in the tube first and the nematogen was added to it, and the solvent was then removed. However, this method needs the sample to be heated in order to dissolve the spin probe in the nematic which may result in the decomposition of the spin probe. The amount of sample materials required in a tube was about 5mm in height. It was then degassed by a repeated freeze-thaw cycle in order to avoid line broadening caused by dissolved oxygen before being sealed under vacuum. As we shall see, tubes with different internal diameters namely 2,4 and 7mm were used to examine the dependence of the result on the sample tube diameter, i.e. the role of the surface effects.

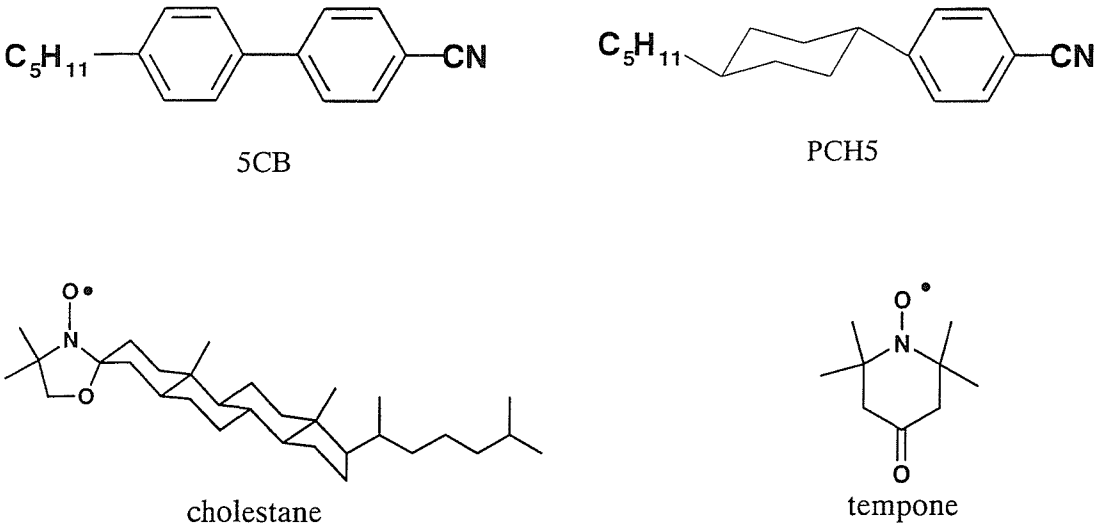

Fig.5 The chemical structures of the nematogens and the spin probes

2.4.2 Nematic-Isotropic Transition Temperature

The nematic-isotropic transition temperature of the ESR samples was determined directly from the temperature dependence of the ESR spectra. When a nematogenic sample is cooled from its isotropic phase, the line shape of the ESR spectrum of a spin probe in this host changes from just three lines to more than three lines which indicates that the sample is biphasic with both isotropic and nematic phase coexisting (we shall refer to this temperature as T_I – the point at which the nematic component first appears). On cooling further, this biphasic spectrum changes to a monophasic spectrum containing just three lines which corresponds to that of the nematic phase (we shall refer to this temperature as T_N). For example, T_I and T_N for ZLI-4792 are 98.3°C and 92.2°C, respectively. The difference is about 6°C and the coexistence of isotropic phase and nematic phase was actually observed by a microscope over this temperature range. This relatively wide biphasic region may be because this mixture consists of two ring compounds and three ring compounds and they tend to separate from each other in the nematic phase. In this Chapter, T_N was used as the nematic-isotropic transition temperature because the

temperature dependence of the order parameter is significant only below T_N. Above this temperature the orientational order is more or less constant until T_I when it vanishes. With regard to the temperature control, the heater jacket which surrounds the sample tube and the digital temperature controller were used to set the temperature. The temperature calibration was carried out before the measurement using a thermocouple placed in a glass tube which is the same as the sample tube. It was placed in the spectrometer at exactly the same position as the samples and the temperature was monitored using a digital multimeter. The calibration line from 25°C to 100°C was almost perfectly linear with an offset value. The stability of the measured temperature was within ±0.1°C over 2.5 hours which is the standard time for one experiment. The temperature gradient over the sample is estimated to be 0.3°C because of the biphasic region of 5CB in the experiment (T_I and T_N were 35.0°C and 34.7°C, respectively). However, because the presence of the spin probe might also contribute the biphasic region, the temperature gradient may be less.

2.4.3 The Rotation-relaxation Experiment using ESR Spectroscopy

The block diagram of the apparatus is shown in Fig.6. The sample in a tube made of glass was inserted into the microwave cavity (rectangular TE_{102}) of the ESR spectrometer (Bruker ECS 106). The axis of the sample tube was perpendicular to the static magnetic field. The magnetic field produced by the electromagnet is in the region of 3000G (0.3T) that is needed to record the spectrum of a nitroxide. The klystron is a microwave source and the power of the microwaves generated was precisely controlled by the attenuator 1. The circulator allows the microwaves to pass in a certain direction as indicated in the block diagram. Via the circulator the reflected microwaves are detected by the diode detector which converts the microwave power to an electric current. To measure the signal intensity quantitatively, we used the reference arm which supplies the detector with a bias microwave power. A technique known as phase sensitive detection is used in this ESR spectrometer to enhance the sensitivity of the spectrometer. This can eliminate noise

and interference. To do this, the strength of the magnetic field was varied at the modulation frequency and the microwaves reflected from the cavity are amplitude modulated at the same frequency. Modulation amplitude also influences the signal intensity. Then the phase sensitive detector filters any signals which do not have the same frequency and phase as the field modulation. For a further improvement of the sensitivity, a time constant, which slows down the response time of the spectrometer, is used to filter out more of the noise.

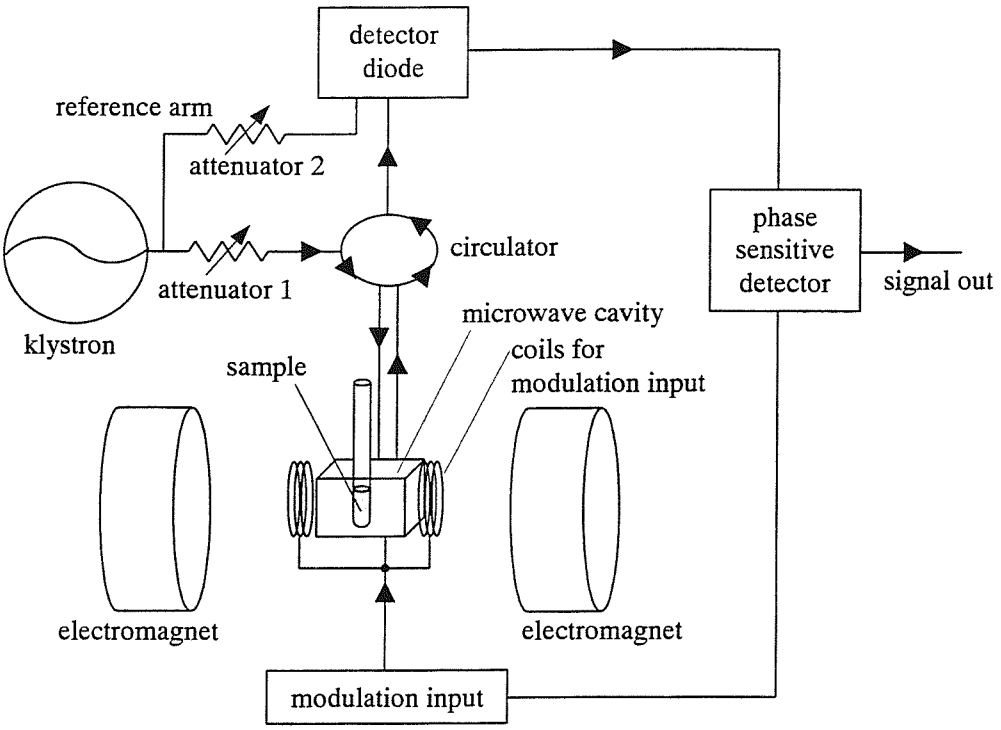

Fig.6 The block diagram of the ESR spectrometer used in the step rotation-relaxation experiment

A schematic view of the sample part of the apparatus is shown in Fig.7. The rotary solenoid (Radio Spares; rotation angle 45°) was used to rotate the sample tube and this was powered independently of the spectrometer although the power supply was controlled via the computer of the spectrometer. It can rotate the sample either when a step voltage is

applied or when it is removed and the spring turns the solenoid back elastically. The time taken for the sample tube to be rotated is estimated to be approximately 10ms [11]. The solenoid was mounted on an aluminium rig attached to the microwave cavity and the drive shaft was connected to the sample tube via a flexible coupler. The procedures of a typical measurement are as follows. First, without rotation, the centre of the magnetic field (3340~3480G or 0.334~0.348T) and the receiver gain were adjusted to obtain a strong three line (field-sweep) spectrum of the spin probe in the centre of the field. The overall width of the field was 70G (7mT) for the cholestane spin probe (50G (5mT) for tempone). Then the time dependence of the ESR signal (time-sweep) was obtained at a fixed magnetic field following step rotation of the sample. The sample started to rotate 0.3s after the start of the signal acquisition and this timing was controlled by the computer of the spectrometer. In this experiment, the time resolution was set by the use of 1024 data points (the time between points, the conversion time, is 5.12ms). The maximum resolution is 0.32ms between data points but because the ESR signal is averaged in this short period, the S/N ratio is much worse than for 5.12ms. In this time-sweep acquisition, the axis of the sample tube was precisely adjusted to be vertical in order not to obtain a spike in the time-sweeps at the time of the step rotation. This may come from the mis-tuning of the microwave cavity due to the sudden change of the sample geometry within it. The time-sweeps generated at each value of the magnetic field were measured with steps of 0.2G (0.02mT) for cholestane and 0.1G (0.01mT) for tempone. Since the linewidths for tempone are smaller than that for cholestane, a smaller step was used for tempone. Typical measurement conditions are shown in Table 1. Fig.8 shows examples of the time-sweep acquisition for cholestane dissolved in ZLI-4792 contained in a 4mm tube. The arrows in Fig.8 (a), (b) and (c) indicate the moment at which the sample was rotated. The magnetic field strengths which correspond to each of the time-sweep acquisitions are indicated in the field-sweep spectrum shown below.

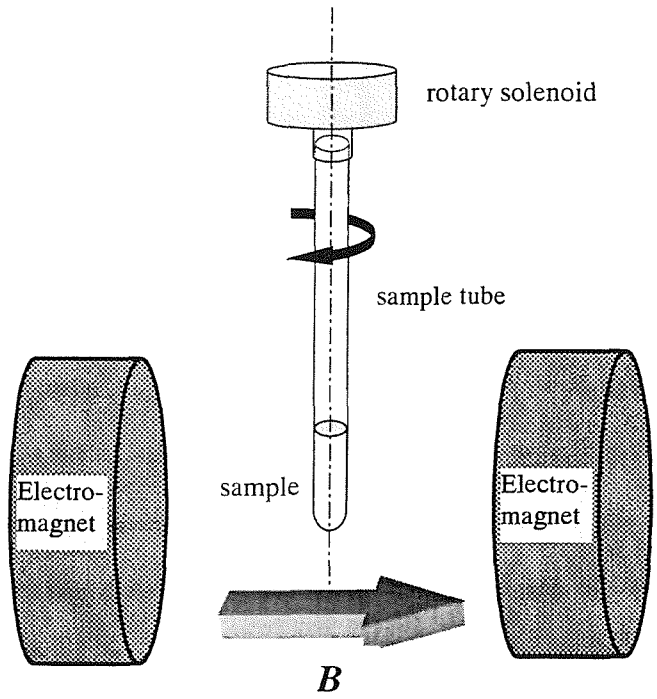

Fig.7 View of the sample part of the apparatus

Table1 Typical experimental conditions used in the time-sweep acquisition

parameters	Spin probes	
	cholestane	tempone
Rotation angle / °	45±0.1	45±0.1
Modulation amplitude / G	1.00	0.50
Modulation frequency / kHz	100	100
Sweep width / G	70	50
Point interval / G	0.2	0.1
Receiver gain	4×10^2	4×10^2
Time constant / ms	1.28	1.28
Conversion time / ms	5.12	5.12
Number of data points acquired	1024	1024
Sweep time / s	5.243	5.243

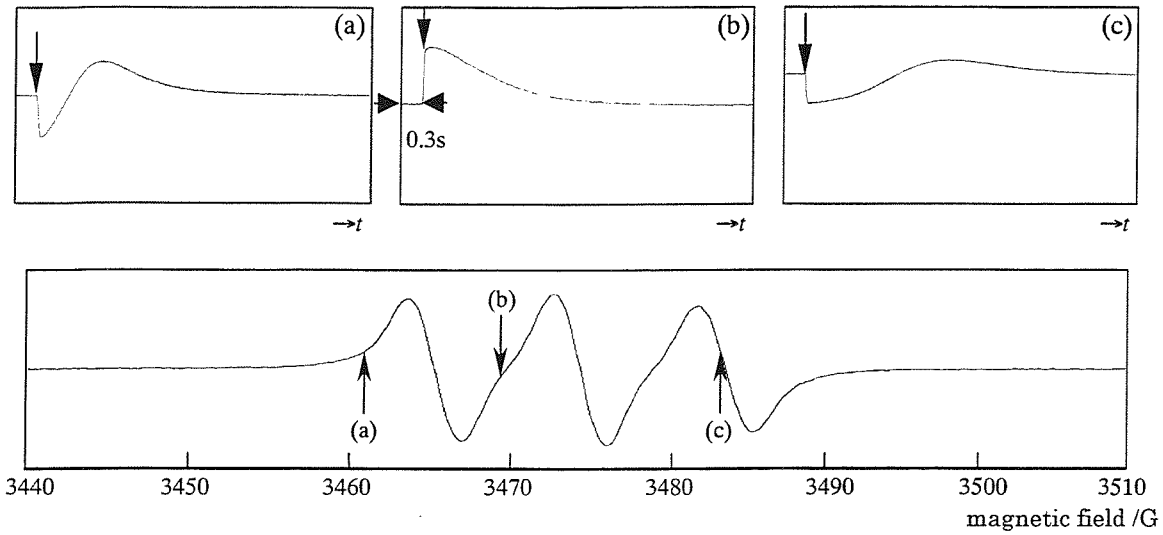

Fig.8 Time-sweep acquisition for cholestane dissolved in ZLI-4792 at room temperature in a 4mm tube and the corresponding field-sweep spectrum at different static fields. The magnetic field strengths shown are (a)3460.9G, (b)3469.4G, (c)3483.1G.

2.5 Analysis of Results

The time-domain spectra were arranged to make a single two-dimensional stack plot where one axis is the time axis and the other axis is the magnetic field. This process was carried out by using the spectrometer analysis software package WIN-EPR. Fig.9 shows this two-dimensional stack plot of time-domain spectra for the cholestane spin probe in ZLI-4792 using a 4mm tube. Here the points are connected to show the field sweeps and so to indicate the variation in the spectra with time. As Fig.9 shows, the lineshape before the rotation, which corresponds to the first three slices at the front of the stack plot, changed sharply immediately after the step rotation (for approximately 70ms). The spectrum then gradually relaxes back towards the initial lineshape during the acquisition time.

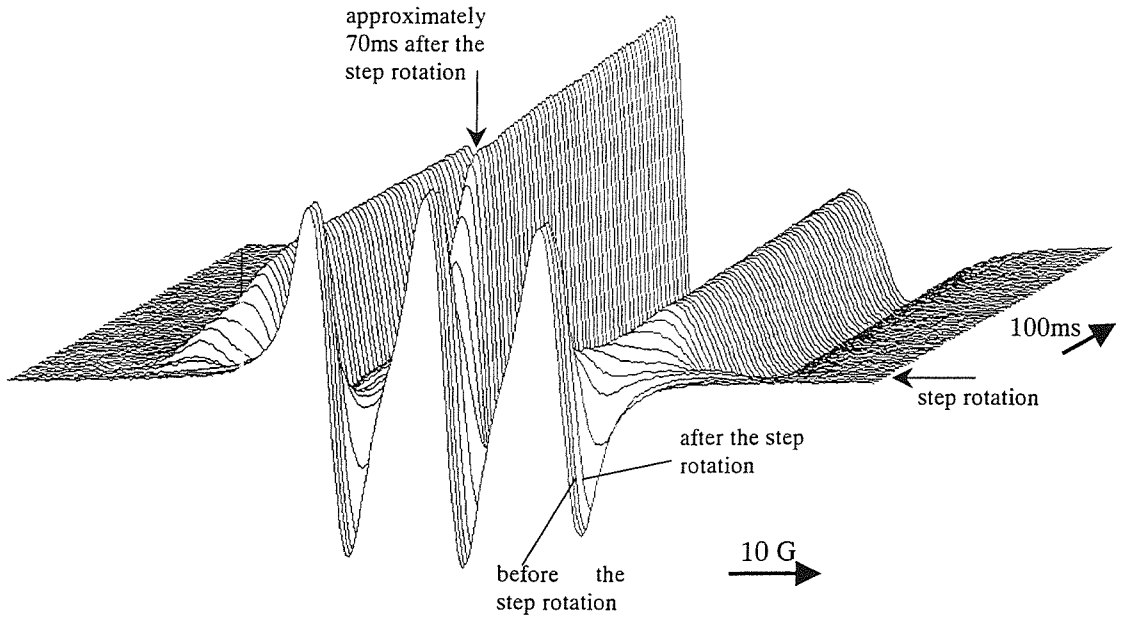

Fig.9 The stack plot of time-sweeps for cholestane in ZLI-4792

In this experiment, 1024 time-sliced spectra were obtained (the time between spectra is 5.12ms). Fig.10 shows examples of the time-sliced spectra taken from the stack plot. In Fig.10 we can see how the spectrum changes; following the powder-like spectrum at 25.60ms it becomes that for a monodomain with just three lines at 66.56ms, then the hyperfine splitting starts to decrease until 4.9s where it takes the same form as the initial spectrum, showing that the director has returned to being parallel to the magnetic field.

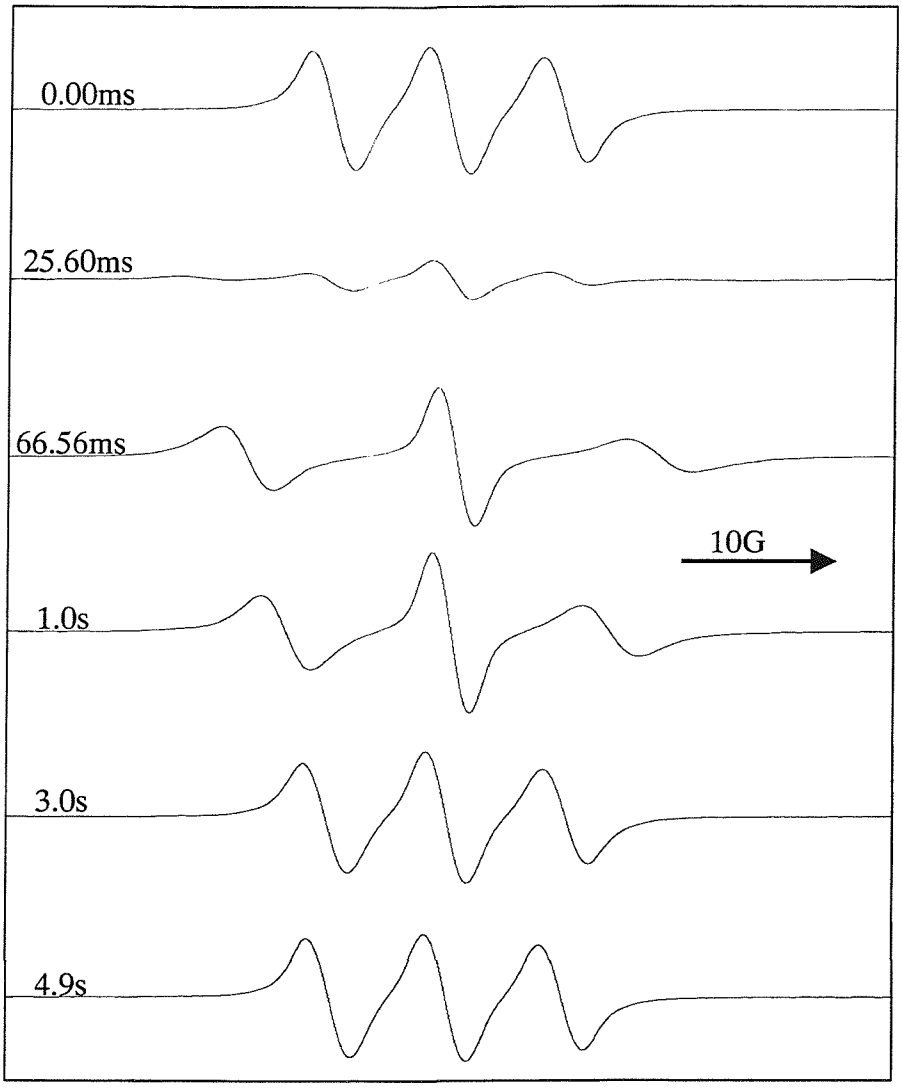

Fig.10 Examples of the time-sliced spectra for cholestane in ZLI-4792

These reconstructed spectra gave the time dependence of the hyperfine splitting. The plot of the time-dependent hyperfine splitting could be fitted to equation (8) by varying the relaxation time τ. However, the time-dependent $\tan\theta_t$ was first fitted to equation (7) because $\tan\theta_t$ is predicted to exhibit a single exponential decay and the fitting process is easy. Fig.11 shows an example of the fit of $\tan\theta_t$ to the data. Although the fit looks good in the shorter time range before 2s, the difference between the theoretical curve and the experimental plots became large after about 2s. This is because the errors in $\tan\theta_t$ are not constant. To solve this problem, a non-linear least squares fit to equation (8) by varying

the relaxation time τ can be used because the errors in the hyperfine splitting are constant. Here, because the time-sweeps were measured at steps of 0.2G, the errors in measuring the hyperfine splitting are within 0.2G. This fit was carried out using a Mathcad program and the function

$$\sum_t \left[(\bar{a}(t))_{\text{experiment}} - (\bar{a}(t))_{\text{theory}}\right]^2$$

was minimised. This gives the value of τ which fits the curve best and an example of the best fit to the data is shown in Fig.12, the agreement is clearly very good.

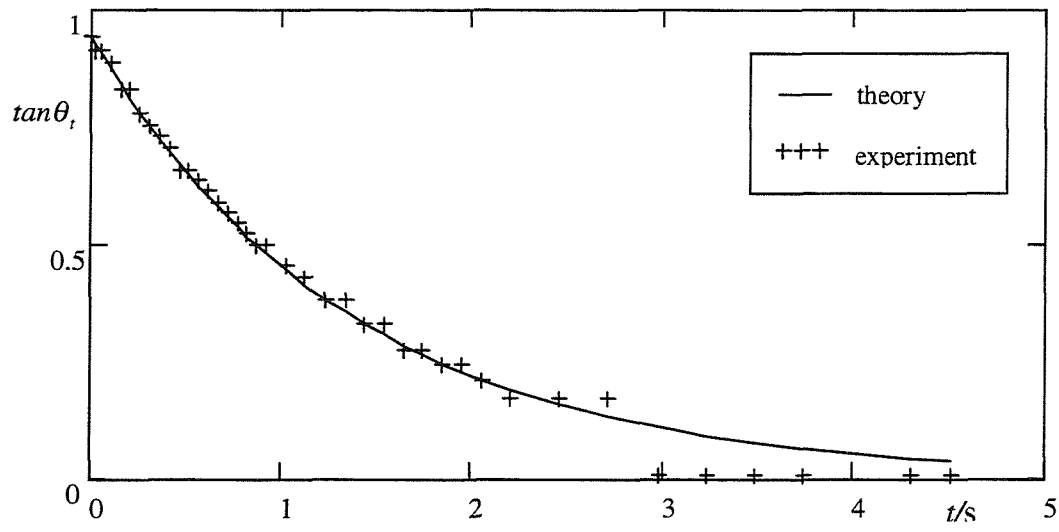

Fig.11 Fitting $\tan\theta_t$ to the theory in equation (7)

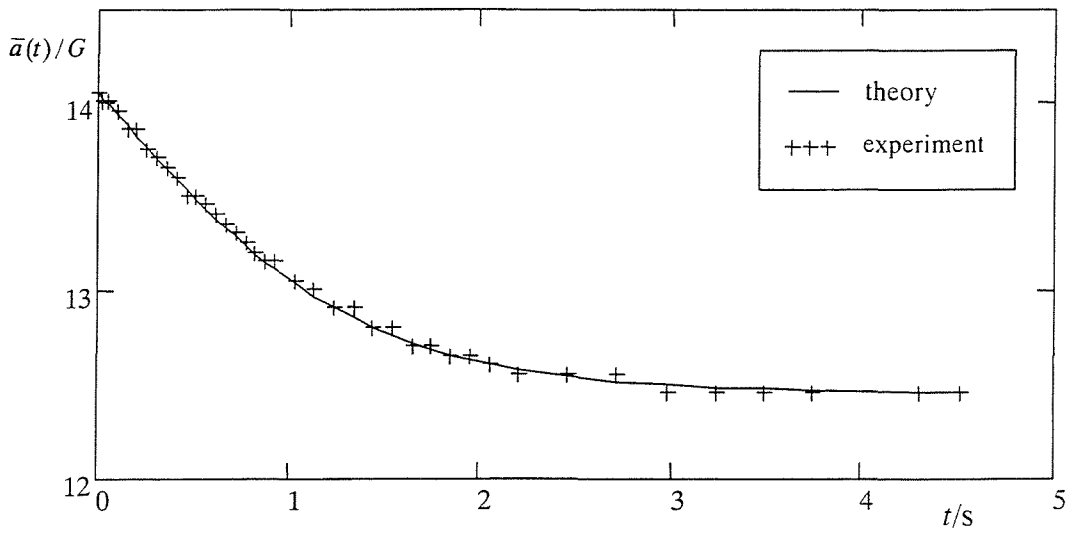

Fig.12 Fitting the hyperfine spacing to the theory in equation (8)

The time origin was identified with that when the hyperfine splitting has its largest value. In the curve fitting process, the values of $\tilde{A}_{\parallel}$, $\tilde{A}_{\perp}$ and $\bar{a}(0)$ in equation (8) should be known and these values were determined in the following way. $\tilde{A}_{\parallel}$ is the value of the hyperfine splitting before the rotation, while $\tilde{A}_{\perp}$ is given by [5]:

$$\tilde{A}_{\perp} = \frac{1}{2}\left(3a_{\text{iso}} - \tilde{A}_{\parallel}\right) \tag{9}$$

in which a_{iso} is the hyperfine splitting for cholestane in the isotropic phase of the nematogen and was measured for each ESR sample before the time-sweep acquisition. Although a_{iso} has a small temperature dependence as shown in Fig.13, the value for each ESR sample was determined as the hyperfine splitting when $T=T_{\text{I}}$ (from Fig.13 the value is 14.56G).

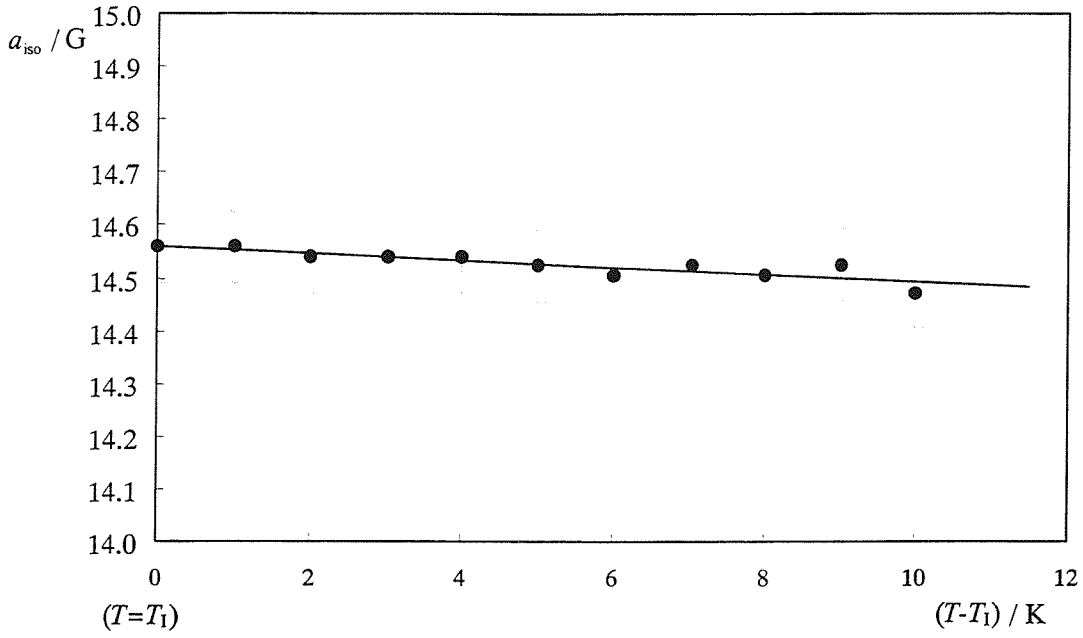

Fig.13 Temperature dependence of a_{iso} for the cholestane spin probe dissolved in ZLI-4792

2.6 Rotational Dynamics of Liquid Crystals

2.6.1 ESR Spectra Immediately after the Step Rotation

We have seen the technique for measuring the field-induced relaxation time using the time-sliced reconstructed spectra. We used the spectra after the nematic has become a monodomain that is when the spectra contain just three anti-symmetric hyperfine lines, normally about 70ms after the step rotation when we use a 4mm sample tube as shown in Fg.10. However, the spectra obtained immediately after the step rotation contain more than three lines or exhibit a powder-like pattern, the spectrum at 25.60ms in Fig.10 for example, this suggests a progressively more randomly distributed director. In other words, the sample is not a monodomain; that is the director adopts a range of orientations. To understand the origin of this distribution, we examined the dependence of the results on the sample tube diameter in this experiment.

When the sample tube is rotated suddenly by 45°, the liquid crystal inside the tube and also the liquid crystals director rotates because the motion of the director should be coupled to that of the tube. However, the extent of this coupling depends on the distance from the surface of the tube. The director which is in the region of the boundary will rotate together with the tube. The motion of the director further from the surface of the tube should, however, depend on both the viscous and elastic coupling between the different regions of the nematic. Because nematogens are expected to have a relatively weak coupling, the director far from the surface of the tube (i.e. close to the middle of the tube) moves slower than that at the interface. Therefore, the director orientation would change from the surface to the middle of the tube, so the director in the tube is non-uniformly distributed. This behaviour will clearly depend on the inner diameter of the tube.

Fig.14 shows the tube diameter dependence of the time-sliced reconstructed spectra immediately after the step rotation. The internal diameter of the tube used was 2mm and 7mm as well as 4mm. Fig.4 shows the clear dependence on the tube diameter. The time taken for the director to be reformed as a monodomain is significantly different for each tube diameter; approximately 41ms for the 2mm tube, 67ms for the 4mm tube and 149ms for the 7mm tube. For the 2mm tube, although no change was observed before about 15ms, a decrease of the intensity of the outer lines were observed at about 20ms which suggests that the director distribution has broadened. At 25.60ms, a powder-like pattern has appeared indicating the director distribution is far from uniform. Then the director reforms as a monodomain with the angle between the director and the field approximately equal to 45° that is the same value as the tube was rotated.

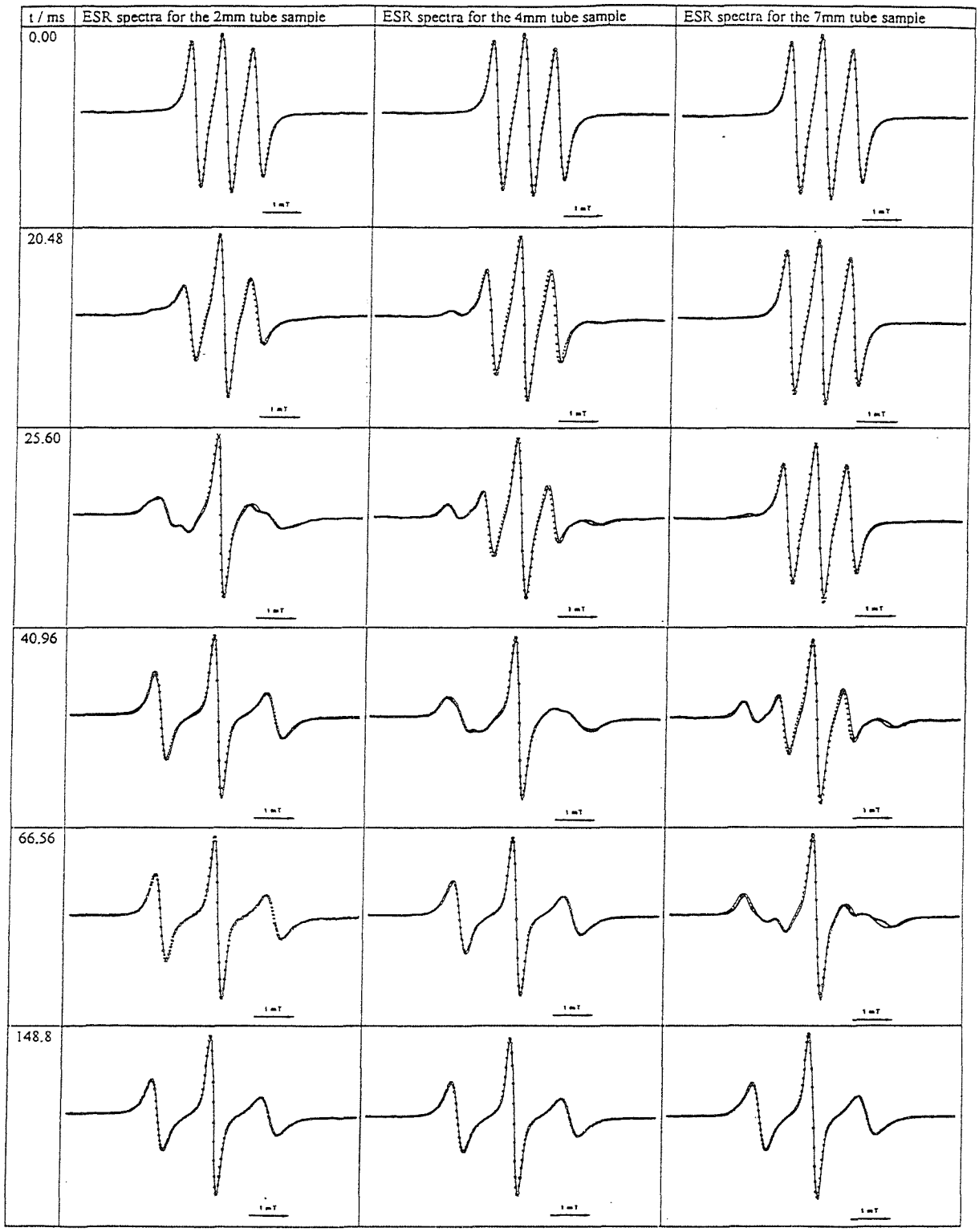

Fig.14 The dependence of the spectra recorded at times immediately after the step rotation of the tube diameter

When we compare the progression with time of the spectra for the 4mm tube with those for the 2mm, a more significant distribution of the director can be clearly observed. The spectrum at about 20ms for the 4mm tube also shows the decrease in the intensity of the outer line but it is less than that for the 2mm tube. However, it becomes a more powder-like pattern than that for the 2mm tube with a new pair of lines in the highest and lowest region of the spectrum at 25.60ms, which indicates that the director in the 4mm tube has become more significantly non-uniform than for the 2mm tube. It then returns to the monodomain spectrum at about 67ms following the slightly powder-like pattern at about 41ms. Finally, the progression of the spectra for the 7mm tube is much more complicated than those for the tubes with smaller internal diameter. First, the spectrum has not changed at about 20ms. This might suggest that the majority of the director has not rotated although close to the surface of the tube it should have rotated. The spectrum at 25.60ms still looks almost unchanged. Secondly, it has the strongest powder-like pattern at about 41ms and it then takes a relatively long time to become a monodomain sample; this does not occur until about 149ms. Thirdly, the powder-like patterns recorded at about 41ms and 67ms contain new lines which are clearly located in the higher and lower field of the spectra than the outer lines for the monodomain sample at about 149ms. This indicates that the director makes an angle greater than 45° with the magnetic field which is that by which the tube was rotated.

Fig.15 shows that the tube diameter dependence of the time between the rotation of the tube and the rotation of liquid crystal director until the hyperfine splitting value reaches its largest value ($\bar{a}(0)$), in other words, the time for the director to become uniform. Here, the lineshape of the spectrum should be that of a monodomain sample. Fig.16 shows the dependence of the angle between the director and the magnetic field with the hyperfine splitting value $\bar{a}(0)$ on the tube diameter. The angle was calculated using equation (7). The smaller the tube diameter is, the closer the largest angle is to 45°. It may be because the director in the tube of larger diameter is distributed more significantly and when it

becomes a monodomain, it has already started to be pulled back to its initial alignment by the applied magnetic field. Thus, the director distribution of the nematic is smallest in the 2mm tube and so it may be better to use the 2mm tube to measure the relaxation time.

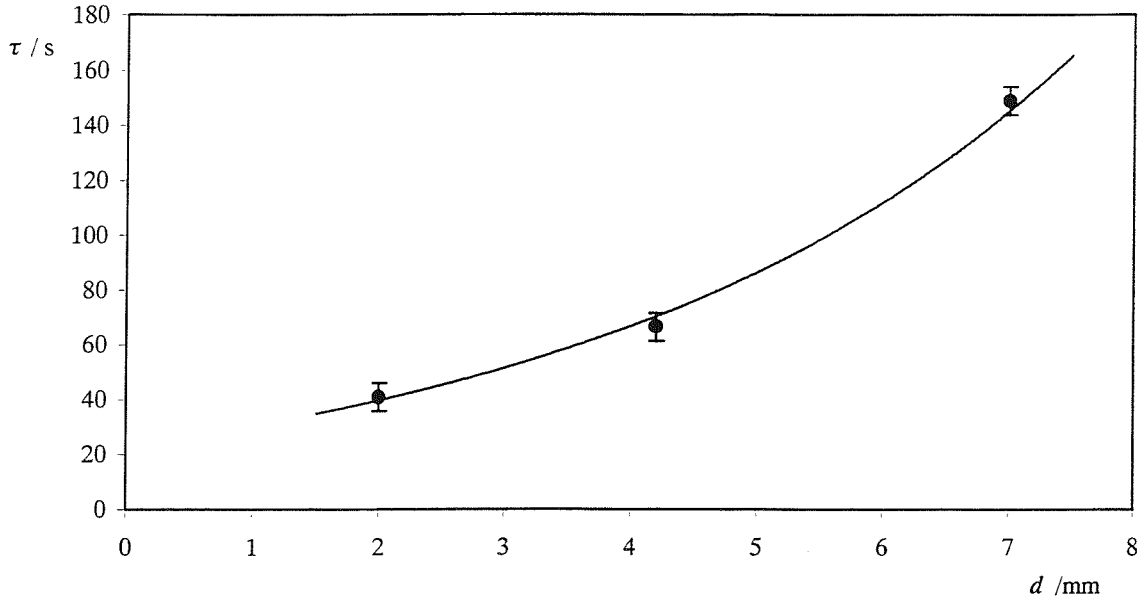

Fig.15 Dependence of the rotation time on the tube diameter, d

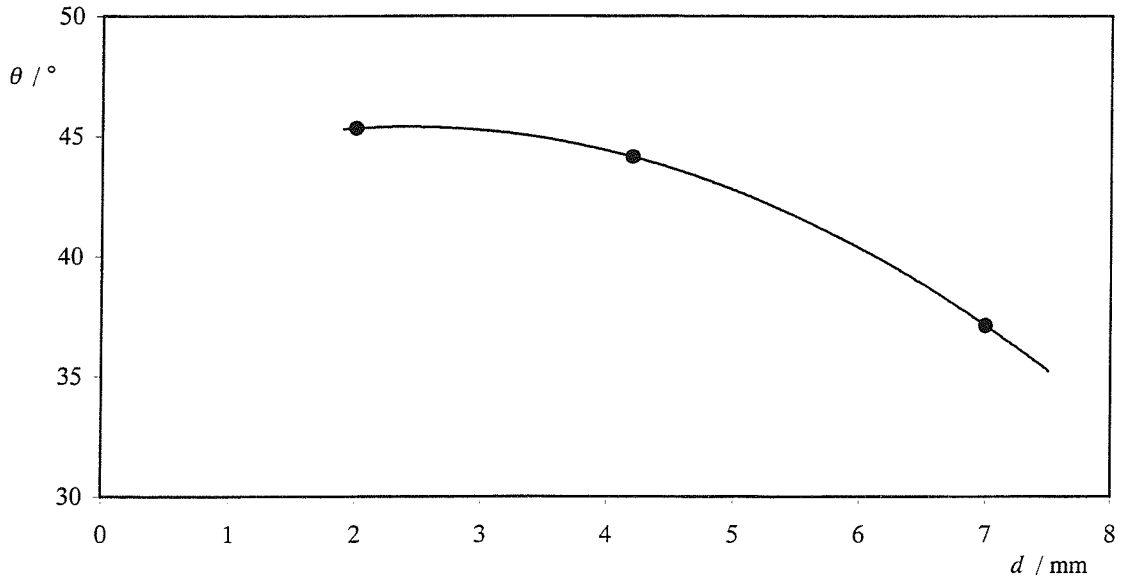

Fig.16 Dependence of the angle between the director and magnetic field on the tube diameter

Fig.17 shows a simple model to account for the tube diameter dependence of the director distribution suggested by the results shown in Figs.15 and 16 as well as shown by the spectra recorded at times immediately after the rotation of the tube (see Fig.14). For the 2mm and 4mm tubes, the angle between the director and the magnetic field is approximately 45° which is the rotation angle of the tube when the director becomes a monodomain. For the 7mm tube, however, the director has already started to relax back to 37° before it becomes uniform. This is because the time taken for the director to become a monodomain after the step rotation is the longest (approximately 150ms) for the 7mm tube.

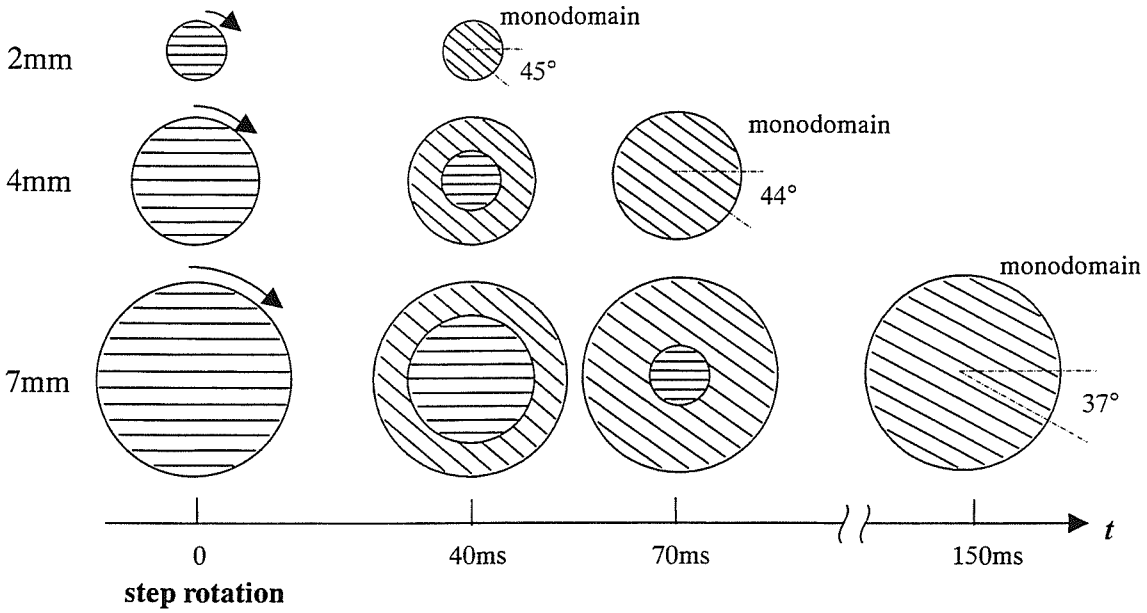

Fig.17 Tube diameter dependence of the director distribution

In this Chapter, we have presented a qualitative analysis of the spectra and obtained some unusual behaviour of the director distribution depending on the tube diameter. For a deeper understanding, a quantitative analysis of the spectra was carried out in collaboration with Drs. C.J.Dunn and D. Ionescu and this is described in the Appendix.

2.7 Results and Discussion

2.7.1 Accuracy of the Measurement of the Relaxation Time

It is important to understand the accuracy of the values for the rotational viscosity coefficient obtained from this method and the factors which control this. Because the field-induced relaxation time is directly measured in this method, the accuracy of the measurement of the relaxation time was examined. The results of five measurements for 5CB using the same sample were 0.386s, 0.391s, 0.396s and 0.389s at 33.3°C. Their average is 0.391s and the standard deviation is 0.004s (the error is ±0.004s). The value of (standard deviation)/(average)×100 is about 1%. This is the statistical error and consistent errors due to any systematic contributions were not taken into consideration. The consistent errors, such as a mechanical error of the spectrometer and an error related to the theory, can be systematically evaluated by the comparison between the values obtained by different experiments or different methods. It will be shown that the difference is small, i.e. the consistent error is small, in the next section. Since this method observes the director orientation using a trace amount of the spin probe added to the nematic sample, the dependence of the relaxation times on the chemical structure of the spin probe should be examined. In this Chapter, two spin probes were used to do this; cholestane which is rod-like and is well-ordered by the nematic host, and tempone which is more or less spherical and so less ordered by the nematic (see Fig.5). The relaxation times determined for ZLI-4792 using tempone and cholestane as spin probes at 25°C were 1.40s and 1.42s, respectively. Although the chemical structures and the orientational order parameters of these two spin probes are quite different, almost no dependence was observed for the relaxation time. Thus, the dependence on the structure of the spin probes is within the experimental error of the method. Here, the reason why τ for ZLI-4792 is larger than that for 5CB is that the ratio $\gamma_1 / \Delta\tilde{\chi}$ for ZLI-4792 is larger than that for 5CB as expected by equation (4). This is partly because $\Delta\tilde{\chi}$ for 5CB at 25°C (approximately 1.1×10^{-7}, see Table 2) is twice as large as that for ZLI-4792 (approximately 5×10^{-8} [7]). Then, the

dependence of the relaxation time on the tube diameter was checked. Because we neglected the surface effect of the tube in the theory of this method, a thicker tube is expected to be appropriate for the measurements. The inner diameters of the tubes used were approximately 2mm, 4mm and 7mm. Fig.18 may show a general trend (τ decreases as the tube diameter increases), this variation is still well within the experimental error of the method. Therefore, it can be said that the dependence of the tube diameter is also within the experimental error of this method. Because smaller director distribution is observed in a 2mm tube as we saw in the previous section and amount of samples required is less for a thinner tube, 2mm tubes were used in all the experiments for measuring τ in this Thesis.

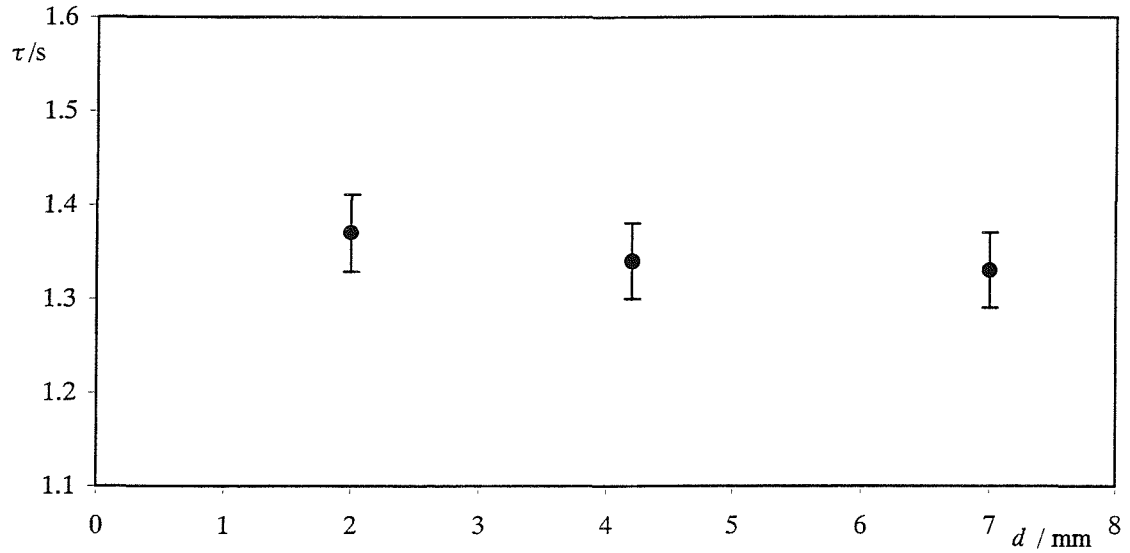

Fig.18 Dependence of the relaxation time τ on the tube diameter

2.7.2 Test of the Methodology for Determining the Rotational Viscosity γ_1

From equation (4), the rotational viscosity is given by:

$$\gamma_1 = \frac{\Delta\tilde{\chi}B^2}{\mu_0}\tau . \qquad (10)$$

For the values of B and μ_0, B =3341G =0.3341T ($JsC^{-1}m^{-2}$) and $\mu_0=4\pi\times10^{-7}Js^2C^{-2}m^{-1}$ were used. In this method, B is taken to be the value of the magnetic field at the centre of the spectrum which is about 70G in width. However, because the variation is only about 1% of the central value, it was ignored. For the test of the methodology, we compared the measured values with the literature values for 5CB and PCH5. The measured values were calculated according to equation (10) using the literature values of $\Delta\tilde{\chi}$ [12,13,14] given in Tables 2 and 3. For 5CB, because the diamagnetic anisotropy was given as the anisotropy of the mass susceptibility, $\Delta\chi^m$ [12], it was multiplied by the density [13]. In addition, $\Delta\tilde{\chi}$ values for both nematics were in the cgs unit system, each value was, therefore, multiplied by 4π in order to change the units to SI [15]. The literature values of γ_1 had been determined by the rotating-field method where the torque is measured directly [8,9]. The error in this method is estimated to be approximately 1.5% [9]. As the comparison in Fig.19 shows, the values measured by ESR spectroscopy are in a good agreement with the literature values.

Table 2 Literature values for the diamagnetic anisotropy for 5CB

$(T_{NI}-T)$ / K	unit system	1.7	4.2	11.9
$\Delta\chi^m$ / $10^{-11}m^3kg^{-1}$ [12]	cgs	8.90	9.60	11.0
ρ / 10^3kgm^{-3} [13]	SI	1.013	1.017	1.023
$\Delta\tilde{\chi}$ / 10^{-8}	cgs	9.02	9.76	11.3
$\Delta\tilde{\chi}\times4\pi$ / 10^{-7}	SI	11.3	12.3	14.2

Table 3 Literature values for the diamagnetic anisotropy for PCH5

$(T_{NI}-T)$ / K	unit system	3.4	7.8	12.5	20.3	29.5	31.1
$\Delta\tilde{\chi}$ / 10^{-8} [14]	cgs	2.85	3.40	3.45	3.72	4.00	4.02
$\Delta\tilde{\chi}\times4\pi$ / 10^{-7}	SI	3.58	4.27	4.33	4.67	5.03	5.05

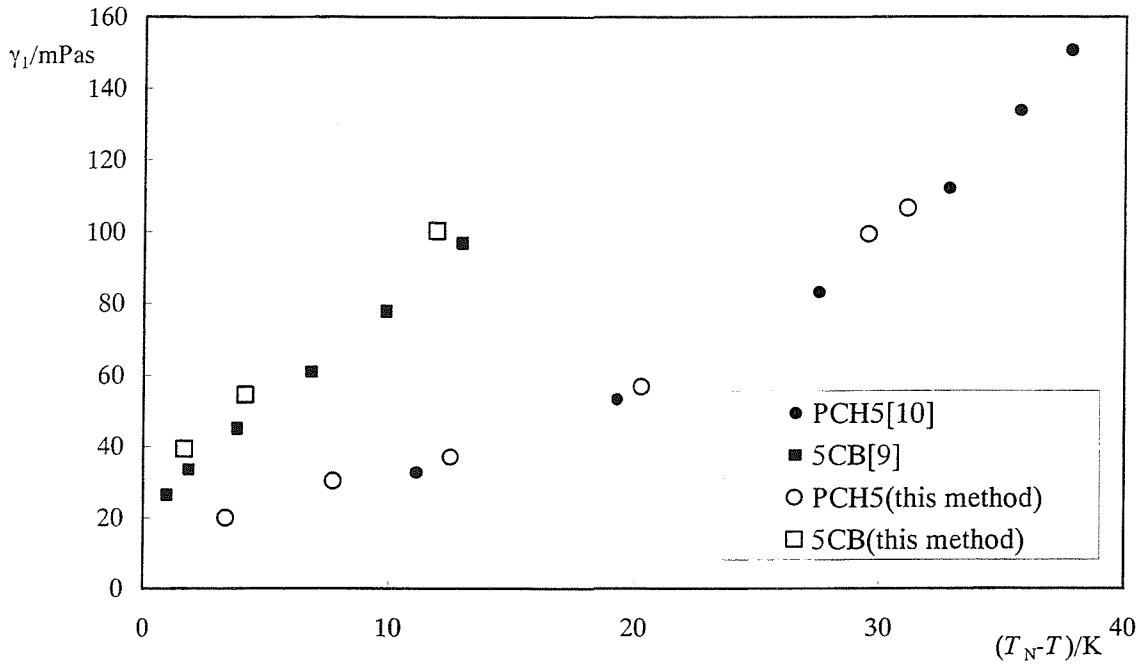

Fig.19 Comparison of the measured values and the values previously reported for PCH5 and 5CB

2.8 Summary

In this Chapter, we have considered the measurement of the field-induced relaxation time using ESR spectroscopy. The relaxation time was obtained from the motion of the director orientation after the step rotation by 45° of the sample tube in a static magnetic field. The rotational viscosity coefficient, γ_1, can be obtained from the relaxation time provided the diamagnetic anisotropy, $\Delta\tilde{\chi}$, is known. The advantage of this method is that we can monitor the orientation of the director of a nematic which is required to be uniform for the theory to be applicable. From this method, we have obtained the following results.

(1) The accuracy of the field-induced relaxation time obtained from the time dependence of the director orientation, monitored by ESR spectroscopy, is about 1%.

(2) γ_1 values for PCH5 and 5CB obtained from the relaxation times together with the $\Delta\tilde{\chi}$ values given in the literature are in good agreement with the literature values of γ_1 where the torque produced on the sample by a rotating magnetic field is measured.

In this experiment, we have observed an unusual behaviour of the nematic director immediately after the step rotation of the sample tube; ESR spectra showed powder-like patterns which indicate that the director is no longer uniformly aligned. This director distribution depends strongly on the diameter of the sample tube. The thicker the tube diameter is, the more the director is distributed. For the thickest tube, we observed a new pair of hyperfine lines in the spectrum which indicates that a part of the director rotates more than the sample tube. We also simulated the ESR spectra and obtained a good agreement with the experimental data. The director then becomes uniform but rotated by about 45° from its original position before it relaxes back to the initial orientation parallel to the field. The time taken for the director to become uniform and the angle between the director and the magnetic field when it becomes uniform depend significantly on the tube diameter. However, there was almost no dependence of the observed relaxation times on the tube diameter.

2.9 References

[1] J.Prost and H.Gasparoux; Phys. Lett., **36A**, 1971, 245.

[2] H.Gasparoux and J.Prost; J. Phys. (Paris), **32**, 1971, 953.

[3] W.H.de Jeu; Physical Properties of Liquid Crystalline Materials, Chapter 7, 1980, Gordon and Breach, London.

[4] E.Ciampi, J.W.Emsley, G.R.Luckhurst, B.A.Timimi, G.Kothe and M.Tittelbach; J. Chem. Phys., **107**, 1997, 5907.

[5] G.R.Luckhurst; Magnetic Resonance Spectroscopy of Liquid Crystals - Non-Amphiphilic Systems, Liquid Crystals and Plastic Crystals Vol.2, Chapter 7, 1974, Ellis Horwood, Chichester.

[6] High resistivity mixtures for active matrix devices, 1st minimum displays Ⅱ, 1990, E. Merck, Darmstadt.

[7] Private communication (Merck Japan).

[8] H.Kneppe, F.Schneider and N.K.Sharma; J. Chem. Phys., **77**, 1982, 3203.

[9] U.Finkenzeller, T.Geelhaar, G.Weber and L.Pohl; Liq. Cryst., **5**, 1989, 313.

[10] G.R.Luckhurst and M.Setaka; Mol. Cryst. Liq. Cyst., **19**, 1972, 179.

[11] C.J.Dunn, D.Ionescu, N.Kunimatsu, G.R.Luckhurst, L.Orian and A.Polimeno; J. Phys. Chem., B, **104**, 2000, 10989.

[12] L. Pohl and U. Finkenzeller; Physical Properties of Liquid Crystals, Liquid Crystals-Application and Uses, Vol.1, Chapter 4, 1990, World Scientific.

[13] D.A.Dunmur and W.H.Miller; J. Phys. (Paris), **40-C3**, 1979, C3-141.

[14] H.D.Schad, G.Baur and G.Meier; J. Chem. Phys., **70**, 1979, 2770.

[15] W.H.de Jeu; Physical Properties of Liquid Crystalline Materials, Chapter 3, 1980, Gordon and Breach, London.

2.10 Appendix (Qualitative Analysis of the ESR Spectra after the Step Rotation)

This work was carried out in collaboration with Drs. C.J.Dunn and D. Ionescu. It is described together with a theoretical analysis in the paper, C.J.Dunn, D.Ionescu, N.Kunimatsu, G.R.Luckhurst, L.Orian and A.Polimeno; J.Phys.Chem., B, **104**, 2000, 10989.

Each of the ESR spectra which we saw in Fig.14 is the sum of spectra from each orientation of the director, and so it contains information on the director distribution. The spectral lineshape is

$$L(B) = \sum_i p_i L(B, B_{r,i}, T_{2,i}^{-1}), \tag{11}$$

where i denotes the orientation of the director with respect to the magnetic field and p_i is the normalised probability that it has this orientation. The lineshape for the spectrum of the spin probe at a particular orientation is denoted by $L(B, B_{r,i}, T_{2,i}^{-1})$ where $B_{r,i}$ gives the three resonance fields for orientation i and $T_{2,i}^{-1}$ is the associated width of the spectral lines. To determine the director distribution, p_i, a model-independent solution was used, for which the discrete probabilities p_i are simply treated as adjustable parameters and the agreement between experiment and simulation is optimised by varying these. We used the NAG Fortran Library Routine E02GAF which minimises the sum of the absolute values of the residuals

$$r(p_i) = \sum_B \left| L^{\exp}(B) - \sum_i p_i L(B, B_{r,i}, T_{2,i}^{-1}) \right|, \tag{12}$$

using a modified simplex method which constrains the p_i to positive values since these are probabilities. To use this, a library of spectra for individual director orientations is required, and we used the experimental spectra for the director immediately following the reformation of the monodomain (see Fig.10) as a part of it. Because the experimental data are for orientations from 0 to 45°, spectra for orientations greater than 45°, which appear in Fig.14, were simulated in the following way. First, we have used a gaussian lineshape

$$L(B, B_{r,i}, T_{2,i}^{-1}) = \left(T_2^3 / \sqrt{2\pi}\right)(B_r - B)\exp\left\{-(T_2^2/2)(B_r - B)^2\right\} \tag{13}$$

since this provides the best description of the observed shape for the spectral lines which are inhomogeneously broadened by unresolved proton hyperfine structure. The widths of

the three nitrogen hyperfine lines vary with the nuclear quantum number m associated with the transition according to

$$T_2^{-1}(m) = A + Bm + Cm^2 . \tag{14}$$

The linewidth coefficients A, B and C also vary with the director orientation and theory [*] gives this variation as, for example,

$$A(\theta) = A_0 + A_2 P_2(\cos\theta) + A_4 P_4(\cos\theta) . \tag{15}$$

The resonance fields, B_r, depend on the principal components of the partially averaged hyperfine tensors and g-tensors according to

$$B_r(\theta) = B_0(\theta) - \frac{h\tilde{K}(\theta)m}{\tilde{g}(\theta)\mu_B} . \tag{16}$$

In this expression the angular variations of the terms are given by

$$B_0(\theta) = \frac{h\nu}{\tilde{g}(\theta)\mu_B}, \tag{17}$$

$$\tilde{g}(\theta)^2 = \tilde{g}_\perp{}^2 + (\tilde{g}_\parallel{}^2 - \tilde{g}_\perp{}^2)\cos^2\theta , \tag{18}$$

$$\tilde{K}(\theta)^2 = \left\{\tilde{A}_\perp{}^2\tilde{g}_\perp{}^2 + \left(\tilde{A}_\parallel{}^2\tilde{g}_\parallel{}^2 - \tilde{A}_\perp{}^2\tilde{g}_\perp{}^2\right)\cos^2\theta\right\}/\tilde{g}(\theta)^2 , \tag{19}$$

where h is the Planck constant, ν is the microwave frequency and μ_B is the electron Bohr magneton. The components of the partially averaged g and hyperfine tensors needed to calculate the positions of the spectral lines for director orientations outside of the range for which spectra are available are listed in table 4, together with the klystron frequency. The parallel components were determined directly from measurements with the director parallel to the magnetic field.

Table 4 The partially averaged magnetic tensors and klystron frequency used to simulate the library spectra in the range 45° to 75°.

$\tilde{A}_{\parallel}$ / mT	$\tilde{A}_{\perp}$ / mT	$\tilde{g}_{\parallel}$	$\tilde{g}_{\perp}$	ν / GHz
0.78	1.78	2.00638	2.00642	9.37802

The angular dependence of the three linewidths for which such measurements are available is shown in Fig.20. It is apparent that the widths of the two outer lines vary markedly with the director orientation whereas that of the central peak does not change. The best fits of equations (14) and (15) to the linewidths are shown as the lines in Fig.20. We can see that the agreement between theory and experiment is not perfect especially for angles close to zero. The widths of the outer lines predicted using the best fit parameters for director orientations beyond 45° appear to be rather small in comparison with those estimated from the experimental powder-like spectra.

In Fig.20, the open symbols indicate the linewidths which were obtained by extrapolating the experimental data in the range 0° to 45° by eye taking into account the widths of the lines in the powder patterns. The linewidths obtained from the results are listed in table 5; they were used to simulate the library of spectra in the range 45° to 75°. The agreement between the simulated and the experimental spectra in the range 0° to 45° was found to be good.

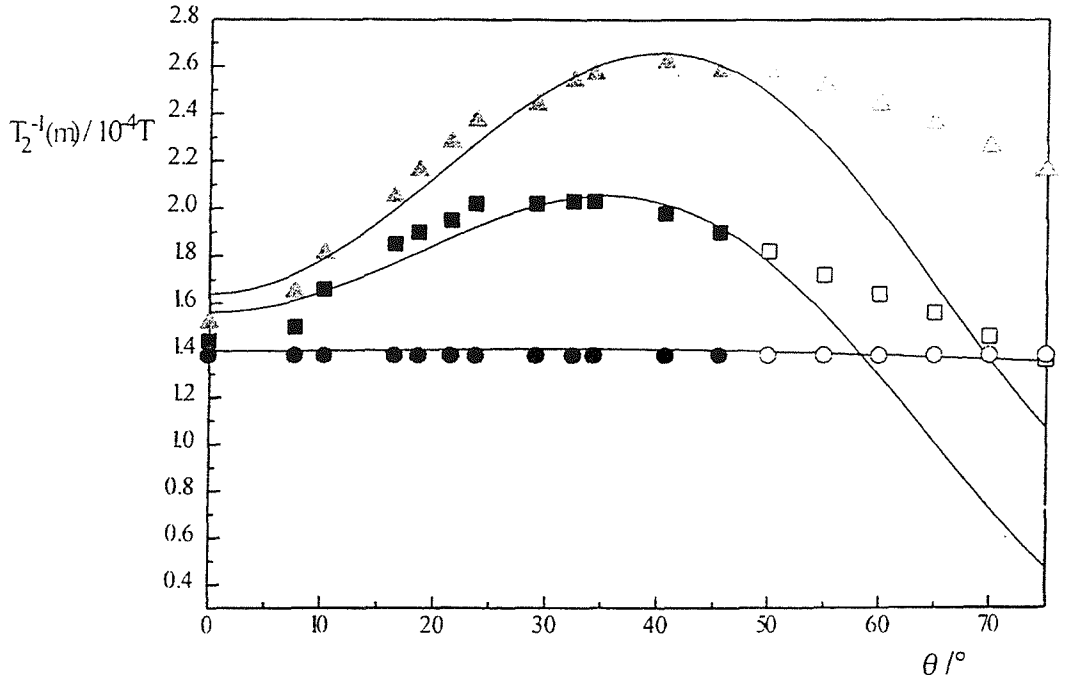

Fig.20 The angular dependence of the widths of the three nitrogen hyperfine lines; m=1(▲) m=0(●) and m=-1(■). The lines are the best fit of the theory and open symbols are the result of extrapolating the experimental data by eye.

Table 5 The angular dependence of the linewidths in the range 45° to 75°

	45°	50°	55°	60°	65°	70°	75°
$T_2^{-1}(1)$ / mT	0.190	0.182	0.172	0.164	0.158	0.146	0.136
$T_2^{-1}(0)$ / mT	0.138	0.138	0.138	0.138	0.138	0.138	0.138
$T_2^{-1}(-1)$ / mT	0.262	0.258	0.252	0.248	0.236	0.226	0.216

The director distribution function can be calculated from the observed powder spectra using the library of spectra for different orientations (both experimental and simulated). We found that the optimum number of director orientations, *i*, is approximately eight by examining the spectra in the library and by trial and error. We distributed the eight

orientations more or less uniformly throughout the range 0° to 75°. In Fig.14, we can see very good agreement between the experimental spectra and the simulated spectra for different tube diameters and different times following the step rotation of the sample tube. The discrete values of the director distribution function obtained in this way are shown in Fig.21 for the three sample tube diameters. For the smallest diameter (2mm), the director is uniformly oriented parallel to the magnetic field, then it moves following the step-rotation of the tube but with a broadening distribution before being refocused after a relatively short period at 45°, the angle through which the tube had been rotated (see Fig.21(a)). Analogous behaviour is observed for the 4mm diameter tube. However the director distribution following the step-rotation of the tube is wider than for the 2mm diameter and moreover, the director orientations are clearly found to extend beyond 45°. Nonetheless at longer times the director is also refocused at 45° (see Fig.21(b)). For the largest diameter (7mm), this unusual behaviour of the director is more outstanding than for the 4mm diameter tube. After the step-rotation, the director is distributed more or less uniformly in the range from 0° to 65° showing that the director orientation has significantly exceeded the rotation angle of the tube. Then with increasing time a peak begins to develop in the distribution function at the rotation angle. However, at the longest time shown in Fig.21(c), the director at 35° is still nearly as strong in intensity as the director at 45°. This is because the director in the largest diameter tube seems to have started to relax back towards its initial orientation before it was refocused at the angle through which the tube had been rotated, since the order-disorder-order process taken for this largest diameter tube is considerably longer than for the smaller diameter tubes.

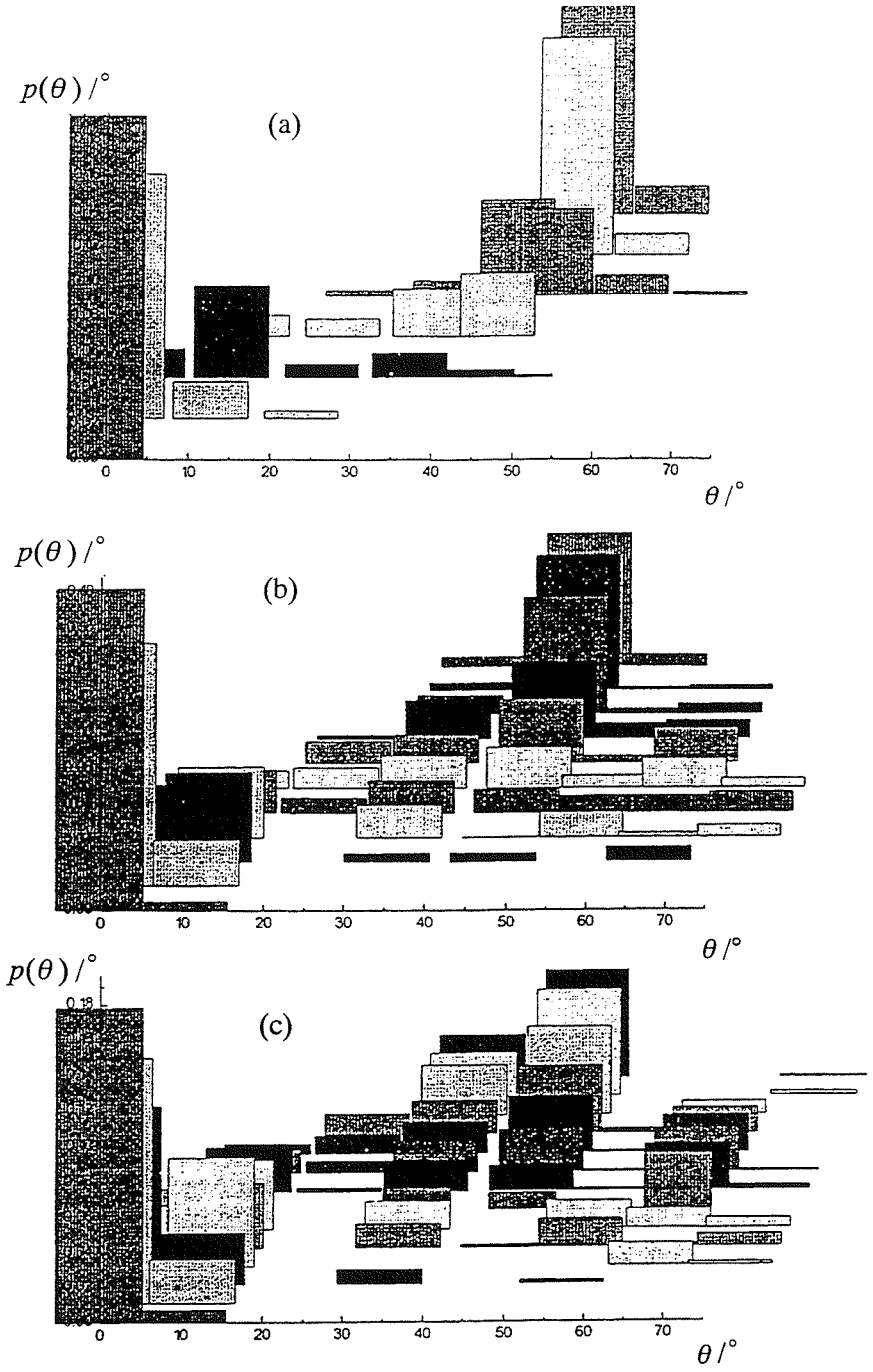

Fig.21 The time dependence of the director distribution function obtained from the model-independent analysis of the ESR spectra following step-rotation of the sample tube for the three different tube diameters (a) 2mm (b) 4mm and (c) 7mm

[*] G.R.Luckhust and A.Sanson; Mol. Phys., **24**, 1972, 1297.

Chapter 3

The Effect of Dopants on the Rotational Viscosity Coefficient for Nematic Liquid Crystals

3.1 Introduction

We have seen in Chapter 1 that the rotational viscosity coefficient, γ_1, is one of the most important properties which controls the response times for LCD. Because response times are proportional to γ_1, we need a small γ_1 to obtain faster response times. This is why to develop liquid crystals with small γ_1 is of importance. Generally, nematic liquid crystals for LCD applications are mixtures which contain many kinds of nematogens. This is because such liquid crystals need to possess desirable properties that is impossible to achieve for a single liquid crystal, such as a high nematic-isotropic transition temperature, T_N (here we will use T_N instead of T_{NI} because the mixture has a biphasic region) together with a low melting point, adequate optical anisotropy, $\Delta\tilde{n}$, and large dielectric anisotropy, $\Delta\tilde{\varepsilon}$. One possible way to develop liquid crystals with small γ_1 is to add a dopant to a base mixture which already has appropriate values for other physical properties and even has a relatively low γ_1. Hence, it is very important to consider the effect of adding dopants to a base liquid crystal mixture as well as which dopants should be used to decrease γ_1 of the base mixture. When we add dopants, we see in many cases a change of T_N provided T_{NI} of the dopants are different from that of the base mixture; this makes the evaluation of the effect of dopants complicated. That is why the effect of dopants should be examined as a function of temperature with appropriate temperature scales, i.e. the absolute temperature scale or the reduced (or shifted) temperature scale. The measurement of the rotational viscosity coefficient, γ_1, using ESR spectroscopy has been investigated in the previous Chapter. We learned that the advantage of this method is

that we can observe whether the director orientation is uniform or not and this allows us to use the approximation of ignoring the elastic term in the torque balance equation. In this Chapter, we will examine the effect of dopants on γ_1 determined by this technique. First, the effect of dopants on T_N will be described. Secondly, the temperature dependence of the field-induced relaxation time will be examined. Next, the temperature dependence of γ_1 will be discussed, this will be carried out by an approximation using the orientational order parameter of the spin probe because we do not obtain the value of the diamagnetic anisotropy, $\Delta\tilde{\chi}$. Then we will discuss the results of the experiment.

3.2 Experimental

3.2.1 The Base Mixture and Dopants

The base mixture chosen was ZLI-4792 (Merck) which was also used in the previous studies described in Chapter 2. Because this is a commercial mixture, chemical structures of its components are unknown. However we believe some of its components are like those shown in Fig.1, where we see that ZLI-4792 consists of mesogenic molecules with two or three rings (phenyl ring or cyclohexane ring) and with polar terminal groups containing fluorine atoms.

In this Chapter 4-pentyl(and pentyloxy) phenylcyclopentenone (5(O)PCP) and 4-pentyl(and pentyloxy) 4'-cyanobiphenyl (5(O)CB) were chosen as examples of the dopants. The reason why these materials were chosen is basically their high $\Delta\tilde{\varepsilon}$ and low γ_1 that can decrease the response times according to equations (33)~(36) in Chapter 1;

(1) two-ring system in the mesogenic core units so that the material has a relatively low viscosity in comparison with three or more-ring systems [1] provided the number of atoms in the flexible group and the type of polar group are the same;

(2) a strong polar group at one end of the molecular structure which gives a higher dipole moment which contributes to the enlargement of $\Delta\tilde{\varepsilon}$ [2];

(3) a conjugated system in the core structures for a high polarisability which also contributes to the enlargement of $\Delta\tilde{\varepsilon}$ [2];

(4) the same length of the terminal group, such as alkyl and alkoxy which is at the other end of the structure because a molecule with a long chain may increase γ_1.

5(O)CB are well-known liquid crystals with two benzene rings in the core structure and with a strongly polar terminal cyano group [3]. 5(O)PCP also have two rings in the core structure, one is benzene but the other is cyclopentenone which possesses the carbonyl group as a polar group [4,5]. Fig.2 shows the chemical structures of the dopants. ZLI-4792 and 5(O)CB were purchased from Merck (Japan) and were used without further purification. 5(O)PCP were synthesised and purified in our laboratory.

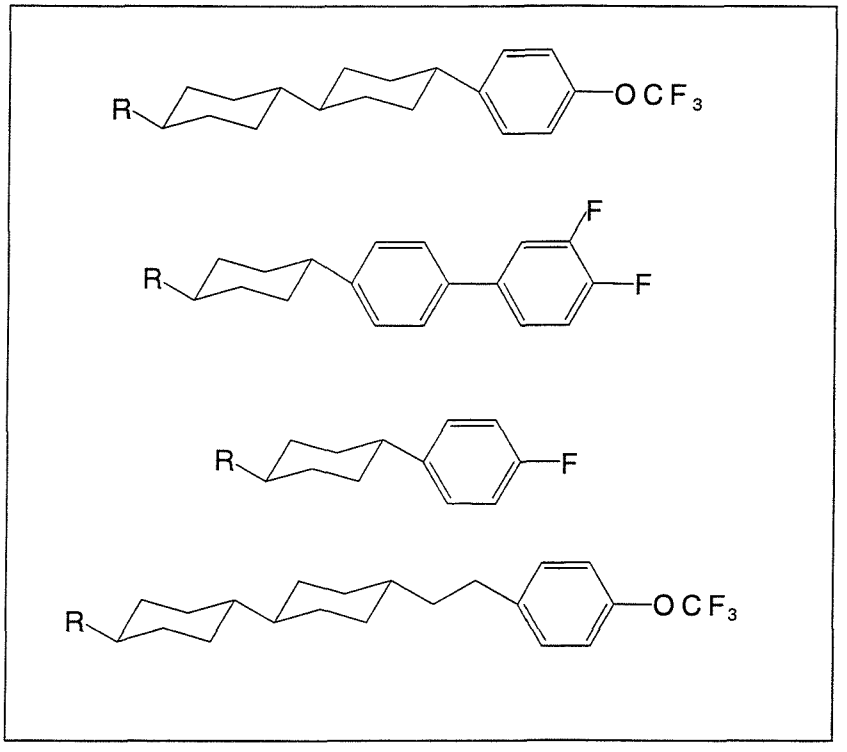

Fig.1 The chemical structures of some of the components of ZLI-4792

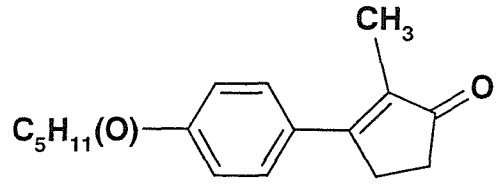

5(O)PCP

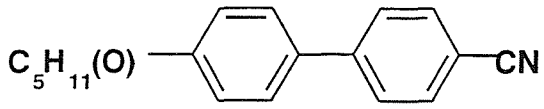

5(O)CB

Fig.2 The chemical structures of the four dopants

Approximately 10wt% of these compounds were added to the base liquid crystal to produce the sample mixtures. The only paramagnetic solute (spin probe) added to the sample mixtures was cholestane, with a concentration of approximately 1×10^{-2}wt%. The ESR samples were prepared in exactly the same way as those described in Chapter 2.

3.3 Results and Discussion

3.3.1 The Effect of Dopants on the Nematic-Isotropic Transition Temperature

First, the nematic-isotropic transition temperature, T_N which is taken to be when the isotropic phase first appears, for all of the ESR samples were measured from the temperature dependence of the ESR spectra. The details about the measurement are described in Chapter 2. Fig.3 shows the effect of the dopants on T_N as a function of the mol% of the dopants. Here, because ZLI-4792 is a mixture, the average molecular weight of 345.3g was used [6]. The lines in Fig.3 are shown simply as guides to the eye. It is obvious that 5(O)PCP decrease T_N of ZLI-4792 significantly while 5(O)CB have a much smaller effect. This is because T_{NI} of 5(O)CB are much higher than 5(O)PCP, in other words, the molecular anisotropy is larger for 5(O)CB than for 5(O)PCP.

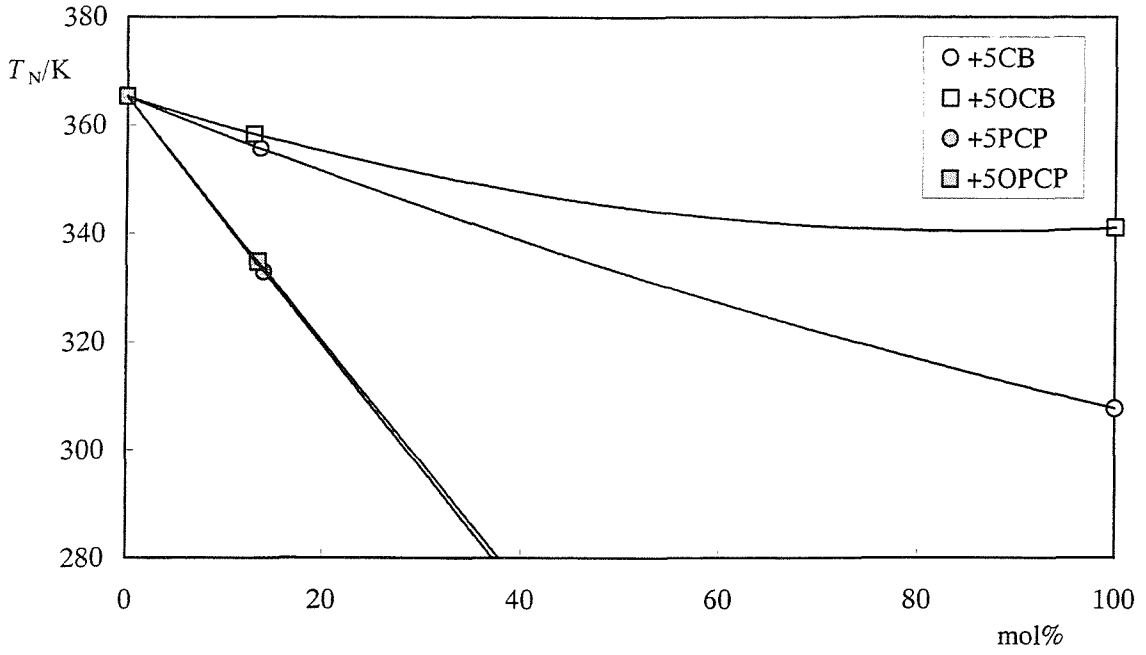

Fig.3 The effect of dopants on T_N

In addition, the pentyloxy compounds decrease T_N less than the pentyl analogues, this reflects the fact that alkoxy compounds generally have higher T_{NI} than those with alkyl chains. For example, T_{NI} for 5OCB and 5CB are 341K(68°C) and 308K(35°C), respectively. From Fig.3, we can see that the dependence of T_N on the mole fraction of 5CB and 5OCB is not linear. Especially, that for 5OCB is very different from a simple straight line. It is well-known that cyano compounds tend to form dimers. It may be difficult to say with such limited experimental data, but it is possible that the dimerization of the cyano compounds is destroyed which would spoil the linear dependence of T_N on the mole fraction. Moreover, the dimerization of 5OCB may be more dominant than that of 5CB.

The effect of dopants on T_I, i.e. when the nematic phase disappears completely, was also measured. Figs.4 and 5 shows this behaviour for 5(O)CB and 5(O)PCP, respectively. Also shown in both figures are T_N, the lines again serve simply as guides to the eye and the area between the two lines corresponds to the biphasic region. In Fig.4, the biphasic

region is larger for 5OCB than for 5CB at the concentration between 0mol% and 100mol%. Similarly in Fig.5, the biphasic region is larger for 5OPCP than for 5PCP.

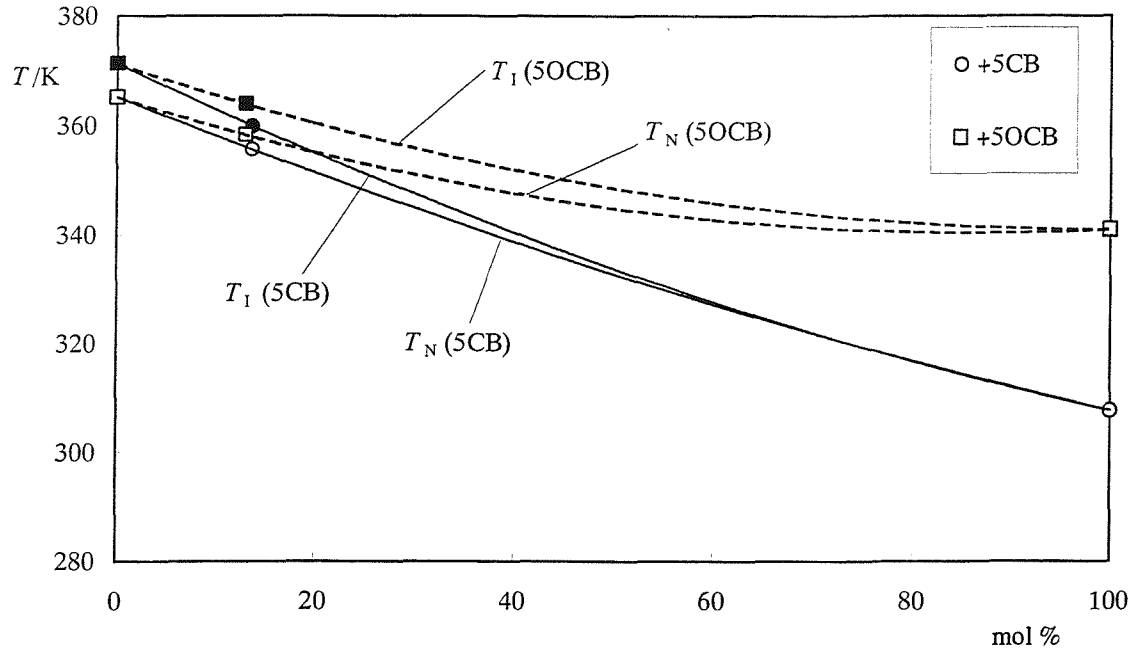

Fig.4 The effect of dopants on T_I and T_N for 5(O)CB dissolved in ZLI-4792

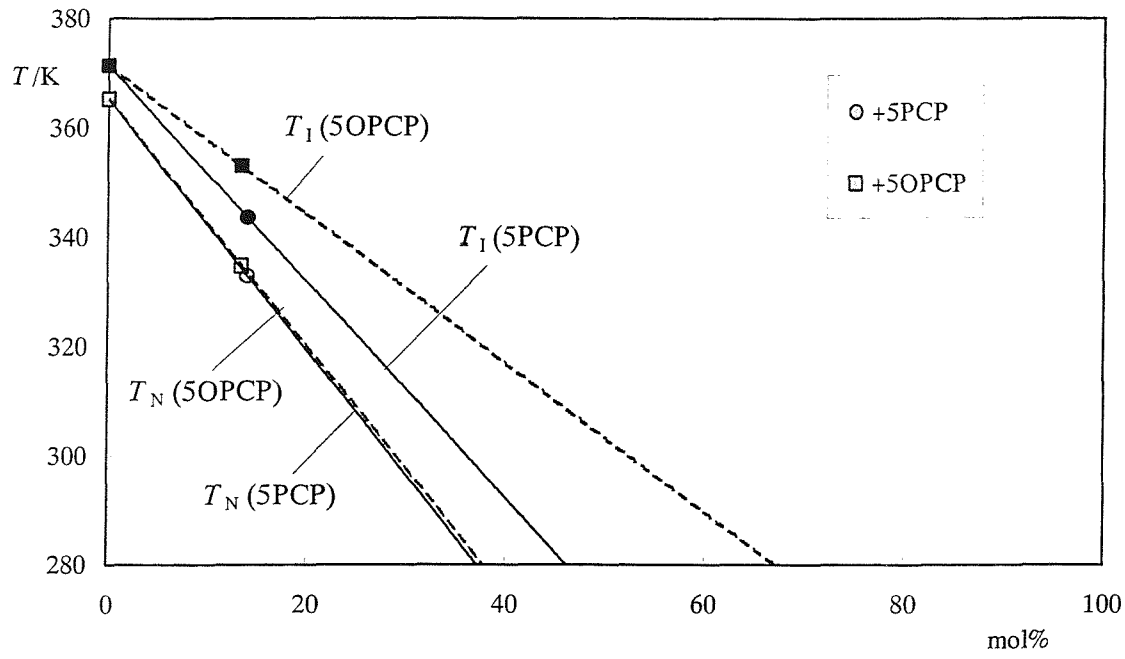

Fig.5 The effect of dopants on T_I and T_N for 5(O)PCP dissolved in ZLI-4792

3.3.2 The Effect of Dopants on the Temperature Dependence of the Relaxation Time

Fig.6 shows the dependence of the relaxation time, τ, on the absolute temperature for the base mixture and with the four dopants. The effect of the dopants is remarkably small on this absolute temperature scale. The line is again just a guide to the eye obtained by an exponential curve fitting for the plots of the base mixture. As Fig.6 shows, the relaxation time varies at lower temperatures more rapidly than at higher temperatures. This behaviour is quite similar to that of the rotational viscosity as expected for an exponential behaviour [7]. Since each sample has different values of T_N, the temperature dependence of the relaxation time for these samples was examined using another temperature scale which takes account of the difference. For the orientational order parameter we expect to use the reduced temperature scale, T/T_N, for different T_N (T_{NI}), it seems reasonable to use the same idea for τ. The observed relationship between the relaxation time, τ, and the reduced temperature is shown in Fig.7. This plot reveals quite clearly the differences between the different dopants. Because there were almost no effect on the absolute

temperature, we can see the effect of T_N on this temperature scale, in other words we can see the effect of the order parameter on this temperature scale.

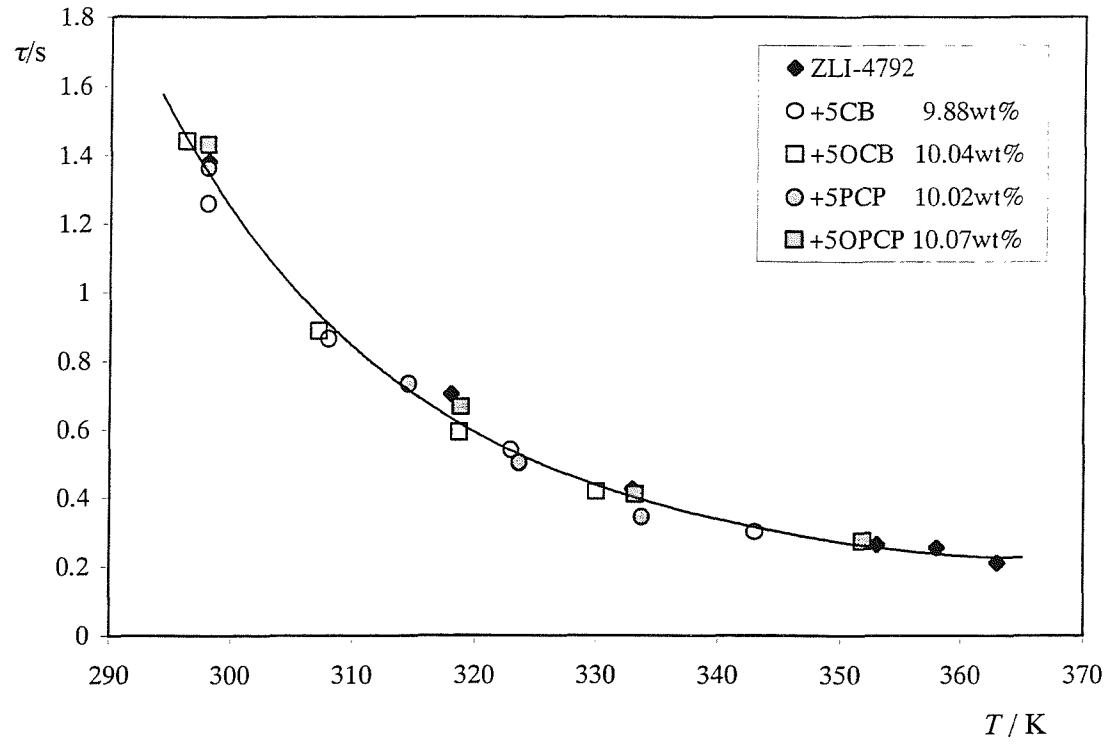

Fig.6 Dependence of the relaxation time for the base mixture with and without the dopants on the absolute temperature

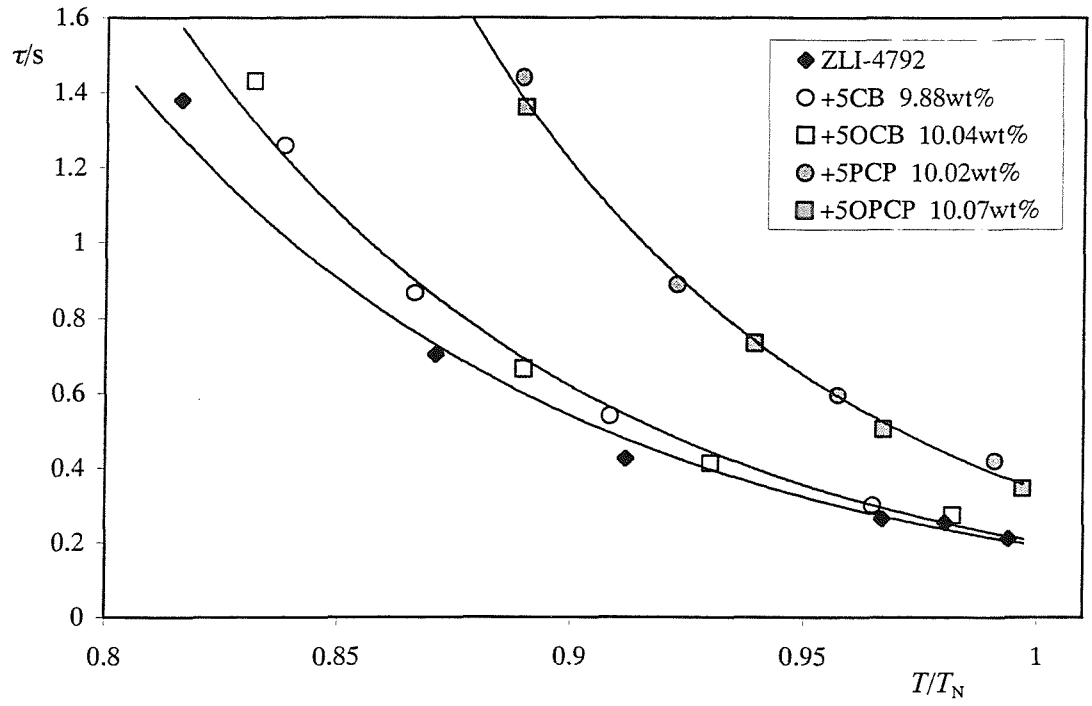

Fig.7 Dependence of the relaxation time for the base mixture with and without the dopants on the reduced temperature, T/T_N

3.3.3 The Effect of Dopants on the Temperature Dependence of the Rotational Viscosity

The rotational viscosity, γ_1, is calculated from the experimental relaxation time

$$\tau = \frac{\mu_0 \gamma_1}{\Delta\tilde{\chi} B^2} \tag{1}$$

together with the value of the anisotropy in the diamagnetic susceptibility, $\Delta\tilde{\chi}$. However, $\Delta\tilde{\chi}$ is not always available experimentally, and so the temperature dependence of γ_1 was examined in another way in this Chapter. From equation (1), we can see that

$$\gamma_1 \propto \tau \Delta\tilde{\chi} \tag{2}$$

and since $\Delta\tilde{\chi}$ is proportional to $\overline{P}_2$ [8], which is the order parameter for a single component mesogen,

$$\gamma_1 \propto \tau\overline{P}_2 . \tag{3}$$

Here we assume that this is also holds, at least approximately, for the multi-component system. Therefore, we can discuss the temperature dependence of γ_1 by taking $\tau\overline{P}_2$ as being equivalent to γ_1. Before showing the temperature dependence of $\tau\overline{P}_2$, we will examine the temperature dependence of $\overline{P}_2$. Although $\overline{P}_2$ determined by this method is the order parameter for the spin probe, and not for the liquid crystal, it is expected to be similar and in any event approximately proportional to each other because the spin probe (cholestane) has a similar molecular anisotropy to the liquid crystal solvent. $\overline{P}_2$ for the cholestane spin probe can be measured from the hyperfine splitting of ESR spectrum according to[9],

$$\overline{P}_2 = 2(a_{\mathrm{iso}} - \tilde{A}_{//}) / A_{33}', \tag{4}$$

where A_{33}' is the major component of the anisotropic nitrogen hyperfine tensor (18.3G for cholestane). Fig.8 shows the dependence of $\overline{P}_2$ on the absolute temperature and Fig.9 shows that on the reduced temperature.

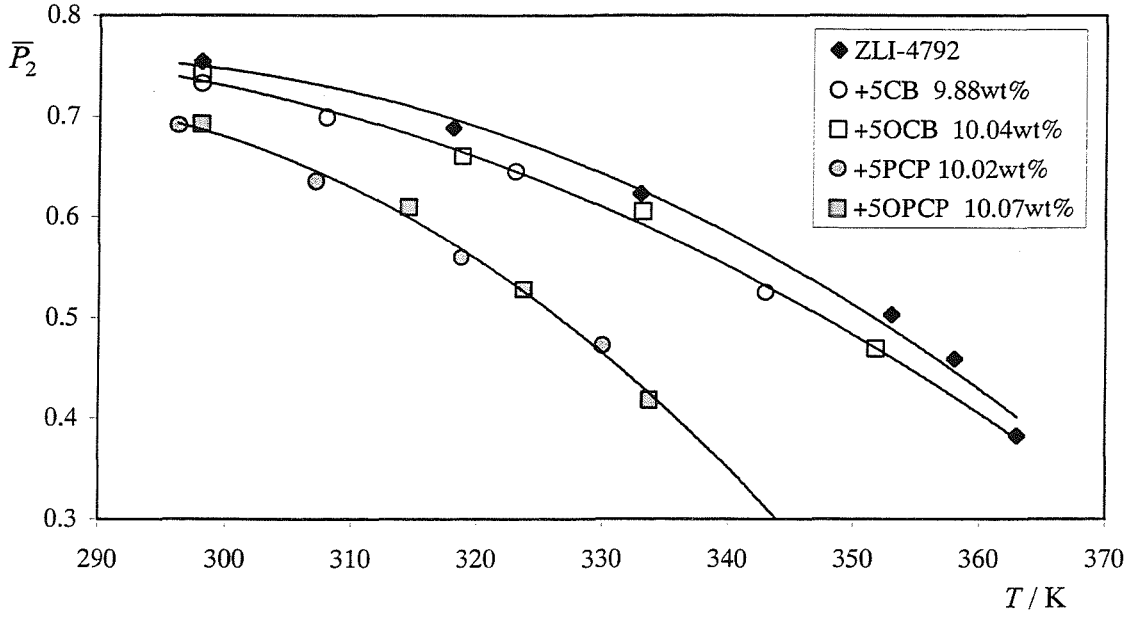

Fig.8 Dependence of the order parameter $\overline{P}_2$ for the cholestane spin probe on the absolute temperature

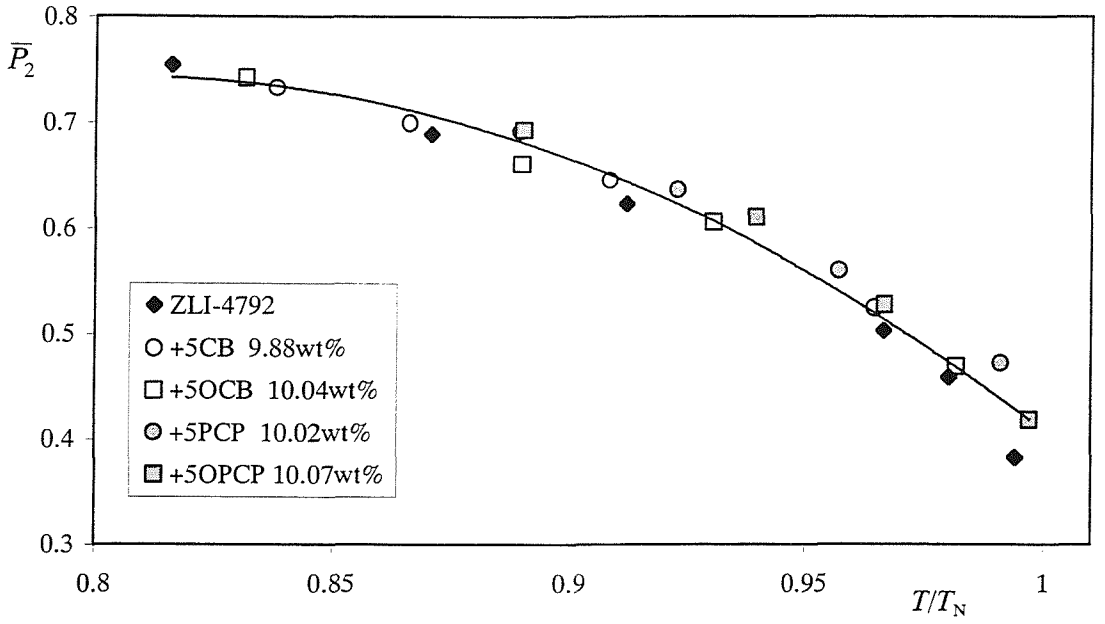

Fig.9 Dependence of the order parameter $\overline{P}_2$ for the cholestane spin probe on the reduced temperature, T/T_N

As Fig.8 shows at the same absolute temperature, the addition of 5(O)PCP decreases $\overline{P}_2$ of the spin probe in ZLI-4792 while the effect of 5(O)CB is relatively small. The decrease of $\overline{P}_2$ is caused only by the decrease of T_N produced by the dopant because the relationship between $\overline{P}_2$ and the reduced temperature does not depend to any significant extent on the structure of the dopants, as is apparent from the results in Fig.9.

We have seen the temperature dependence of τ in Figs. 6 and 7, and that of $\overline{P}_2$ in Figs.8 and 9. The temperature dependence of $\tau\overline{P}_2$ which is proportional to γ_1 will be the combination of the temperature dependence of these two parameters. Fig.10 shows the dependence of $\tau\overline{P}_2$ on the absolute temperature and Fig.11 shows that on the reduced temperature.

The effect of each dopant on $\tau\overline{P}_2$ is found to be similar on the absolute temperature scale whilst it is significantly different on the reduced temperature scale. This behaviour is almost the same as for τ shown in Fig.6 and Fig.7. However, on the absolute

temperature scale, the addition of 5(O)PCP slightly decreases the value of $\tau\overline{P}_2$ for ZLI-4792 while the addition of 5(O)CB does not change it. This can be explained by the results in Fig.7 which shows that 5(O)PCP decrease $\overline{P}_2$ on the absolute temperature scale whilst 5(O)CB do not change it to any significant extent. To help us understand this behaviour we consider the factors which are predicted to influence γ_1 in the following section.

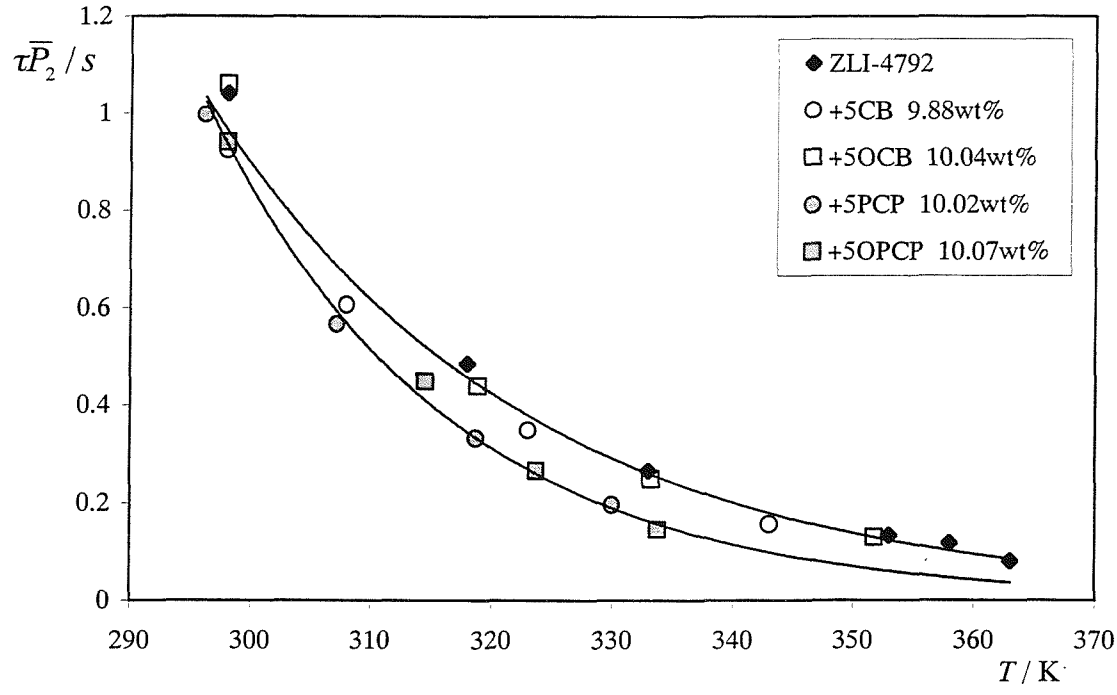

Fig.10 Dependence of $\tau\overline{P}_2$ for the cholestane spin probe on the absolute temperature

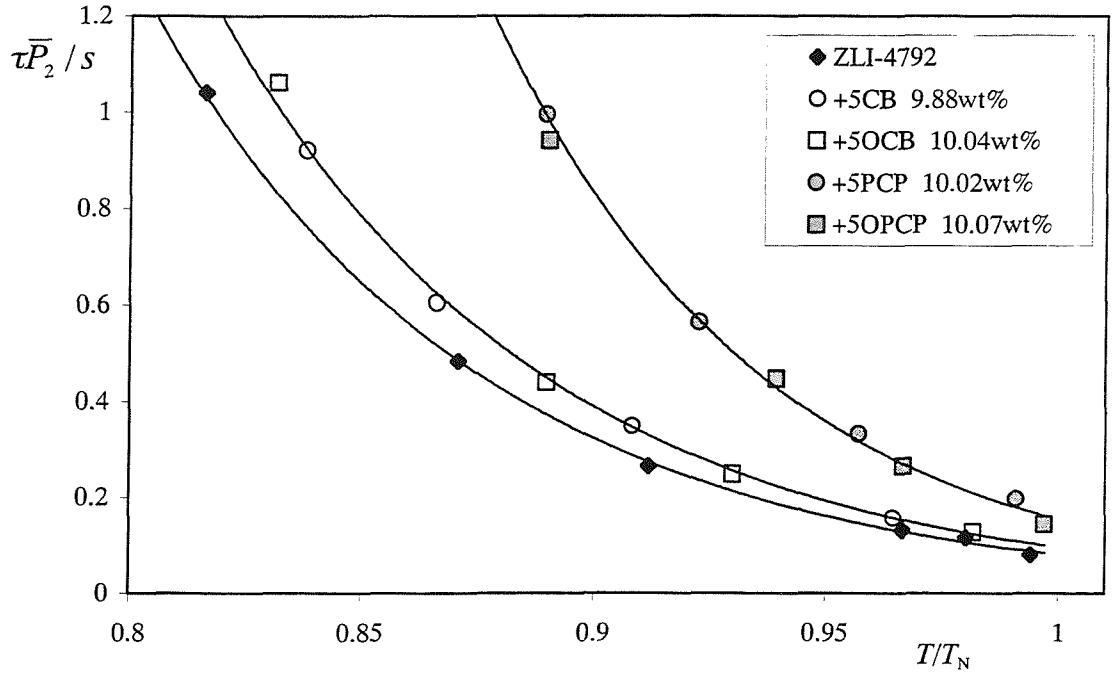

Fig.11 Dependence of $\tau\overline{P}_2$ for the cholestane spin probe on the reduced temperature, T/T_N

3.3.4 Analysis of the Temperature Dependence of the Relaxation Time

According to theory, the rotational viscosity, γ_1, has a temperature dependence given both by the Arrhenius behaviour and by that of the order parameter [7,10];

$$\gamma_1 \propto \overline{P}_2 \exp(E_a / RT) \tag{5}$$

in which $\overline{P}_2$ is the order parameter of the nematic sample, E_a is an activation energy which normally takes a positive value, R is the gas constant and T is the absolute temperature. As we have seen $\gamma_1 / \Delta\tilde{\chi}$ is expected to be proportional to $\gamma_1 / \overline{P}_2$ and so we have

$$\tau \propto \gamma_1 / \overline{P}_2 \propto \exp(E_a / RT). \tag{6}$$

Thus, the relaxation time should be given by the simple Arrhenius behaviour

$$\tau = \tau^{\infty} \exp(E_a / RT), \tag{7}$$

where τ^{∞} is a constant corresponding to the relaxation time which is obtained by extrapolating τ to infinite temperature. However, because the system is not nematic above T_I, τ^{∞} cannot be determined directly although it is available indirectly from the plot of $\ln\tau$ versus T^{-1} which also gives the activation energy, E_a:

$$\ln\tau = \ln\tau^{\infty} + (E_a / R)T^{-1}. \tag{8}$$

Fig.12 shows this plot; here the results for the different systems tend to fall on a common line as is expected from the behaviour of τ shown in Fig.6, and this proves to be linear in accord with the prediction of equation (8). The straight line in Fig.12 was fitted by the linear least squares method to all of the data which appears in this figure. The calculated value of the average activation energy E_a obtained in this way is 25.8±0.8kJ/mol.

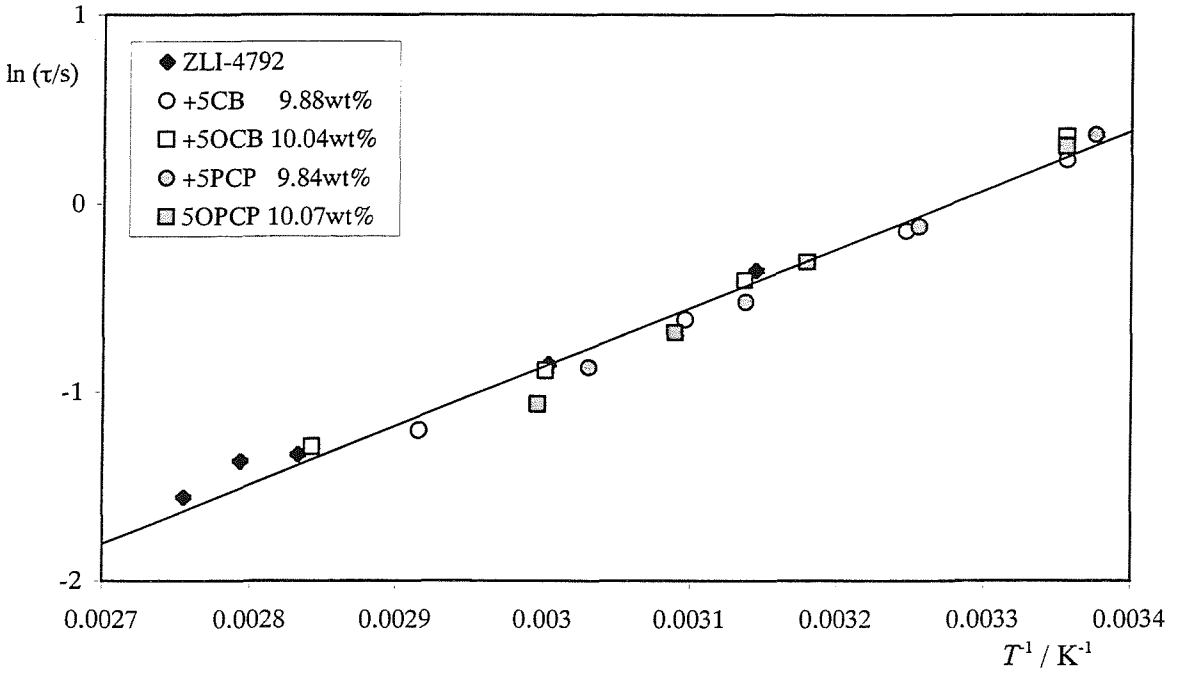

Fig.12 Logarithm of the relaxation time for the cholestane spin probe versus T^{-1}

Because according to equation (6) τ may depend only on the absolute temperature, this is clearly the appropriate temperature scale with which to compare the effect of dopants on τ. Nonetheless, as we compared the temperature dependence of τ not only on the absolute temperature but also on the reduced temperature in Figs.6 and 7, we will attempt the same comparison for this logarithmic plot using another temperature scale which includes T_N, namely

$$\tau = \tau^N \exp\{(E_a/R)(T^{-1} - T_N^{-1})\}. \quad (9)$$

This gives

$$\ln\tau = \ln\tau^N + (E_a/R)(T^{-1} - T_N^{-1}) \quad (10)$$

in which τ^N is the relaxation time at the transition, T_N. In Fig.13, the logarithm of the relaxation time is plotted against the shifted inverse temperature T^{-1}-T_N^{-1}. The use of the inverse temperature scale does not change the value of the activation energy E_a but the pre-exponential factor is altered. Table 1 shows E_a, τ^∞ and τ^N which were estimated from the slope and the intercept via equations (8) and (10) for the individual systems.

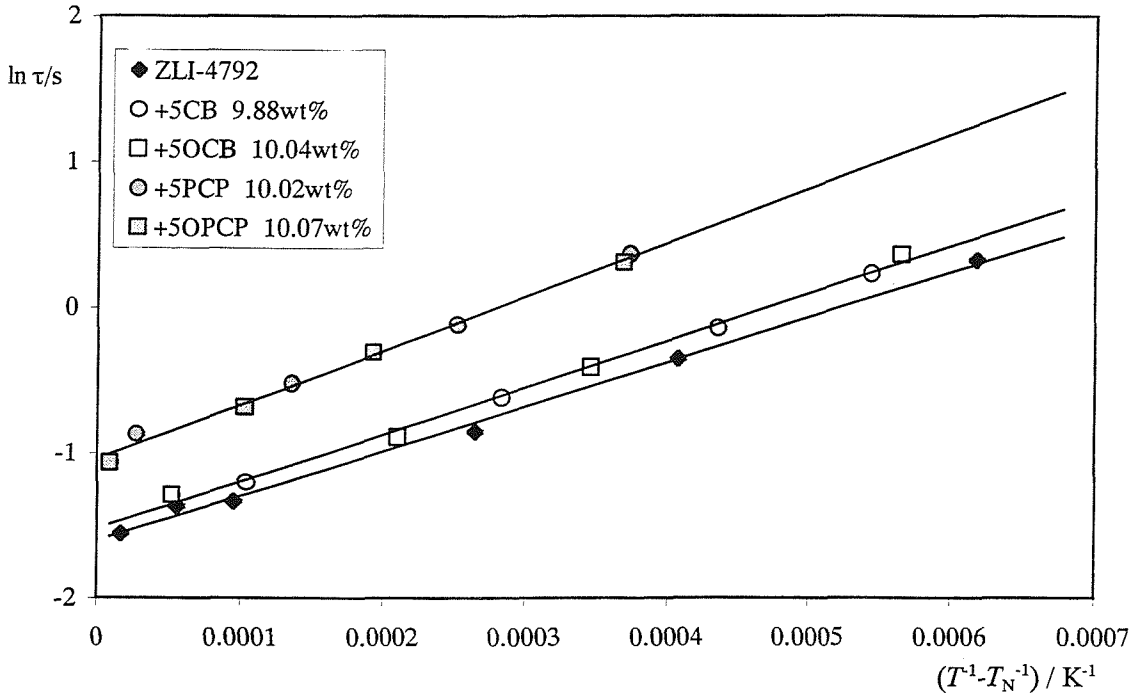

Fig.13 Logarithm of the relaxation time for the cholestane spin probe versus T^{-1}-T_N^{-1}

Table1 Calculated E_a, τ^∞ and τ^N for the various systems

samples	wt%	mol%	E_a/kJmol^{-1}	τ^∞ / 10^{-5}s	τ^N /s
ZLI-4792	0	0	25.6±0.8	4.5±1.4	0.20±0.01
+5CB	9.88	13.19	27.0±0.3	2.3±0.3	0.21±0.01
+5OCB	10.04	12.69	27.0±1.4	2.5±1.7	0.22±0.01
+5PCP	9.84	13.47	30.2±0.5	0.63±0.13	0.42±0.01
+5OPCP	10.07	13.03	31.7±1.0	0.39±0.17	0.34±0.01

The addition of the various dopants makes the activation energy slightly higher than that of the base mixture. Because the activation energy of γ_1 for 5CB is reported to be 0.46(±0.02)eV [11] which is equal to 44(±2)kJmol^{-1} and is larger than ZLI-4792, the result for adding 5CB seems to be reasonable. From Table1, we see that the

phenylcyclopentenones (5(O)PCP) increase E_a more than the cyanobiphenyls (5(O)CB). The changes are not large but they are in excess of the experimental error. For τ^N and τ^∞, the changes are large, although the pair of dopants 5(O)CB do not change τ^N significantly, in contrast to the 5(O)PCP pair, it is almost doubled. In terms of τ^∞, the addition of these dopants decreases the value and the addition of 5(O)PCP makes the values of τ^∞ considerably smaller than that of ZLI-4792 while the addition of 5(O)CB makes it about half. The behaviour of both of the Arrhenius pre-exponential parameters with 5(O)CB are almost the same, however 5PCP and 5OPCP show different values to some extent.

We have discussed two temperature scales with which to compare the values of the experimental relaxation times τ and the rotational viscosity coefficients, γ_1. From a practical point of view, that is for LCD applications, the absolute temperature scale gives information which is particularly relevant to the switching time of the display. However if a dopant decreases T_{NI}, it will also affect the other physical properties and this may change the characteristics of the LCD. Moreover, the lower T_{NI} is, the more difficult it is to use the liquid crystal in an LCD because the temperature ranges for the use of the display will be restricted.

Theoretically, equation (5) predicts that γ_1 should depend on both the absolute temperature and the orientational order parameter, $\overline{P}_2$, whose behaviour for the different systems is well-characterised by a reduced temperature scale. In addition the activation energy might also be expected to depend on the molecular organisation and hence the order parameter. Therefore, it is important to consider both of temperature scales when γ_1 values are compared for different systems. For τ, the absolute temperature scale is predicted to be most appropriate (see equation (6)) in agreement with our experiments. The values, E_a, τ^N and τ^∞, may be appropriate parameters with which to compare the effect of dopants provided they are independent of temperature. However, we should treat

them carefully since they may be a function of the order parameter which is usually a universal function of T/T_{NI} and so is not expected to show conformal behaviour on an absolute temperature scale.

3.4 Summary

(1) Addition of 5(O)PCP decreases T_N (when the isotropic phase first appears) of the base mixture ZLI-4792 significantly whilst that of 5(O)CB does not decrease it so much.

(2) The alkoxy compounds have a slightly smaller effect on T_N than the alkyl compounds because alkoxy compounds have higher T_{NI} than alkyl compounds.

(3) The effect of dopants on the field-induced relaxation time is small on the absolute temperature scale.

(4) The reduced temperature scale reveals a large difference of the effect of dopants; thus the addition of 5(O)PCP increases the relaxation time far more than for 5(O)CB.

(5) The addition of 5(O)PCP decreases $\overline{P}_2$ significantly whilst 5(O)CB decreases it slightly, which is equivalent to (1) because $\overline{P}_2$ is essentially a universal function of T/T_N.

(6) The addition of 5(O)PCP decreases $\tau\overline{P}_2$ slightly which is proportional to γ_1 at the same absolute temperature, while 5(O)CB does not change it to any significant extent.

3.5 References

[1] L.Pohl and U.Finkenzeller; Physical Properties of Liquid Crystals, Liquid Crystals-Application and Uses, Vol.1, Chapter 4, 1990, World Scientific.

[2] W.H.de Jeu; Physical Properties of Liquid Crystalline Materials, Chapter 5, 1980, Gordon and Breach, London.

[3] G.W.Gray; J. Phys. (Paris), **36-C1,** 1975, C1-337.

[4] R.Brettle, D.A.Dunmur, L.D.Farrand and C.M.Marson; J. Chem. Soc., Chem. Commun., 1994, 2305.

[5] L.D.Farrand, Y.Utsumi, H.Kagawa and K.Kondo; Liq. Cryst., **20**, 1996, 751.

[6] Private communication (Merck Japan).

[7] W.H.de Jeu; Physical Properties of Liquid Crystalline Materials, Chapter 7, 1980, Gordon and Breach, London.

[8] W.H.de Jeu; Physical Properties of Liquid Crystalline Materials, Chapter 3, 1980, Gordon and Breach, London.

[9] G.R.Luckhurst; Magnetic Resonance Spectroscopy of Liquid Crystals - Non-Amphiphilic Systems, Liquid Crystals and Plastic Crystals Vol.2, Chapter 7, 1974, Ellis Horwood, Chichester.

[10] J.Prost, G.Sigand and B.Regaya; J. Phys. Lett. (Paris), **37**, 1976, L-341.

[11] H.J. Coles; in The Optics of Thermotropic Liquid Crystals, Eds. S. Elston and R. Sambles, Chapter 4, 1998, Taylor&Francis, London.

Chapter 4

Determination of the Diamagnetic Anisotropy for Nematic Liquid Crystals by ESR Spectroscopy

4.1 Introduction

In Chapters 2 and 3, we discussed the determination of the field-induced relaxation time τ, which is proportional to $\gamma_1 / \Delta\tilde{\chi}$, by ESR spectroscopy. Although we found the temperature dependence of the rotational viscosity γ_1 using the quantity $\tau\overline{P}_2$ (here $\overline{P}_2$ is the orientational order parameter of the paramagnetic spin probe) that is proportional to γ_1, we could not obtain the absolute value of γ_1. To do this, we need the value of the magnetic anisotropy $\Delta\tilde{\chi}$. There are several techniques with which to measure $\Delta\tilde{\chi}$, for example, (1) the classical Faraday-Curie method [1], (2) measurement of the bulk susceptibility using NMR spectroscopy [2] and (3) the field-balance method between a magnetic field and an electric field [3] for which a variety of techniques can be used to determine the director orientation [3,4]. In method (1), a sample is placed in a magnetic field that has a gradient in the vertical direction, and the force acting on the sample is determined using a sensitive balance. Numerous measurements have been carried out for many kinds of materials. However, some of the reported values are not accurate in the sense that results for some of the materials by different authors disagree considerably [5-9]. In method (2), the proton NMR signal is recorded of a reference sample, such as p-xylene, contained in the outer annulus of a coaxial, cylindrical tube with the liquid crystalline sample placed in the inner tube [2,10]. $\Delta\tilde{\chi}$ is obtained from the difference of the splitting of the doublet proton NMR signal when the liquid crystal is nematic and isotropic. However, the precision is not high because the difference of these two splittings is normally small; for example the overall precision is 20% for a liquid crystal with negative $\Delta\tilde{\chi}$ [10].

In this Chapter, the last method listed above, the field-balance method in which ESR spectroscopy is used to determine the director orientation, will be used. The basic idea of this method is to monitor the director alignment under the influence of two competing fields. As we saw in Chapters 2 and 3, ESR spectroscopy is useful for monitoring the director orientation and uniformity. Moreover, exactly the same sample doped with a spin probe as used in Chapters 2 and 3 can be studied with this method.

In this Chapter, we shall be concerned with the methodology itself and its use to determine the absolute value of $\Delta\tilde{\chi}$ for a typical nematic liquid crystal. This will then employed to evaluate γ_1.

4.2 Theory

The basic idea of the experiment described in this Chapter is the competition between a magnetic field and an electric field for the alignment of the director of a nematic liquid crystal. The ESR technique was used to monitor the director alignment by measuring the nitrogen hyperfine splitting for the nitroxide spin probe dissolved in the nematogen, as we saw in Chapter 2. The system required in this experiment is a nematic liquid crystal, with positive diamagnetic and dielectric anisotropy, in a static magnetic field and together with a variable electric field, with a non-zero angle between the two fields. Experimentally, an electric field can be applied by containing the liquid crystal between two parallel conducting plates, for example glass plates coated with electrodes, and then applying a voltage to them. Although interfacial effects exist between the surface of the plates and the nematic liquid crystal, we shall simply assume that the surface effects are negligible. In other words, the anchoring energy of the surface and the nematogen is small, or the field coherence length is small in comparison with the sample thickness. To achieve this, a relatively thick sample is needed. Fig.1 shows the sample geometry with two conducting plates (the distance between the plates is d), an electric field E, a static

magnetic field B and the director of the nematic liquid crystal $\hat{n}$. Here, $\hat{n}$ is in the plane formed by the two fields. Without an electric field, the director aligns uniformly along the magnetic field since we ignore the surface effects, i.e. the magnetic coherence length is small in comparison with the sample thickness d. When an electric field is applied, the director moves towards the electric field if the magnitude of the electric field is large enough. Here, the angle, α, between the two fields is non-zero. In an equilibrium condition, the director orientation is determined as the result of balancing the orientational energies of the two fields except for the special case when α=90°, where the director jumps from parallel to B to parallel to E, as we discuss later.

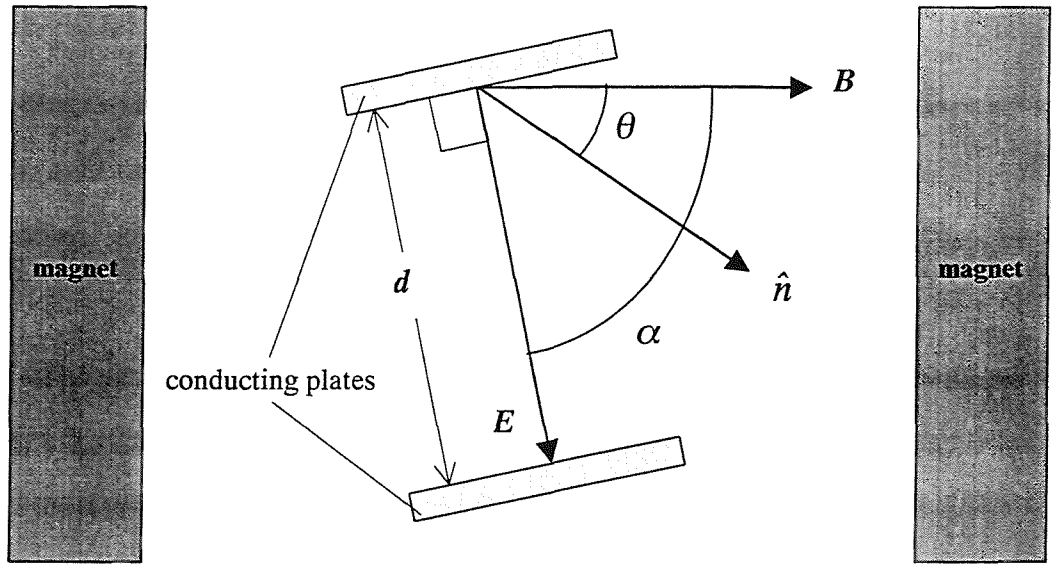

Fig.1 Sample geometry: two conducting plates, electric field, magnetic field and the nematic director

This situation can be described using the orientational free energy of the nematic. Because we ignore the contribution of the surface anchoring energy, the distortion or elastic energy of the director is zero since the director is uniformly aligned. Then we need only take the

two fields into consideration. One is the electric energy per unit volume U_e, and the other is the magnetic energy per unit volume U_m, which are given by [11]

$$U_e = -\frac{1}{2}\varepsilon_0 \Delta\tilde{\varepsilon} E^2 \sin^2(\alpha - \theta) \tag{1}$$

and

$$U_m = -\frac{1}{2}\frac{1}{\mu_0}\Delta\tilde{\chi} B^2 \sin^2\theta . \tag{2}$$

Here ε_0 is the dielectric constant of free space, $\Delta\tilde{\varepsilon}$ is the dielectric anisotropy, E is the magnitude of the electric field, μ_0 is the magnetic constant, $\Delta\tilde{\chi}$ is the diamagnetic anisotropy and B is the magnetic flux density. Then the total energy per unit volume of the liquid crystal, U_t, is given by

$$U_t = U_e + U_m . \tag{3}$$

At equilibrium the director adopts an orientation which minimises the total energy; this occurs when

$$\frac{1}{2}\varepsilon_0 \Delta\tilde{\varepsilon} E^2 \sin 2(\alpha - \theta) - \frac{1}{2}\frac{1}{\mu_0}\Delta\tilde{\chi} B^2 \sin 2\theta = 0 . \tag{4}$$

The solution of this equation is

$$\cos 2\theta = \frac{\lambda \cos 2\alpha + 1}{\sqrt{\lambda^2 + 2\lambda\cos 2\alpha + 1}}, \tag{5}$$

where λ is defined as

$$\lambda = \mu_0 \varepsilon_0 \frac{\Delta\tilde{\varepsilon} E^2}{\Delta\tilde{\chi} B^2} .$$

According to this equation, we can obtain the relationship between $\Delta\tilde{\chi}$ and $\Delta\tilde{\varepsilon}$ by determining λ from the experiment which monitors θ as a function of E. Fig.2 shows

plots of θ versus E calculated using equation (5) with varying λ when the angles between the two fields, α, are 0°, 40°, 80° and 90°. The values used for $\Delta\tilde{\varepsilon}$, $\Delta\tilde{\chi}$ and B are listed in Table 1. As the results in Fig.2 show, θ takes just the value 0° when α=0° since the director aligns along the magnetic field with the electric field parallel to the director. When α=90°, θ can take just two values as equation (5) has just two solutions; if the parameter λ is smaller than 1, i.e. $E^2 \leq (1/\varepsilon_0\mu_0)(\Delta\tilde{\chi}/\Delta\tilde{\varepsilon})B^2$, θ takes 0° and if the parameter λ is larger than 1, i.e., $E^2 \geq (1/\varepsilon_0\mu_0)(\Delta\tilde{\chi}/\Delta\tilde{\varepsilon})B^2$, θ takes 90°. When α is not 90°, for example 40° or 80°, θ increases continuously as E increases to the limiting situation when the director is parallel to the electric field.

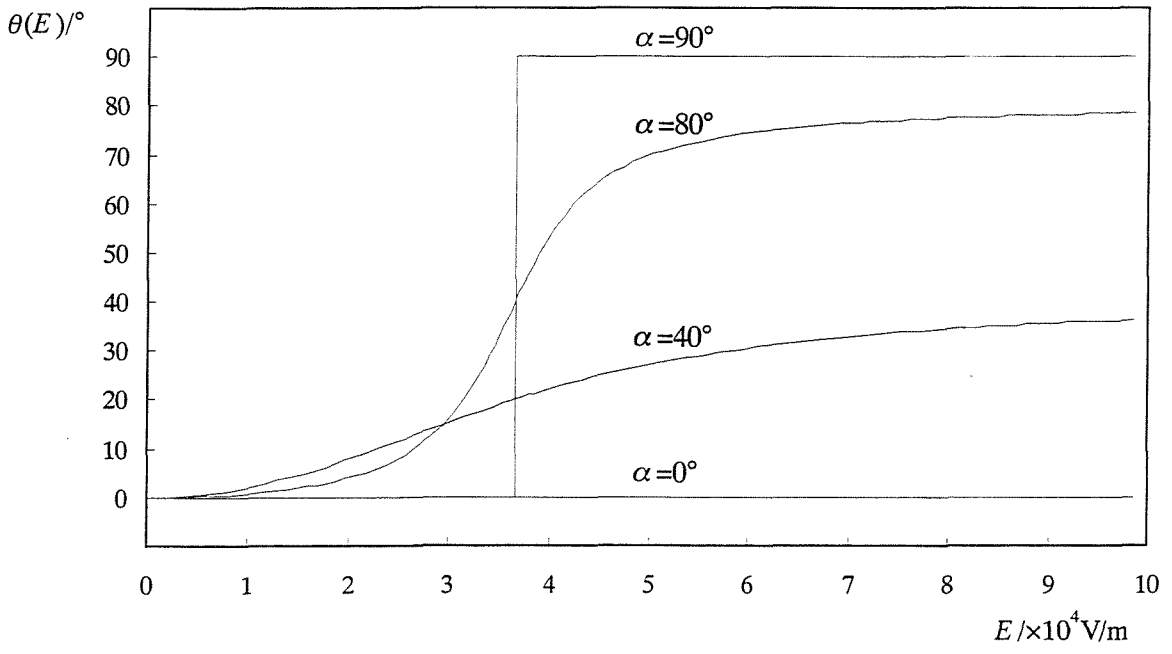

Fig.2 Plot of θ versus E for different values of the angle, α, between the two fields: 0°, 40°, 80° and 90°

To measure the orientation of the director, ESR spectroscopy can be used, as we saw in Chapter 2. Thus the nitrogen hyperfine splitting in the ESR spectrum of a nitroxide spin probe dissolved in the nematic phase is determined by the angle between the director and

the magnetic field. The nitrogen hyperfine splitting, $\bar{a}(\theta)$, of the nitroxide spin probe is given by

$$\bar{a}(\theta) = \left(\tilde{A}_{\parallel}^{\,2}\cos^2\theta + \tilde{A}_{\perp}^{\,2}\sin^2\theta\right)^{\frac{1}{2}}, \tag{6}$$

in which $\tilde{A}_{\parallel}$ and $\tilde{A}_{\perp}$ are the hyperfine splittings when the director and the magnetic field are parallel and perpendicular, respectively. The equation for $\bar{a}(\theta)$ can also be written as

$$\bar{a}(\theta) = \left(\frac{1}{2}\left(\tilde{A}_{\parallel}^{\,2} - \tilde{A}_{\perp}^{\,2}\right)(\cos 2\theta + 1) + \tilde{A}_{\perp}^{\,2}\right)^{\frac{1}{2}} \tag{7}$$

which facilitates its combination with equation (5) to give the field dependence of the hyperfine splitting $\bar{a}(\theta)$ as

$$\bar{a}(E) = \left(\frac{1}{2}\left(\tilde{A}_{\parallel}^{\,2} - \tilde{A}_{\perp}^{\,2}\right)\left(\frac{\lambda\cos 2\alpha + 1}{\sqrt{\lambda^2 + 2\lambda\cos 2\alpha + 1}} + 1\right) + \tilde{A}_{\perp}^{\,2}\right)^{\frac{1}{2}}. \tag{8}$$

Because the electric field is controlled experimentally by the applied voltage, V, between the two electrodes, it may be convenient to rewrite the equation for $\bar{a}(E)$ using the relationship between the electric field and V

$$E = \frac{V}{d}. \tag{9}$$

$$\bar{a}(V) = \left(\frac{1}{2}\left(\tilde{A}_{\parallel}^{\,2} - \tilde{A}_{\perp}^{\,2}\right)\left(\frac{\lambda' V^2\cos 2\alpha + 1}{\sqrt{\lambda'^2 V^4 + 2\lambda' V^2\cos 2\alpha + 1}} + 1\right) + \tilde{A}_{\perp}^{\,2}\right)^{\frac{1}{2}}. \tag{10}$$

where λ' is defined as

$$\lambda' = \frac{\mu_0\varepsilon_0\Delta\tilde{\varepsilon}}{\Delta\tilde{\chi}B^2d^2}.$$

Thus, the ratio of $\Delta\tilde{\varepsilon}$ and $\Delta\tilde{\chi}$ can be calculated from the measured voltage dependence of the hyperfine splitting $\bar{a}(V)$ using known values of $\tilde{A}_{\parallel}$, $\tilde{A}_{\perp}$, B, d and α via a non-linear least squares fit. Fig.3 shows the voltage dependence of the hyperfine splitting, $\bar{a}(V)$, for a selection of the angles between the magnetic and the electric field. This was simulated according to equation (10) with the parameters listed in Table 1.

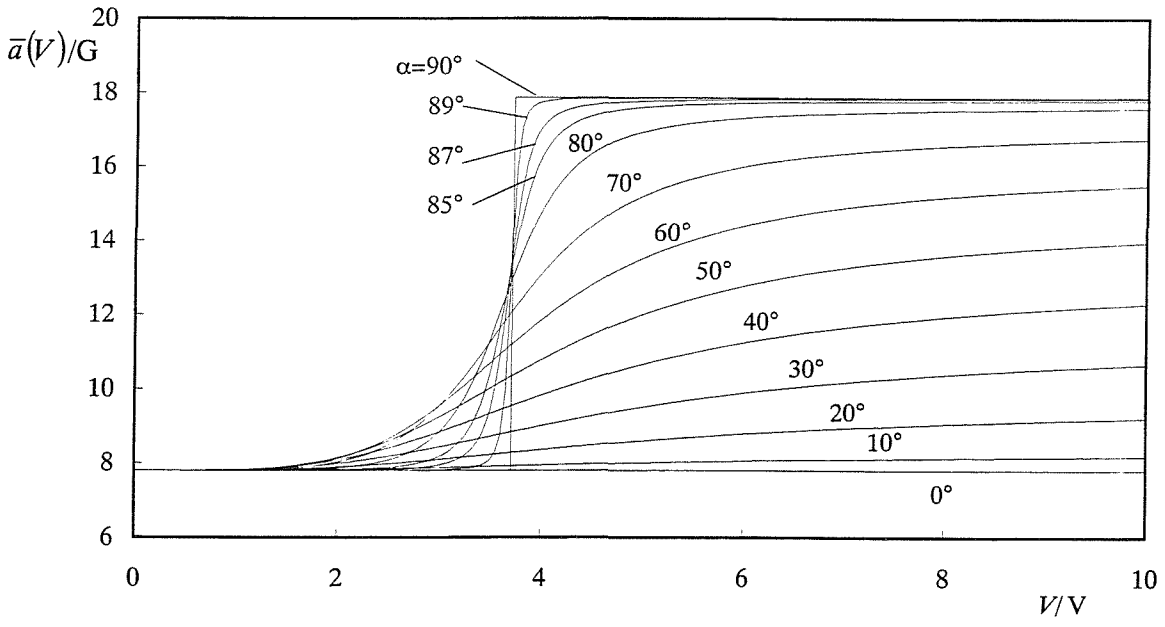

Fig.3 The simulated voltage dependence of $\bar{a}(V)$ for a selection of angles between the two fields

Table 1 Parameters used in the simulation

parameters	value	comments
$\tilde{A}_{\parallel}$/G	7.8	value for the same sample but in a tube
$\tilde{A}_{\perp}$/G	17.9	value for the same sample but in a tube
$\Delta\tilde{\varepsilon}$	5.2	value at 20°C [12]
$\Delta\tilde{\chi}$	6.7×10^{-7}	value at 20°C [13]
B/T	0.3401	centre field
d /m	101.7×10^{-6}	measured value for the empty cell
μ_0/ $Js^2C^{-2}m^{-1}$	$4\pi\times10^{-7}$	-
ε_0/ $J^{-1}C^2m^{-1}$	8.854×10^{-12}	-

For $\tilde{A}_{\parallel}$ and $\tilde{A}_{\perp}$, the values for the same sample but in a tube were used; the measurement of these for ZLI-4792 are described in Chapter 2. The values for $\Delta\tilde{\varepsilon}$ and $\Delta\tilde{\chi}$ are those taken from the Merck data sheet of liquid crystal mixtures for display applications [12] and a private communication [13]. From the simulated results shown in Fig.3, it is clear that the hyperfine splitting takes just two values when the angle between the two fields, α, is 90°. This behaviour is the same as in the plot of θ versus E and as Fig.3 shows, the hyperfine splitting jumps discontinuously at a certain voltage. This threshold voltage, V_{th} is calculated from equation (10) to be

$$V_{th} = \frac{dB}{\sqrt{\mu_0\varepsilon_0(\Delta\tilde{\varepsilon}/\Delta\tilde{\chi})}}. \qquad (11)$$

When $V<V_{th}$, the hyperfine splitting takes the smaller value, $\tilde{A}_{\parallel}$, and it takes the larger value, $\tilde{A}_{\perp}$, when $V>V_{th}$. If α is not 90°, the hyperfine splitting changes continuously as a function of the applied voltage.

4.3 Experimental

4.3.1 Sample Cell Preparation

The sample used in this experiment was ZLI-4792 doped with the cholestane spin probe; this was prepared as described in Chapters 2 and 3. The ESR sample was placed in a sandwich cell to which a voltage can be applied and the construction of the cell is shown in Fig.4. The method used to fabricate the cell is shown in Fig.5. First, a pair of well-washed soda-lime glass plates coated with ITO (Indium Tin Oxide) as an electrode were prepared. The thickness of the glass plate was 1.1mm and the thickness of the ITO was approximately 100nm. Surface treatment, such as casting an alignment film or rubbing the surface, was not carried out. Secondly, a polymer film about 90μm thick was cut into two 40mm×2mm strips as spacers for the cell. Some epoxy adhesive (Mitsui Chemical) was printed on certain positions of the electrode side of both glass plates where the polymer spacer strips were to be placed. After two spacer strips were placed on one glass plate, another was placed on top of it. The ITO side of the two glass plates faced each other. Then, pressure was applied by fastening them together using several clips. Interference lines that originated from the variation of the cell thickness were observed using a sodium light source (589nm). If there were many interference lines, the positions of the clips were changed until the number was reduced to a minimum. Next, the cell was heated at 150°C for 2 hours in an oven in order that the epoxy adhesive reacted and hardened. The cell thickness and its uniformity were evaluated for the empty cell as we shall describe later. Then the empty cell was filled with the liquid crystal sample by capillary action. After filling the cell, epoxy adhesive (Araldite) was put on the edges of the cell to prevent it leaking. Finally, a pair of conducting wires was attached to the surfaces of both ITO sides of the two glass plates using solder (Indium) and they were covered with Teflon tape in order to insulate the exposed metals.

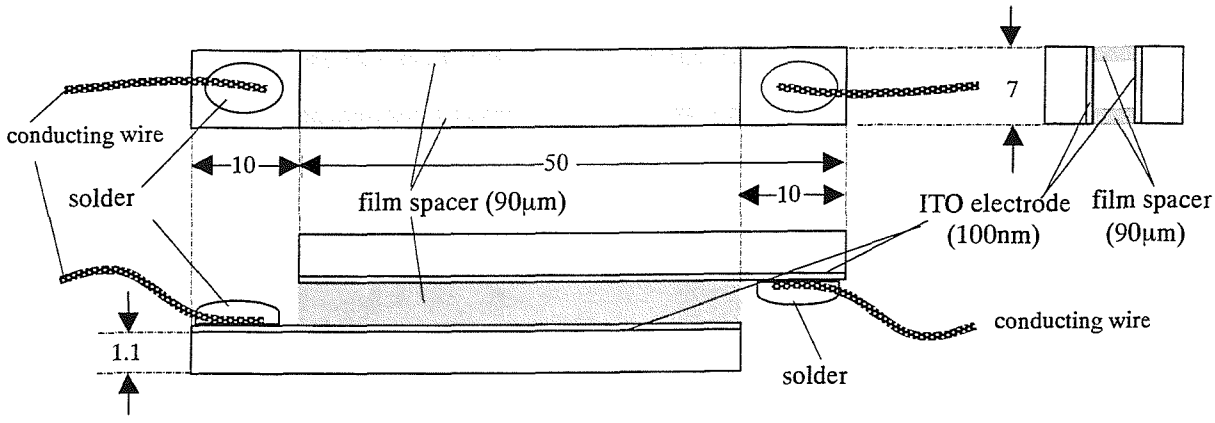

Fig.4 Structure of the cell used in the field balance experiment

(the sizes of the cell are in mm)

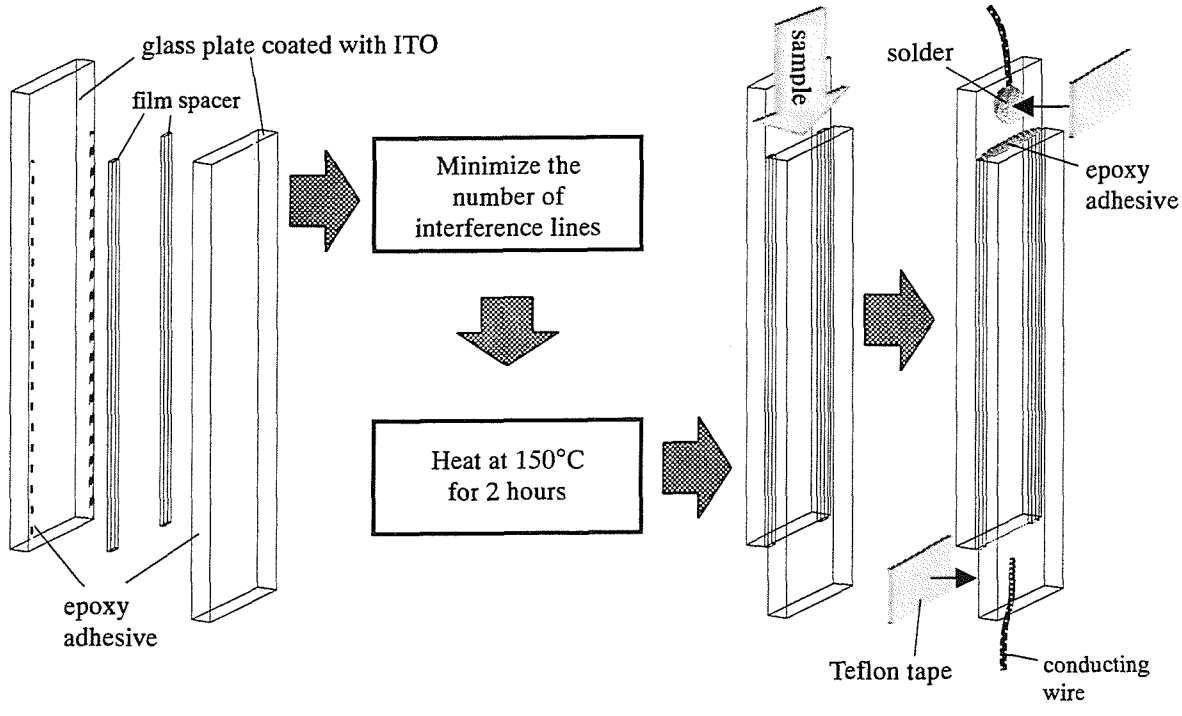

Fig.5 Procedure for fabricating the cell

The thickness of the empty cell was determined by measuring the wavelength of the multi-reflected interference peaks using a UV-VIS spectrometer. The relationship between the cell thickness and wavelength of the interference peaks is given by

$$d = \frac{n}{2}\frac{\lambda_i \lambda_{i+n}}{\lambda_{i+n} - \lambda_i}, \tag{12}$$

in which λ_i is the wavelength of an interference peak and λ_{i+n} is the wavelength of the nth interference peak from λ_i. The measured cell thickness of the cell used in this experiment was 101.7±0.2μm at the centre of the cell (about 3mm in diameter). The value is larger than the thickness of the polymer spacers which is about 90μm because some epoxy adhesive intrudes between the glass plates and the spacers. The uniformity of the cell gap was evaluated by counting the interference lines under a sodium light source (589nm). The number of interference lines over an area 20mm in length at the centre of the cell was five which meant that the difference of the thickness in this area was about 3μm (±1.5μm) provided the slope between two glass plates was linear. Thus the fractional variation over the area of sample observed in the ESR experiment is approximately 0.15μm/mm. The uniformity of the cell thickness will cause the electric field to vary, and this, in turn, gives different hyperfine splittings according to equation (10).

4.3.2 The Field-Balance Experiment

The sample cell was placed in the ESR spectrometer described in Chapter 2 using the Teflon holder shown in Fig.6. This sample holder was inserted in the spectrometer being held at the top and bottom of the microwave cavity. The conducting wires from the cell were connected to the wave generator (Linstead Signal Generator G120; RS components Ltd. Black star 4503) as shown in Fig.6. The voltage available to apply to the cell was in the range 0V to 9V and the frequency of the signal was 1kHz and the voltage accuracy is approximately 0.1%. The sample holder can be rotated by a goniometer (Bruker) with

respect to the axis perpendicular to the direction of the magnetic field thus changing the angle between the two fields, as shown in Fig.7.

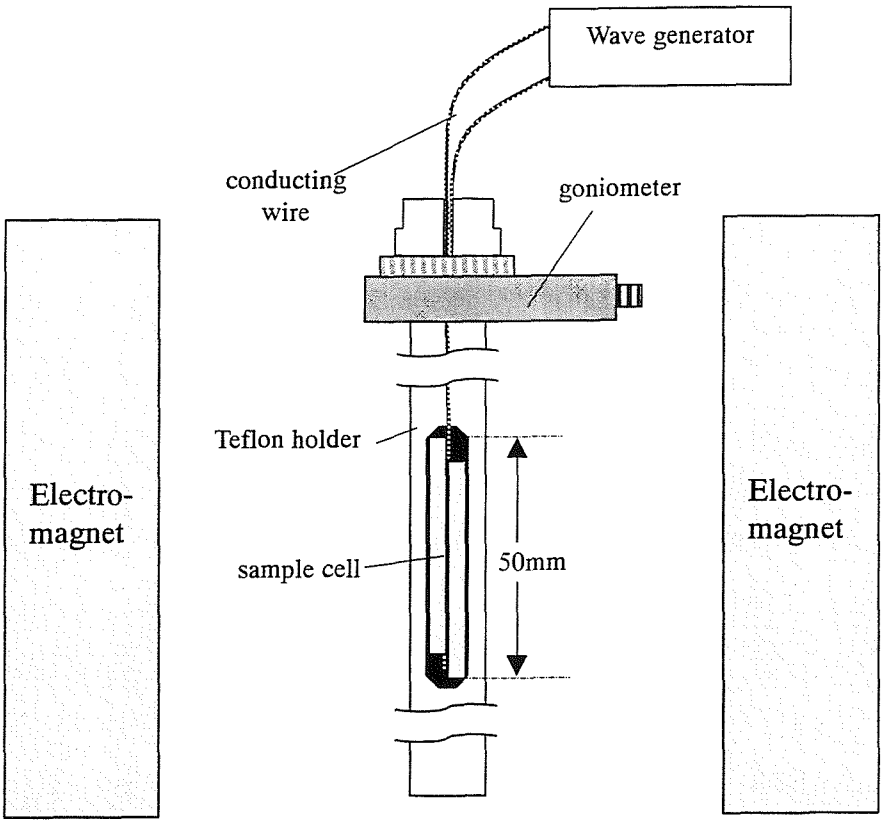

Fig.6 A sketch of the measurement system

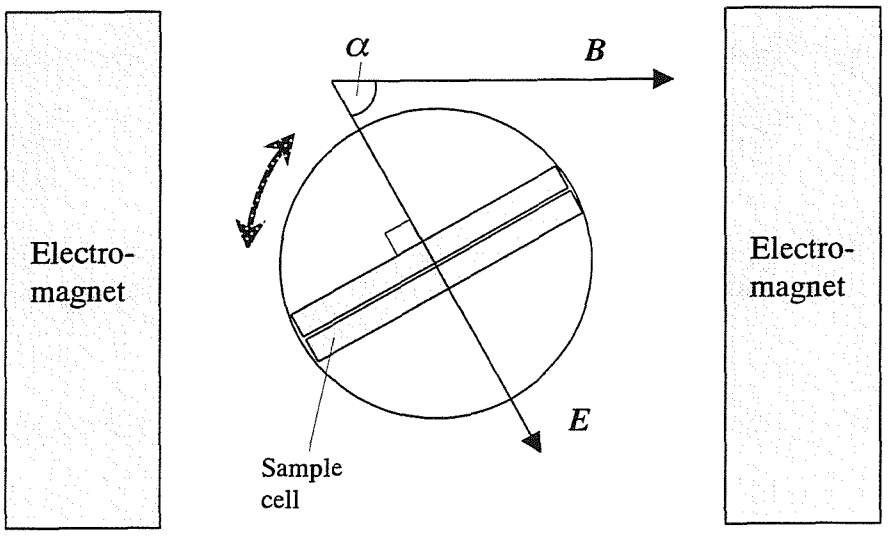

Fig.7 The view of the sample cell and the angle between the two fields

Although the principle of this experiment is exactly the same as that described in Chapter 2, tuning the ESR microwave cavity was slightly different in this experiment. When a sample tube was used as in Chapters 2 and 3, the tuning process was carried out completely automatically by the spectrometer. However, when we used the conducting plates (glass plates with electrodes) in this experiment, the automatic tuning process could not be completed in most cases. This is because of the coupling between the electrodes, which have a low resistance, and the electric vector of the microwave radiation in the cavity which prevents the creation of a standing wave. To minimise the effects of this, the cell needs to be vertical and the wires need to be straight and also vertical. In addition, a careful positioning of the cell was required by rotating the cell in the cavity, with the angle α as close as possible to 90°. If the angle is far from 90°, then we are unable to tune the cavity. Under these conditions it was necessary to perform the iris coupling process manually. This process controls the amount of microwaves which will be reflected back from the cavity by adjusting the position of a conducting disc with respect to a hole between the waveguide and the cavity. We can check how this process is achieved by the display of the klystron power output reflected from the microwave cavity and the reference arm power; no incident microwaves are reflected back from the cavity and this is independent of the microwave power when we have achieved critical iris coupling. After the correct iris coupling, the remaining tuning processes were successfully carried out automatically. The width of the cell affects this tuning process. For example, when the width of the cell was 10mm, the signal was never tuned. However, when the width was 7mm, the tuning was available. This may be because the amount of conducting material in the microwave cavity is larger for 10mm glass plates than for 7mm.Because the amount of the nitroxide spin probe was less in the flat sample cell than in the sample tube used in Chapter 2 (2mm diameter or more), the receiver gain was set to about 1000 times higher in this field-balance experiment. In addition, a longer conversion time was used in order

to improve the S/N ratio. The operating conditions for the ESR spectrometer are listed in Table 2. The measurement temperature is ambient temperature (approximately 23°C)

Table 2 The operating conditions of the spectrometer for the field-balance experiment

Conditions	Values
Modulation amplitude / G	1.00
Modulation frequency / kHz	100
Sweep width (field centre) / G	70 (3401)
Receiver gain	2.00×10^5
Time constant / ms	10.24
Conversion time / ms	40.96
Number of data points acquired	1024
Sweep time / s	41.943

4.4 Results and Discussion

4.4.1 Results of the Field Balance Measurements

First, we visually tried to make the angle between two fields, α, as close as possible to 90°. Then, a voltage was applied to the cell and the ESR signal was measured at each voltage. The voltage range applied was from 0.01V to 9.01V which is the maximum voltage available with the wave generator. The voltage was changed in steps of 0.1V between 3.0V to 4.1V and in 0.5V or 1.0V steps in the other voltage range where the splitting does not change significantly with the voltage.

Fig.8 is the stack plot of this measurement (from 2.5V to 6.5V). As we can see, the spectra have a small hyperfine splitting value at low voltages and the value changes quite suddenly at about 3.1V.

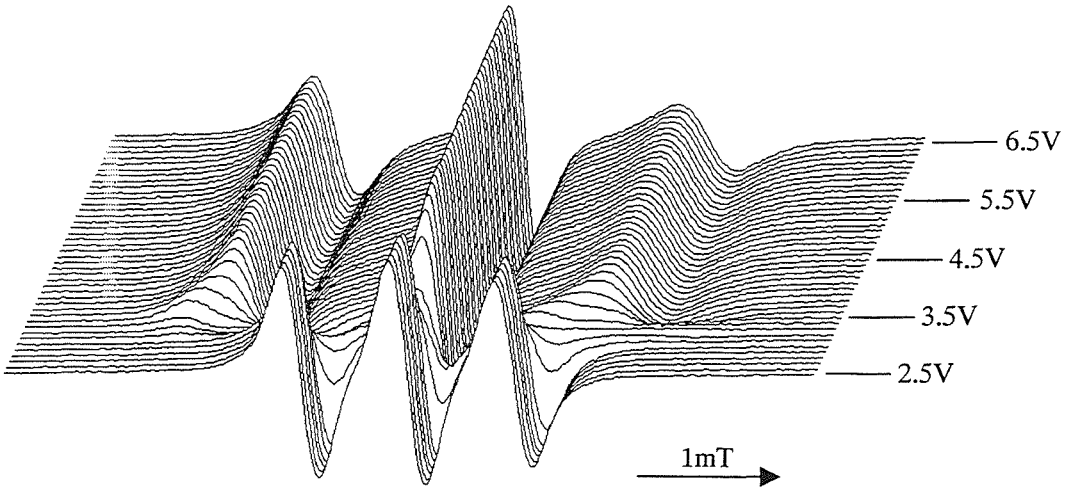

Fig.8 Stack plot of the ESR spectra when the angle between the two fields was approximately 90°

Fig.9 shows a selection of the individual ESR spectra for which we can see the change of the spectra with respect to the applied voltage more clearly. The spectra when V=0.00V has a pair of weak lines outside of the three strong peaks. It may be because the director close to the surface of the cell does not align parallel to the magnetic field. This may occur if the director of the nematic has been aligned by the flow during the filling process since no surface treatment, such as casting an alignment film or rubbing, was carried out. The spectra at 3.20V has a stronger pair of outer lines than at 0.00V, this powder pattern indicates the appearance of a new director orientation, i.e. the director aligned parallel to the electric field. These outer lines increase in intensity as the applied voltage increases and at the same time, two of the initial inner lines decrease. Here, the intensity of the centre line does not change to any significant extent since its position is, to a good approximation, independent of the director orientation. The pair of initial lines have almost disappeared at 3.89V, but the initial lines still remain because the spectral lines are not anti-symmetric. These powder patterns indicate that two different director orientations

coexist. Since the angle between the two fields was supposed to be 90°, the director can only take one of two orientations, either parallel or perpendicular to the electric field depending on the applied voltage. However, because of the non-uniformity of the cell thickness, the electric field varies over the active area of the sample. Therefore, a part of the sample may be above the threshold voltage and the other part of the sample may be below the threshold voltage.

The spectrum at 5.00V contains three lines each with an anti-symmetric shape and this indicates that the director is uniformly oriented. This conclusion is confirmed by the observation that the spectra at 5.00V and at 9.01V are essentially the same and that at the higher voltage is expected to come from a monodomain.

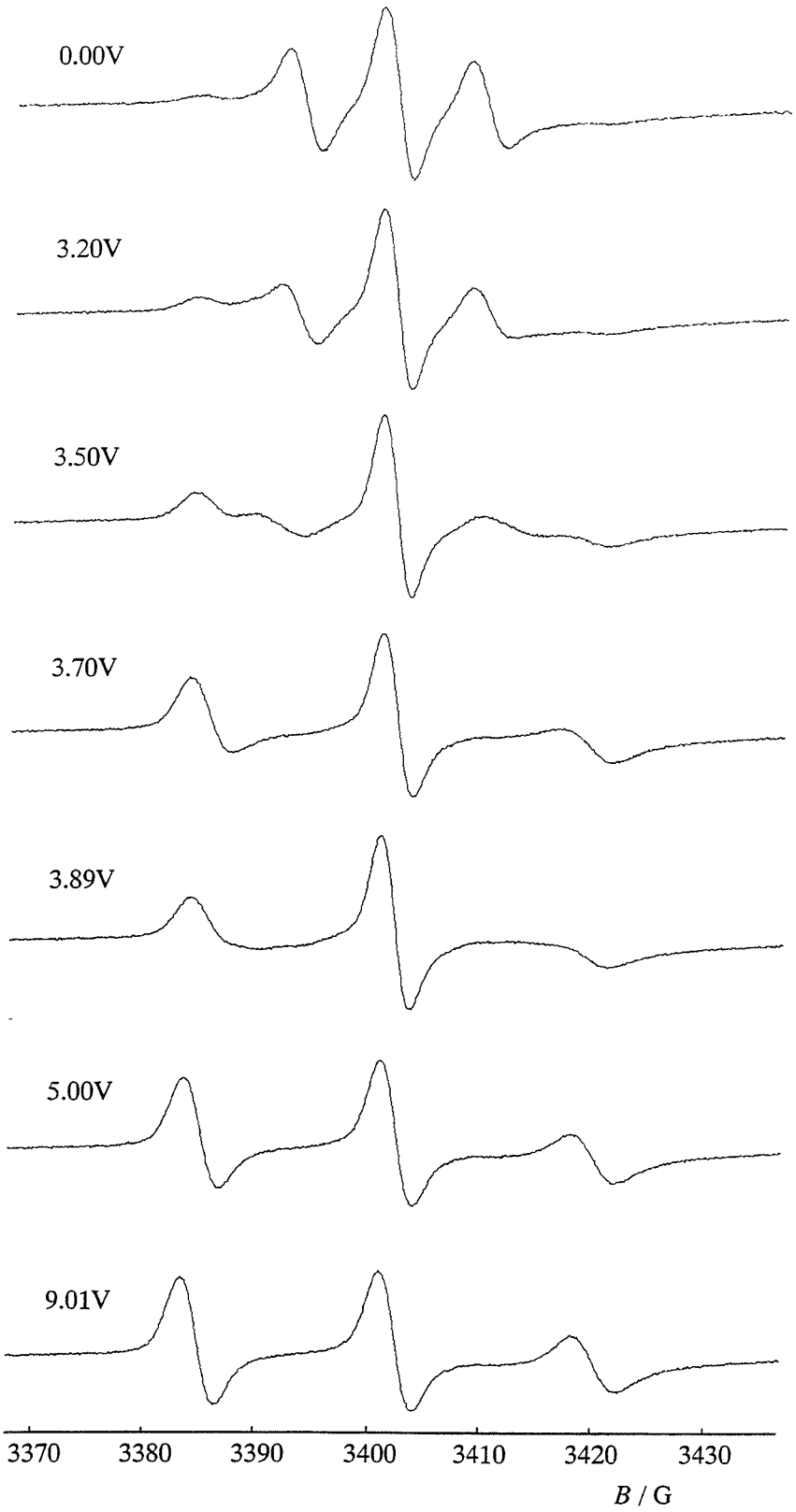

Fig.9 The voltage dependence of the ESR spectra when the angle between the two fields was approximately 90°

The voltage dependence of the nitrogen hyperfine splitting determined from the spectra in the stack plot is shown in Fig.10. The spectra below 5.0V in Fig.9 have a powder-like appearance, so there is not a single hyperfine splitting. What is measured from these spectra is an averaged hyperfine splitting (draw a horizontal baseline on the centre of a spectrum and pick the value of the magnetic field at which the spectrum crosses the horizontal baseline). The experimental data (open circles) in Fig.10 shows a relatively large change at about 3.5V. Although the set angle between the two fields, α, was supposed to be 90°, the results are different from the predicted dependence shown in Fig.3 for α =90° which is also given in Fig.10 as a step function with dashed line. In order to determine α for this experiment, the plots were fitted by the theory. The theoretical curve is also shown in Fig.10 (using $\tilde{A}_{\parallel}$ as the value when V=0 and $\tilde{A}_{\perp}$ as the value when V=9.01).

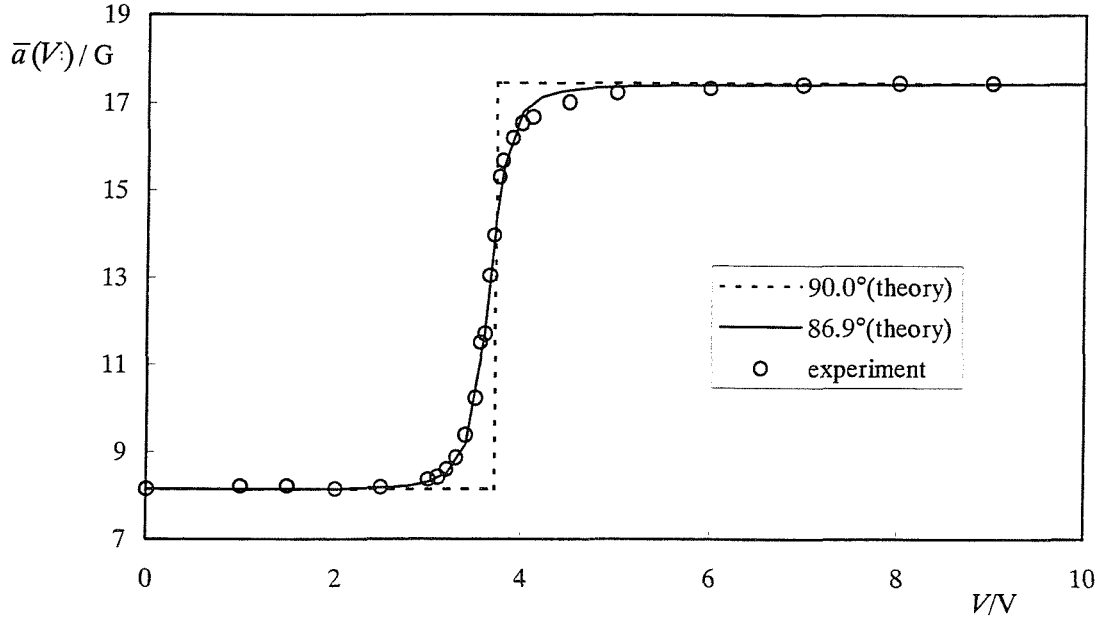

Fig.10 The voltage dependence of the experimental hyperfine spacing and the best fit to the theoretical expression in equation (10)

The experimental data could be fitted to equation (10) using a non-linear least squares fit by varying $\cos 2\alpha$ and $(\mu_0\varepsilon_0\Delta\tilde{\varepsilon})/(\Delta\tilde{\chi}B^2d^2)$. This was carried out using a Mathcad program to minimise the function

$$\sum_V\left[(\bar{a}(V))_{\text{experiment}}-(\bar{a}(V))_{\text{theory}}\right]^2.$$

$\text{Cos}2\alpha$ and $(\mu_0\varepsilon_0\Delta\tilde{\varepsilon})/(\Delta\tilde{\chi}B^2d^2)$ that gave the best fit were -0.9937±0.0008 and 0.0742±0.0002, respectively, thus, α=86.9±0.2° and $\Delta\tilde{\varepsilon}/\Delta\tilde{\chi}$=(7.9±0.3)×10^6. The value $\Delta\tilde{\varepsilon}/\Delta\tilde{\chi}$ is in a very good agreement with the literature value 7.8×10^6 calculated from the data in Table 1.

4.4.2 Results for a Selection of the Angles between the Two Fields

Other measurements were carried out using the same cell for a selection of angles between the two fields. The angles chosen were 84°, 100°, 110°. Because of the symmetry of the system, only the deviation from 90° is important, so the deviations of these angles from 90° are 6°, 10° and 20°. A selection of the individual ESR spectra for α of 84° are shown in Fig.11. The initial spectrum (when V=0.00V) again has a pair of weak lines outside of the three strong peaks. However, these weak lines do not increase at 3.21V and higher applied voltages. Spectra in Fig.11 always show three lines, and they do not exhibit powder patterns. We can observe that a pair of strong outer lines shifts towards the outside gradually as the applied voltage increases. However, these outer lines become broader and smaller in intensity from 3.21V to 3.56V. Then they become sharper and stronger in intensity from 3.75V to 9.02V. This behaviour of the spectra indicates that the director is distributed to a small extent at a lower voltage but that it is more or less uniform. Then it becomes uniform to a greater extent at higher voltages. Here, as we have seen in Fig.9, the intensity of the central line does not change to any significant extent. These experimental results were then fitted by theory as we did in the previous section. Each of Figs.12, 13 and 14 shows the fitting of these for each angle between the two

fields. These figures show that the larger the deviation of the angle from 90° is, the less steep the change of the hyperfine splitting in the threshold region, this is expected from the simulations. The values for the parameters, $\cos 2\alpha$ and $(\mu_0\varepsilon_0\Delta\tilde{\varepsilon})/(\Delta\tilde{\chi}B^2d^2)$, obtained from the non-linear least squares fit are listed in Table 3. In this experiment, larger deviations from 90° could not be studied. This is because tuning the cavity became more difficult due to the coupling between the electrodes of the cell and the electric vector of the microwave radiation in the cavity, as described in section 4.3.2. From this experiment, the largest deviation from 90° was about 20°, i.e. the set angle 110°.

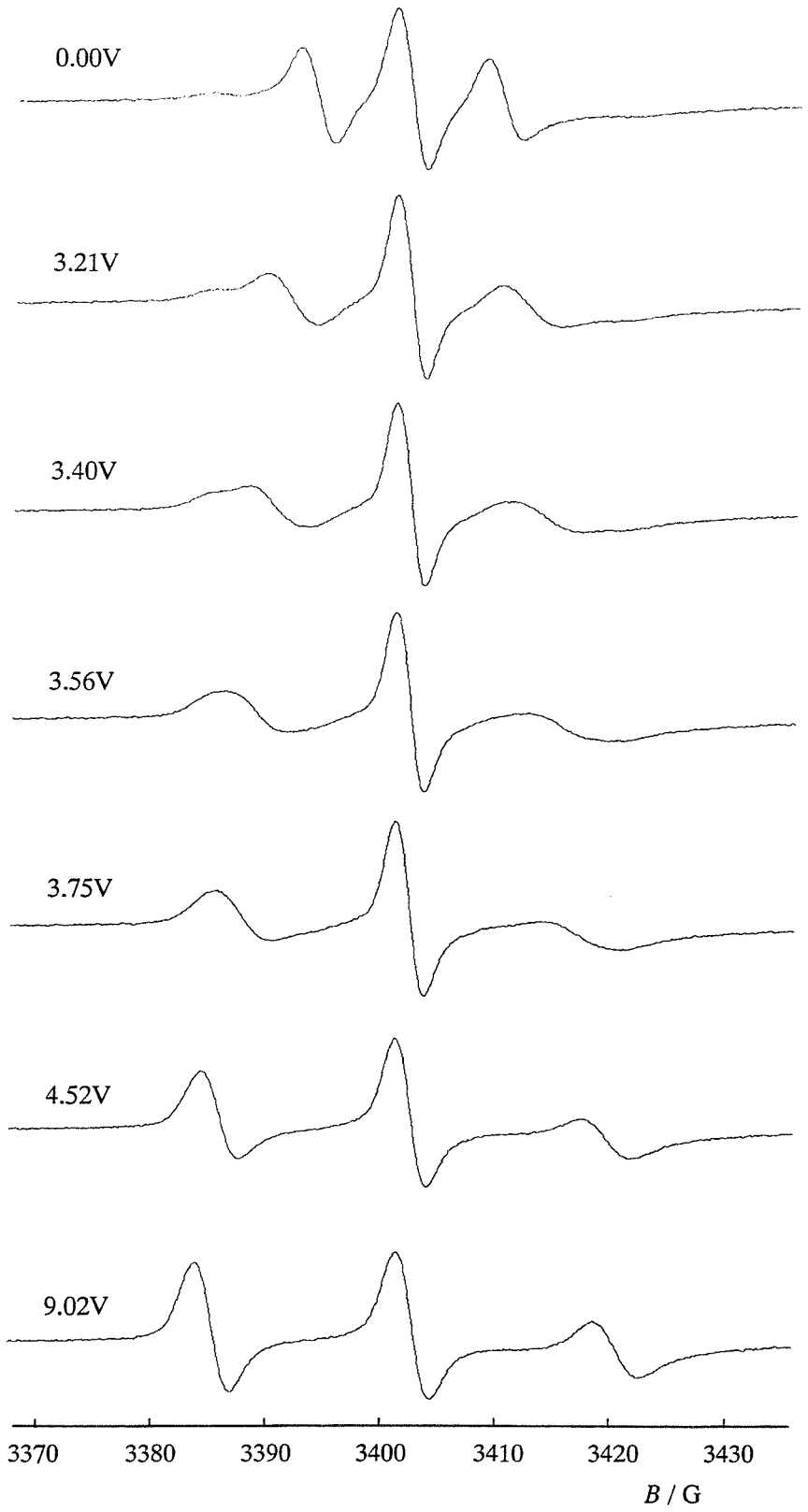

Fig.11 The voltage dependence of the ESR spectra when the angle between the two fields was approximately 84°

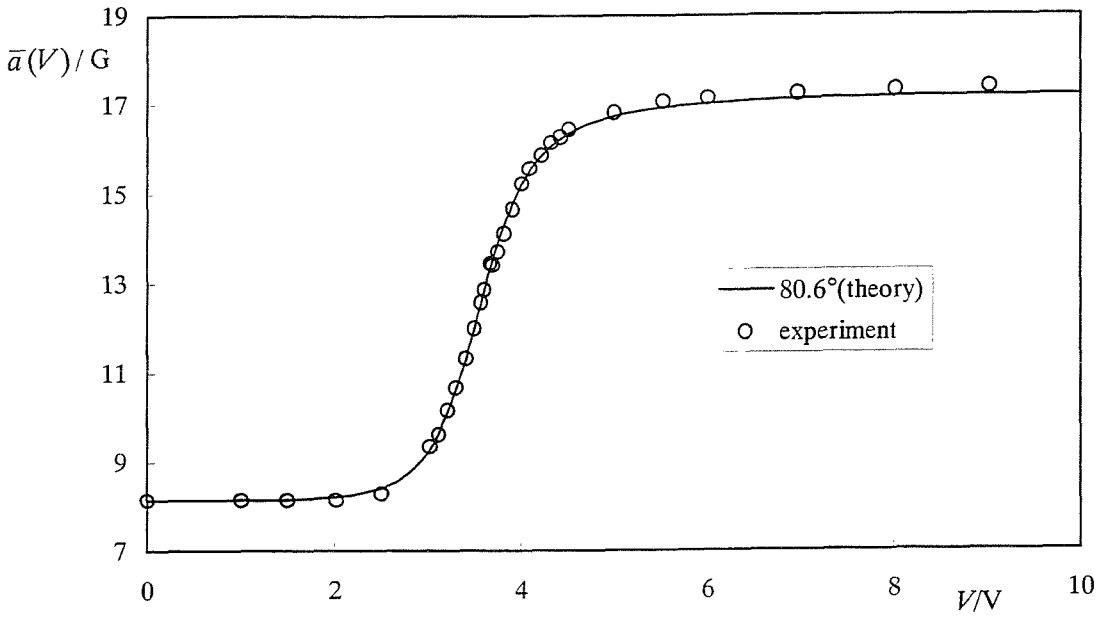

Fig.12 The voltage dependence of the hyperfine splitting when α was set to be approximately 84°

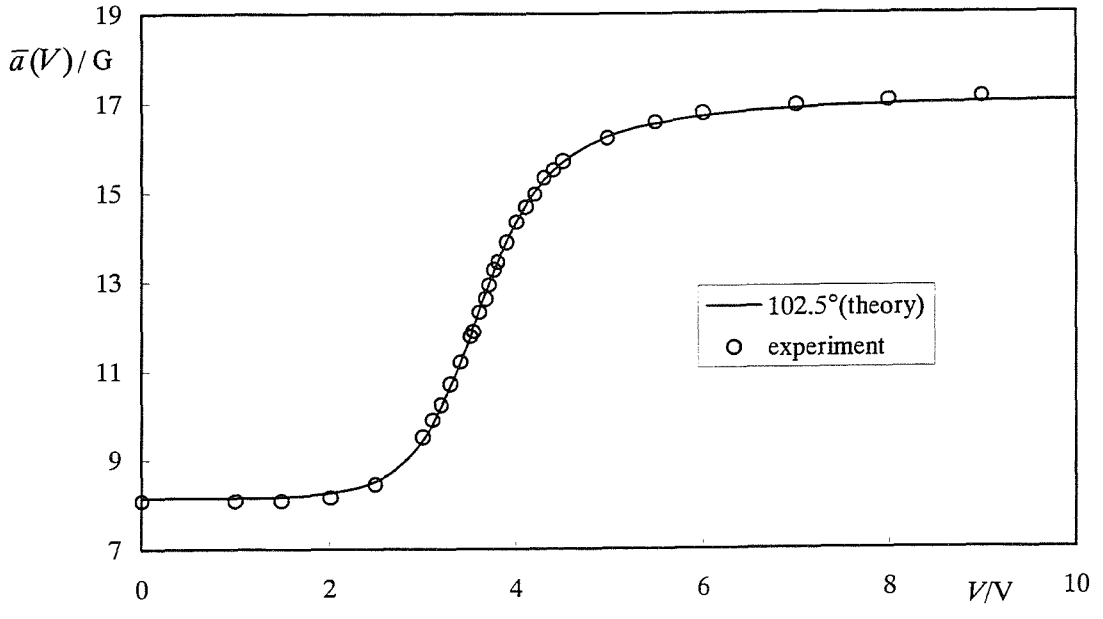

Fig.13 The voltage dependence of the hyperfine splitting when α was set to be approximately 100°

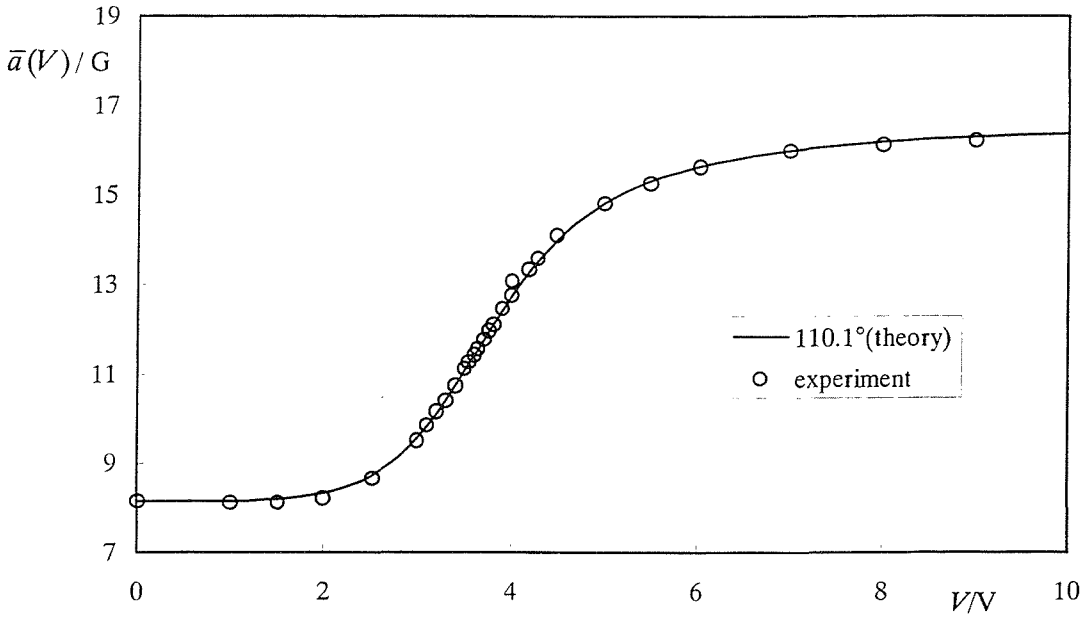

Fig.14 The voltage dependence of the hyperfine splitting when α was set to be approximately 110°

Table 3 Results of fitting

set α /°	fitted $\cos 2\alpha$	fitted α /°	fitted $(\mu_0\varepsilon_0\Delta\tilde{\varepsilon})/(\Delta\tilde{\chi}B^2d^2)$ / $J^{-2}C^2$	fitted $\Delta\tilde{\varepsilon}/\Delta\tilde{\chi}$ /10^6
84	-0.947±0.003	80.6±0.3	0.0768±0.0008	8.2±0.1
90	-0.9937±0.0008	86.9±0.2	0.0742±0.0002	7.9±0.0
100	-0.906±0.005	102.5±0.3	0.0749±0.0010	8.0±0.1
110	-0.763±0.010	110.1±0.4	0.0703±0.0017	7.5±0.2

In Table 3, the errors for the fitted parameter $\cos 2\alpha$ are about 1 % or less and those for the fitted ratio $(\mu_0\varepsilon_0\Delta\tilde{\varepsilon})/(\Delta\tilde{\chi}B^2d^2)$ are about 2.5% or less. These are caused by the error of determining the nitrogen hyperfine splitting from the spectra, which is ±0.068G (1024

data points over the range of 70G). The errors in α obtained from the fitted parameter cos2α are less than 0.5%, these were calculated from those for the fitted cos2α. The errors for the fitted $\Delta\tilde{\varepsilon}/\Delta\tilde{\chi}$ calculated from the fitted ratio $(\mu_0\varepsilon_0\Delta\tilde{\varepsilon})/(\Delta\tilde{\chi}B^2d^2)$ were 2.5% or less. According to Table 3, $\Delta\tilde{\varepsilon}/\Delta\tilde{\chi}$ does not have a clear dependence on α. The average for these values is 7.9×10^6 and the standard deviation is 0.3×10^6 (approximately 4% of the average value). The errors mainly result from the variation of the thickness of the cell over the active area and the director near the surface of the cell which aligns perpendicular to the magnetic field presumably by flow during the filling process. The measurement temperature is ambient temperature (approximately 23°C). The result for $(\mu_0\varepsilon_0\Delta\tilde{\varepsilon})/(\Delta\tilde{\chi}B^2d^2)$ of 7.9×10^6 is in good agreement with the literature value of 7.8×10^6 which is obtained at the slightly lower temperature of 20°C [12,13].

4.5 Summary

In this Chapter, measurement of the diamagnetic anisotropy, $\Delta\tilde{\chi}$, has been discussed. Here, the method used was the field balance method of magnetic and electric fields using ESR spectroscopy to determine the director orientation. The basic idea of this measurement is to monitor the director orientation in an equilibrium state under the competition between the two fields. ESR spectroscopy was used to determine the director orientation. Here we have been mainly concerned with the methodology and the following results were obtained.

The dependence of the hyperfine splitting of the ESR spectrum on the applied voltage to the sample cell was measured.

(1) A steep change was observed when the angle between the two fields was close to 90°. However, the director was not uniform, which might be come from the non-uniform cell thickness.

(2) The larger the deviation of the angle between the two fields from 90°, such as 84°, 100° and 110°, the less steep the change in the hyperfine spacing in the threshold region.

The plots of the hyperfine splitting versus the applied voltage were well fitted by the theory.

(3) The fitted angles between the two fields was slightly shifted from the set angles, for example, the fitted angle was 87° when the set angle was 90°.

(4) The fitted ratio, $\Delta\tilde{\varepsilon} / \Delta\tilde{\chi}$, was almost independent of the angle between the two fields and is in very good agreement with the literature value where each anisotropy was measured individually; $\Delta\tilde{\varepsilon}$ was obtained from capacitance measurements with a planar and perpendicular cell, and $\Delta\tilde{\chi}$ was obtained from the Faraday-Curie method.

(5) The error in $\Delta\tilde{\varepsilon} / \Delta\tilde{\chi}$ was approximately 4% and mainly contributed by the variation of the thickness of the sample cell over the active area in the cavity, and also by the director near the surface of the cell which was aligned perpendicular to the magnetic field by flow during the filling process.

4.6 References

[1] W.H.de Jeu and W.A.P.Claassen; J. Chem. Phys., **68**, 1978, 102.

[2] R.A.Bernheim, T.R.Krugh; J. Amer. Chem. Soc., **89**, 1967, 6784.

[3] P.G. Cummins, D.A. Dunmur and D.A. Laidler; Mol. Cryst. Liq. Cryst., **30**, 1975, 109.

[4] Hp. Schad, G. Baur and G. Meier; J. Chem. Phys., **71**, 1979, 3174.

[5] I.Haller, H.A.Huggins, H.R.Lilienthal and T.R.McGuire; J. Chem. Phys., **77**, 1973, 950.

[6] W.H.de Jeu, W.A.P.Klaassen and A.M.J.Spruijt; Mol. Cryst. Liq. Cryst., **37**, 1976, 269.

[7] H.Kneppe, V.Reifenrath and F.Schneider; Chem. Phys. Lett., **87**, 1982, 59.

[8] P.L.Sherrell and D.A.Crellin; J. Phys. (Paris), **40-C3**, 1979, C3-211.

[9] J.D.Bunning, D.A.Crellin and T.E.Faber; Liq. Cryst., **1**, 1986, 37.

[10] E.Ciampi and J.W.Emsley; Liq. Cryst., **22**, 1997, 543.

[11] W.H.de Jeu; Physical Properties of Liquid Crystalline Materials, Chapter 6, 1980, Gordon and Breach, London.

[12] High resistivity mixtures for active matrix devices, 1st minimum displays Ⅱ, 1990, E. Merck, Darmstadt.

[13] Private communication (Merck Japan).

Chapter 5

The Effect of Dopants on the Twist Elastic Constant and the Rotational Viscosity Coefficient for Nematics Studied by Dynamic Light Scattering

5.1 Introduction

The twist elastic constant and the rotational viscosity coefficient are important physical properties which determine the performance of liquid crystal displays (the response times and the threshold voltage), especially the in-plane switching mode as described in Chapter 1. For the rotational viscosity, we have discussed the effect of dopants on this and on its temperature dependence using the ESR technique to determine γ_1 (see Chapters 2, 3, 4). The twist elastic constant can be measured by a few techniques, such as the Freedericksz transition [1] and dynamic light scattering [2]. In the former method, the twist elastic constant is determined by measuring the threshold magnetic field applied parallel to a sample cell where the liquid crystal has a uniform planar alignment [3,4]. It is also possible to determine the twist elastic constant by measuring the threshold voltage applied perpendicular to the surface of the sample cell, but this measurement requires a twist alignment cell together with a uniform planar alignment cell. On the other hand, the dynamic light scattering method in the presence of a stabilizing electric field allows us to measure both the twist elastic constant and the rotational viscosity coefficient at the same time using a single cell [5]. Therefore, we can obtain the twist elastic constant for a nematic liquid crystal and, at the same time, we can compare the rotational viscosity coefficient determined by this method with that obtained by the ESR method. The aim of the work described in this Chapter is to investigate the twist elastic constant together with the rotational viscosity coefficient by the dynamic light scattering method. The materials

studied are the same as those used in the previous Chapters; this means that a comparison between values by the two methods can be made. Because these materials decrease T_{NI} of the base mixture, a dopant which increases T_{NI} of the base mixture was also used in this investigation to discuss its effect on both the rotational viscosity coefficient and the twist elastic constant.

5.2 Theory

Thermal fluctuations of the director of liquid crystals combined with their birefringence causes strong scattering of light [6]. According to the Orsay group [2,7], light scattering by nematic liquid crystals produces a Lorentzian lineshape broadening by two overdamped director modes. The first mode (Mode 1) is due to a combination of splay and bend elastic distortions, and the second mode (Mode 2) is due to a combination of twist and bend elastic distortions. The linewidth resulting from Modes 1 and 2 are given by [8,9]:

$$\Gamma_1 = \frac{K_1 q_\perp^2 + K_3 q_\parallel^2}{\gamma_1 - \beta}, \tag{1}$$

$$\Gamma_2 = \frac{K_2 q_\perp^2 + K_3 q_\parallel^2}{\gamma_1 - \delta}, \tag{2}$$

where

$$\beta = \frac{2(q_\perp^2 \alpha_3 + q_\parallel^2 \alpha_2)^2}{q_\perp^4(\alpha_2 + 2\alpha_3 + \alpha_4 + \alpha_5) + 2q_\perp^2 q_\parallel^2(\alpha_1 + \alpha_3 + \alpha_4 + \alpha_5) + q_\parallel^4(-\alpha_2 + \alpha_4 + \alpha_5)} \tag{3}$$

and

$$\delta = \frac{2\alpha_2^2 q_\parallel^2}{q_\perp^2 \alpha_4 + q_\parallel^2(\alpha_4 + \alpha_5 - \alpha_2)}. \tag{4}$$

In these equations, K_i (i=1,2,3) are the splay, twist and bend elastic constants, α_i (i=1,2,3,4,5) are the Leslie viscosity coefficients, γ_1 is the rotational viscosity ($\gamma_1=\alpha_3-\alpha_2$) and $q_\perp$ and $q_\parallel$ are the scattering vectors perpendicular and parallel to the director, respectively.

In this Chapter, where only the twist elastic constant K_2 and the viscosity coefficient γ_1 will be discussed, we shall concentrate just on the line broadening caused by Mode 2 (see equation (2)). Although equation (2) contains terms other than the twist elastic constant and the rotational viscosity, it can be a simplified if the director alignment and scattering geometry are chosen such that $q_\parallel$ is zero. For example, the twist mode can be isolated by using a homeotropically aligned director, vertically polarised incident light, horizontally polarised scattered light and scattering angles less than 15° for which $(q_\parallel / q_\perp)^2 << 1$. This scattering geometry is shown in Fig.1. In this case, the width of the Lorentzian line for Mode 2 is given simply by

$$\Gamma_2 = \frac{K_2 q_\perp^{\,2}}{\gamma_1}. \tag{5}$$

In this expression the wavevector $q_\perp$ is given by

$$q_\perp = \frac{2\pi}{\lambda} n_{\text{air}} \cos\theta\,, \tag{6}$$

where λ is the wavelength of the incident light (632.8nm), n_{air} is the index of refraction for air which is nearly equal to 1 and θ is the scattering angle measured in the laboratory frame.

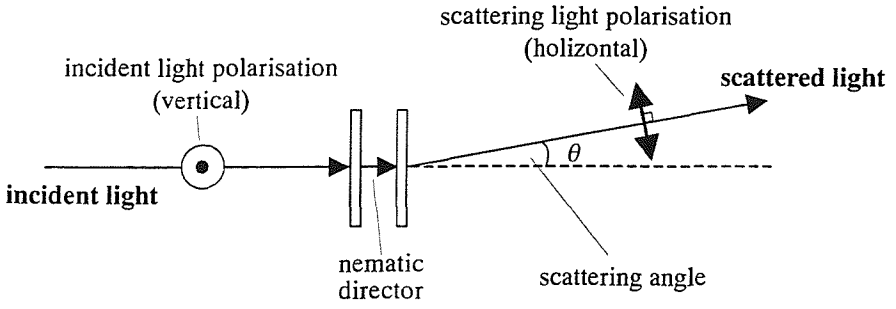

Fig.1 The simplified scattering geometry

According to equation (5), the ratio of the elastic constant to the viscosity coefficient, K_2/γ_1, is obtained by measuring the linewidth. However, what we wish to discuss in this Chapter are the individual values of K_2 and γ_1. In order to obtain these, the distortion free energy of the director fluctuations should be modified by the application of a stabilising external field. Applying an electric field to the nematic is experimentally the easiest way [5]. When the field is applied parallel to the nematic director for materials with $\Delta\tilde{\varepsilon} > 0$, equation (2) becomes

$$\Gamma_2 = \frac{K_2 q_\perp^2 + K_3 q_\parallel^2}{\gamma_1 - \delta} + \frac{\varepsilon_0 \Delta\tilde{\varepsilon} E^2}{\gamma_1 - \delta}. \tag{7}$$

Using the same director alignment and the scattering geometry described previously, equation (7) can be further simplified to give

$$\Gamma_2 = \frac{K_2 q_\perp^{\,2}}{\gamma_1} + \frac{\varepsilon_0 \Delta\tilde{\varepsilon}}{\gamma_1} E^2. \tag{8}$$

Therefore, by plotting the Γ_2 as a function of E^2, γ_1 and K_2 will be obtained individually provided the dielectric anisotropy $\Delta\tilde{\varepsilon}$ is known.

5.3 Experimental

5.3.1 Sample Preparation

The nematic samples used in this Chapter are partly the same as those investigated in Chapter 3, that is 5(O)CB and 5(O)PCP as dopants (their chemical structures are shown in Chapter 3) and ZLI-4792 as the base mixture. The concentration of these dopants was about 10wt% which is approximately 13mol%. As we saw in Chapter 3, all of the dopants decrease the nematic-isotropic transition temperature, T_{NI}, of the base mixture. In addition, 4-pentyl-4'-cyanobiphenylcyclohexane (5CBC) was used as another dopant. Although this mesogen has the same cyanobiphenyl structure as 5CB, the additional cyclohexyl ring causes a major increase in T_{NI} which is 219°C in comparison with 35°C for 5CB. As T_{NI} of ZLI-4792 is 92°C, adding 5CBC increases T_{NI} significantly while the addition of 5CB decreases T_{NI} to a lesser extent than the increase caused by 5CBC. Therefore, these cyanobiphenyl derivatives form the basis for a good comparison for the temperature dependence of the elastic constants and the rotational viscosity coefficient. The temperature dependence of the effect of the dopants 5CBC and 5CB on the elastic constants and the rotational viscosity coefficient was investigated at various concentrations. These mixtures differ slightly from those studied by ESR spectroscopy in that they do not contain the nitroxide spin probe. The procedure of making the mixture is the same as that in Chapter 3, that is, the weight of the dopant is measured and a given weight of base mixture, ZLI-4792, was added to it to make the desired concentration. Then the mixture was repeatedly heated above T_{NI} and shaken well to be uniformly mixed. The concentrations used were approximately 10wt%, 15wt% and 23wt%, which are approximately 13mol%, 20mol% and 29mol% for 5CB, and 10mol%, 16mol% and 24mol% for 5CBC, respectively.

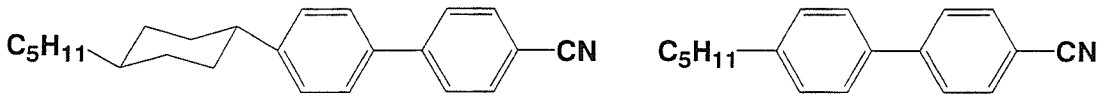

Fig. 2 The chemical structures of 5CBC (left) and 5CB

5.3.2 Sample Cell Preparation

In the work described in this Chapter, two kinds of sample cell were used; one was for the measurement of the dielectric anisotropy and the other for the dynamic light scattering measurement. The dielectric anisotropy, $\Delta\tilde{\varepsilon}$, for each sample needs to be measured in order to obtain the twist elastic constant, K_2, and the rotational viscosity coefficient γ_1 individually from the dynamic light scattering results, as discussed in the previous section. The dielectric anisotropy was measured at the same temperature as the dynamic light scattering experiment using cells with uniform planar alignment [10]. The structure of the cells used for measuring $\Delta\tilde{\varepsilon}$ is shown in Fig.3, the basic procedure of the cell fabrication is described in Chapter 3. The uniform planar alignment was achieved using a polyimide alignment film (Hitachi Chemicals). An NMP (N-methylpirolidone) solution (about 5% by weight) of the alignment film was spin coated onto the faces of the glass plates with the patterned ITO transparent electrode. Then they were cured in an oven at 250°C for 30 minutes. Next, the surface of the polyimide film was rubbed in one direction by a rubbing roller coated with a synthetic cloth. Then two of the glass plates were sandwiched together so that the rubbing directions are anti-parallel. The cell thickness was measured in the same way as described in Chapter 3; it varied from 40 to 45 μm depending on the cell when 40μm glass fibres were used as the spacers. The uniformity of the cell thickness was evaluated using a sodium light source (589nm) and there were a few interference lines observed over the ITO electrode. Because two interference lines were observed in an area of the cell, the cell gap variation for this area is approximately 0.6 μm, a cell which

has a few interference lines may have the uniformity within 1 or 2μm. Finally, the nematic mixtures described in section 5.3.2 were filled into the cells by capillary action.

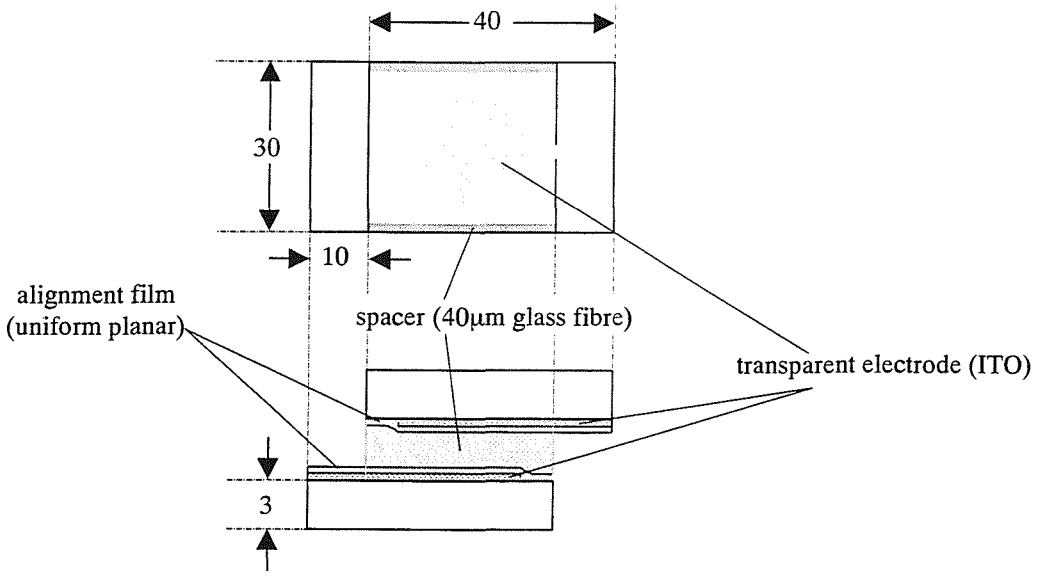

Fig.3 Structure of the cell used in the dielectric measurement

(the sizes of the cell are in mm)

Cells with homeotropic alignment were used for the dynamic light scattering measurements. Fig.4 shows the structures of these cells. The main differences with this cell fabrication compared to that for the dielectric measurement cells are the alignment direction, the electrode pattern and the sizes of the glass plates. The cell size fits the temperature-controlled sample holder of the light scattering apparatus. Polyimide film (50μm) or glass fibre (40μm) was used for the spacer. Because the director should be aligned homeotropically for the measurement, the surface treatment used was a homeotropic alignment film. A solution with about 5 wt% of NMP, an alignment film [11], was spin coated onto the face of the glass plate coated with the ITO transparent electrode (not patterned) and they were cured in an oven at 200°C for 15 minutes. The resulting films were not rubbed. The individual cell thickness ranged from 60 to 70μm for the cells

with the polyimide spacer and from 40 to 45μm for the cells with the glass fibre spacer. The uniformity of the cell thickness was evaluated in the same way as for the other cells; there were no interference lines observed in the measuring area (1 or 2 mm diameter), which indicates that the thickness variation was less than 0.6 μm over the measuring area since the wavelength of the light source is approximately 0.6μm. The quality of the homeotropic alignment was checked with the cells between crossed polarisers. The cells filled with a liquid crystal sample looked black when viewed orthogonal to the surface, which confirms that all of the cells used had good homeotropic alignment. A pair of conducting wires were soldered to the electrodes to allow a voltage to be applied.

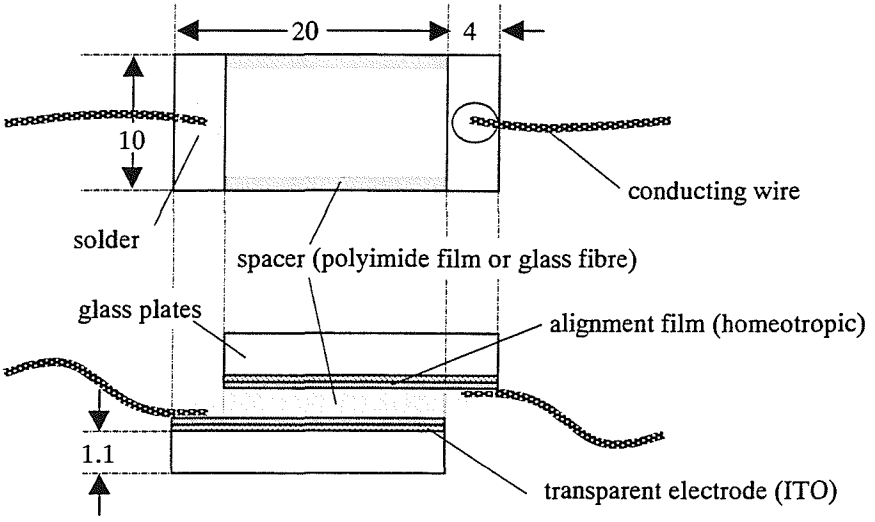

Fig.4 Structure of the cell used in the dynamic light scattering measurement (the sizes of the cell are in mm)

5.3.3 Dielectric Anisotropy Measurement

The dielectric anisotropy of a sample was obtained by measuring the voltage dependence of the capacitance of a sample in the cell described in the previous section. As the voltage applied to the cell increases, the director orientation of the nematic changes non-uniformly because of the strong anchoring condition which causes the change of the dielectric constant of the nematic throughout the cell. Therefore, by measuring the voltage dependence of the capacitance, we can obtain information of the voltage dependence of the dielectric constant and thus the dielectric anisotropy. The principle of the measurement is described elsewhere [10,12] and the background theory will be described briefly later. The voltage dependence of the capacitance was measured with an LCR meter with a built-in amplifier (Hewlett Packard HP4284A) which was controlled by a personal computer. The applied voltage was a 1 kHz square wave, produced by the LCR meter, for all of the dielectric measurements. The capacitance was independent of frequency at least for the range 100 Hz to 10 kHz. The range of the applied voltage was from 0 to 20 V, and this was changed in steps of 0.025 V in the range where the capacitance changes significantly with the voltage and in steps of 0.1V in the other voltage range. The sample was placed in an oven and the temperature was precisely controlled (with an accuracy of less than 0.1°C). Because a cell has its own floating capacitance, this was measured for each cell by the following procedure. First, the capacitance of the empty cell (filled with air) was measured. Then the cell was filled with a liquid with known dielectric value and the capacitance was measured. The floating capacitance C_f can then be calculated from

$$C_f = \frac{\varepsilon_{liq} C_{air} - \varepsilon_{air} C_{liq}}{\varepsilon_{liq} / \varepsilon_{air}}, \tag{9}$$

where ε_{liq} and ε_{air} are the dielectric values for the liquid and air, respectively; C_{liq} and C_{air} are the capacitance values for the cells filled with the liquid and air, respectively. Then the liquid was removed from the cell and the voltage dependence of the capacitance was measured after the cell was filled with the nematic sample. The floating capacitance

calculated from equation (9) for each cell was subtracted from all of the measured capacitance values for the samples. Cyclohexane was used as the liquid in this experiment because it does not affect the properties of the alignment film significantly and is easy to remove from the cell by flushing with air.

The dielectric anisotropy was measured by the following method. The threshold voltage V_c in the voltage-capacitance dependence for a nematic sample in a cell, with strong anchoring conditions, is given by [10,12]

$$V_c = \pi\left(\frac{K_1}{\varepsilon_0 \Delta\tilde{\varepsilon}}\right)^{\frac{1}{2}}, \tag{10}$$

where K_1 is the splay elastic constant. The voltage dependence of the capacitance is given by

$$\frac{C}{C_\perp} - 1 = \zeta - \frac{2\gamma}{\pi}(1+\zeta\psi_m^{\,2})^{\frac{1}{2}} \frac{V_c}{V} \int_0^{\psi_m} \left\{ \frac{(1+\kappa\psi^2)(1-\psi^2)}{(1+\zeta\psi^2)(\psi_m^{\,2}-\psi^2)} \right\}^{\frac{1}{2}} d\psi, \tag{11}$$

where

$$\psi = \sin\theta,$$

$$\psi_m = \sin\theta_m,$$

C is the capacitance of the sample in the cell and $C_\perp$ is the capacitance when the applied voltage V is less than V_c, θ is the tilt angle of the nematic director from the surface of the substrate which varies throughout the cell thickness and θ_m is the largest value of θ. The parameters ζ and κ are given by

$$\zeta = \Delta\tilde{\varepsilon} / \tilde{\varepsilon}_\perp \tag{12}$$

and

$$\kappa = K_3 / K_1 - 1, \tag{13}$$

in which $\tilde{\varepsilon}_\perp$ is the dielectric constant perpendicular to the director and K_3 is the bend

elastic constant. When the voltage applied to the cell is high enough to make the director essentially parallel to the electric field (i.e. θ=90°), equation (11) can be simplified to

$$\frac{C}{C_{\perp}} \cong \zeta + 1 - \frac{2\zeta}{\pi}(1+\zeta)^{\frac{1}{2}} \frac{V_c}{V} \int_0^1 \left(\frac{1+\kappa\psi^2}{1+\zeta\psi^2} \right)^{\frac{1}{2}} d\psi \qquad (14)$$

According to this result, a plot of $C/C_{\perp}$ against V_c/V is linear, so ζ ($= \Delta\tilde{\varepsilon}/\tilde{\varepsilon}_{\perp}$) can be obtained from the intercept of the line. $\varepsilon_{\perp}$ is obtained from the ratio of the capacitances of the cells with and without the sample when V is less than V_c. From this method, the elastic constants K_1 and K_3 could be obtained from the slope of the line, however, we shall not discuss these elastic constants in this Chapter.

5.3.4 Dynamic Light Scattering Measurement

A photon correlation spectrometer [13,14] was used to measure the linewidth Γ_2; this system is shown schematically in Fig.5. The light source used is a He-Ne gas laser (the power output is about 10 mW). The sample cell was placed in the temperature-control unit which can vary the temperature from ambient temperature (25 °C) to 200 °C. The accuracy of the temperature was 0.05±°C from the ambient temperature to at least 60 °C, which is the highest temperature of our experiment, for the typical measurement time of 30 minutes. A half wavelength plate (λ/2 plate) and polariser sheet (P) are available to be rotated to choose the appropriate polarisation of the input light for the determination of either Γ_1 or Γ_2. Because the main purpose for this experiment was to measure γ_1 and K_2, the determination of Γ_2 with vertically polarised input light was required. The analyser (AN) was used to define the polarisation of the scattered light in the horizontal scattering plane. The detector, a photo multiplier tube (PMT), was mounted in order to capture the scattered light in the direction of the scattering angle θ defined with respect to the direction of the incident beam. Then the output signal from the PMT was amplified by the amplifier system (pre-amplifier and amplifier) and any small noise was eliminated by the discriminator to improve the signal-to-noise ratio. The output of the discriminator was fed

into the correlator system. The correlator counts the number of photomultiplier output pulses, $n(t)$, arriving during a fixed time interval, Δt, that is much less than the average time of the fluctuation due to the director motion, and then it produces a digital representation of the autocorrelation function given by [14]

$$C(m\Delta t) = \langle n(t)n(t + m\Delta t)\rangle = \lim_{T \to \infty} \frac{1}{T}\int_0^T n(t)n(t + m\Delta t)dt\,, \tag{15}$$

where $m\Delta t$ is the delay time for the m^{th} channel of the correlator. The correlator output was collected and fitted to a single exponential decay as the theory predicts [2]. The linewidth Γ_2, which is the final aim of this measurement, is obtained as the inverse of the time constant of this exponential correlation function. At low scattering angles, it is difficult to avoid static scattering from surface imperfections, etc. If only the scattered light due to the director fluctuation is detected, which is called the homodyne mode, such spurious signals affect the linewidth. To solve this problem, the heterodyne beam, a static light beam which usually comes from the same laser light source, was combined with the dynamic scattered light. If the intensity of the heterodyne beam is about 25 times or more the dynamic scattering intensity, the spurious signals become negligible and the fully heterodyned linewidth is determined. The fully heterodyned linewidth is half the value of the pure homodyne linewidth. In this light scattering apparatus, the heterodyne beam was split from the input beam via the beam splitter (BS). Then this reference signal was combined with the scattered signal after the sample by the recombination beam splitter (RBS).

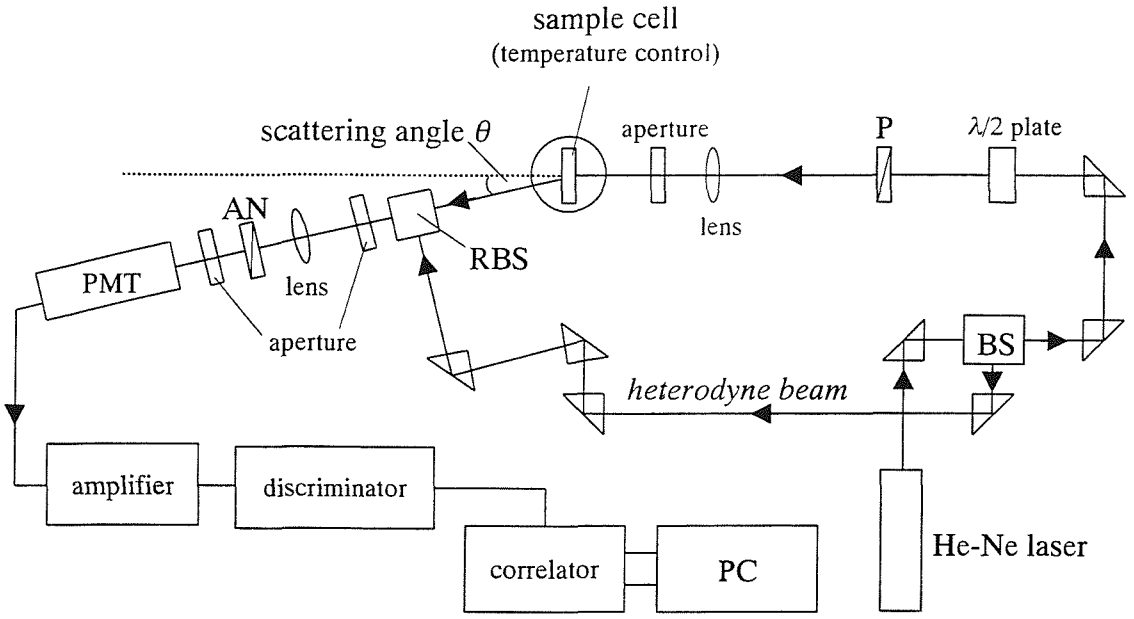

Fig.5 The dynamic light scattering apparatus

5.3.5 The Rotational Viscosity Coefficient and the Twist Elastic Constant for 5CB

First, the rotational viscosity coefficient and the twist elastic constant for 5CB were measured to test the methodology. Fig.6 shows the relationship between the linewidth and the square of the applied electric field, determined at 28.4 °C to facilitate comparison with earlier measurements [13,14]. The scattering angle chosen was 14 ° and the frequency of the applied field was 10 kHz. In the earlier measurements [13], the frequency dependence of the linewidth was examined from 1Hz to 15Hz and no changes were observed over this frequency region. These values of the scattering angle and the frequency of the applied field were used for all of the measurements described here. Because the plot shows a straight line as expected from the theory (see equation (8)), the slope and the intercept were calculated using a least squares fit to a straight line. From the intercept we find $(K_2/\gamma_1)q_\perp^{\,2} = 3.20\times10^2\ s^{-1}$ and the standard deviation is 3.22 s^{-1} which is about 1 % of the intercept value. From the slope we determine $\varepsilon_0\Delta\tilde{\varepsilon}/\gamma_1 = 1.89\times10^{-9}\ m^2V^{-2}s^{-1}$ and the

standard deviation is 2.12×10^{-11} $m^2V^{-2}s^{-1}$ which is about 1.1% of the slope value. γ_1 and K_2 can then be calculated from equation (8). These values are shown in Table 1 using the dielectric anisotropy value, $\Delta\tilde{\varepsilon}$, of 12.4 at 28.4 °C which has a ±0.5 % accuracy [15]. The experimental error for this experiment is estimated as approximately 2 % for γ_1 and approximately 3 % for K_2, however, this error depends strongly on the linearity in the plot of Γ_2 versus E^2. Table 1 also shows the literature values together with the γ_1 value which was obtained by the ESR experiment (see Chapter 2). The literature value for γ_1 is obtained by the rotating field method where the torque is directly measured [16,17]. The literature value for K_2 is obtained by measuring the Freedericksz transition for the twist deformation using a conoscope [18]. As the results in the Table 1 show, the values of K_2 and γ_1 for this system are in good agreement with their literature values and the value determined by ESR.

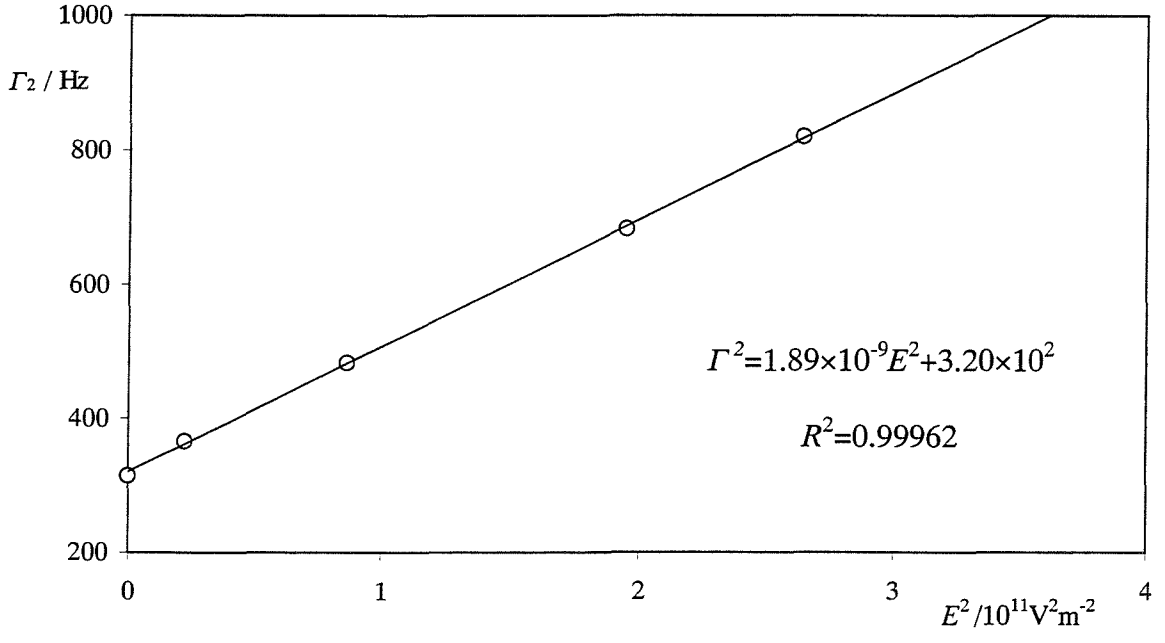

Fig.6 The dependence of the linewidth on the square of the electric field for 5CB at 28.4 °C

Table1 Values for γ_1 and K_2 obtained for 5CB

	This work	literature value	ESR value
γ_1/mPa·s	58.2 (28.4 °C)	60.7 (29.0 °C)[16] 58 (28.7 °C)[17]	54.4 (30.8 °C)
K_2/N	3.23×10^{-12} (28.4 °C)	3.2×10^{-12} (28.7 °C)[18]	—

5.4 Results and Discussion

5.4.1 The Effect of Dopants on the Nematic-Isotropic Transition Temperature

The effect of 5(O)CB and 5(O)PCP on the nematic-isotropic transition temperature T_{NI} was described in Chapter 3 and it is clear that both of these dopants decrease T_{NI} of the base mixture, ZLI-4792. However, the effect of adding 5CBC to ZLI-4792 is qualitatively different as we can see from Fig.7, now because T_{NI} of 5CBC is higher than that of the base mixture, T_{NI} increases with the concentration of 5CBC whilst, in comparison, the addition of 5CB decreases T_{NI}. In Fig.7 the solid lines indicate the temperature at which the isotropic phase first appears which we named T_N and the dashed lines indicate the temperature at which the nematic phase disappears, that is T_I; thus the area between the solid and dashed lines corresponds to the biphasic region. We have found that these lines are not linear over the entire concentration range. As predicted by the Humphries-James-Luckhurst theory [19], T_{NI} of a binary mixture is given by

$$T_{NI}^{mixture} = xT_{NI}^{A} + (1-x)T_{NI}^{B}, \tag{16}$$

where T_{NI}^{A}, T_{NI}^{B} and $T_{NI}^{mixture}$ are the T_{NI} for component A, component B and the resulting mixture, respectively and x is the mole fraction of component A. In this experiment, T_{NI}^{A} and T_{NI}^{B} correspond to T_{NI} of a dopant and the base mixture, respectively. According to equation (16) the dependence of T_{NI} on the mole fraction of a dopant should be linear.

This ideal case occurs when the three intermolecular energy parameters, ε_{AA}, ε_{BB} and ε_{AB}, are related by the geometric mean approximation

$$\varepsilon_{AB} = (\varepsilon_{AA}\varepsilon_{BB})^{\frac{1}{2}}. \tag{17}$$

However, the lines in Fig.7 show negative deviations, which may indicate that equation (17) is not obeyed by this system. According to Humphries et al. [19], a negative deviation indicates

$$\varepsilon_{AB} < (\varepsilon_{AA}\varepsilon_{BB})^{\frac{1}{2}}. \tag{18}$$

Therefore, the intermolecular energy parameter for the mixture in this experiment is predicted to be less than that from the geometric mean rule.

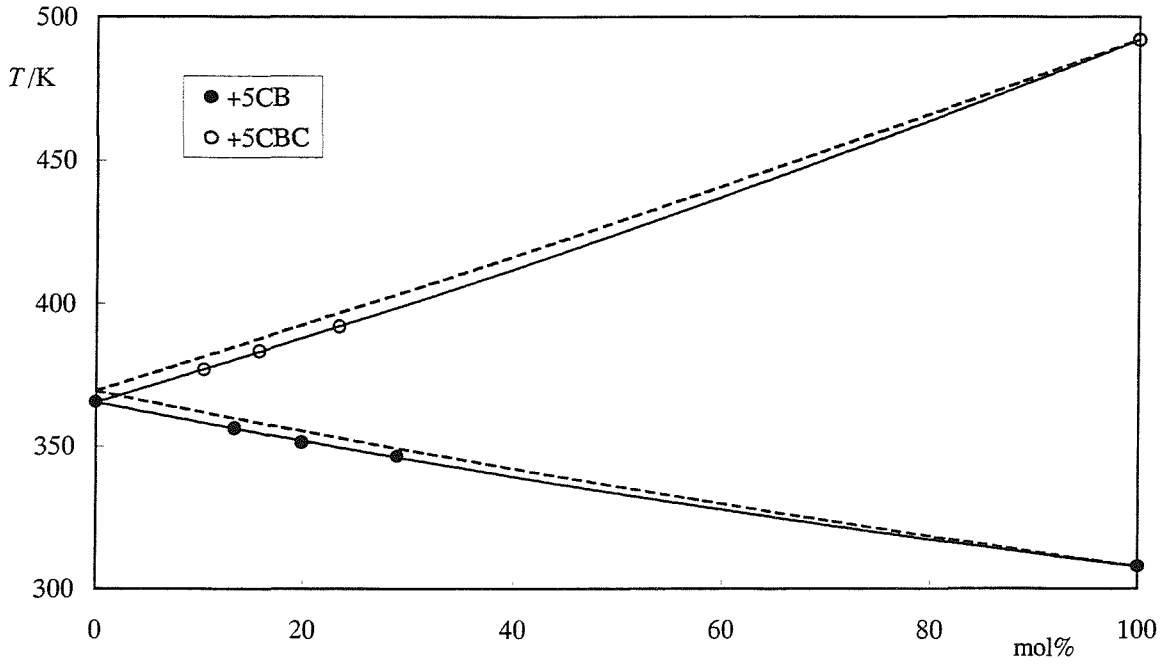

Fig.7 The effect of the dopants 5CB and 5CBC on T_{NI} of ZLI-4792

5.4.2 Temperature Dependence of the Dielectric Anisotropy

The dielectric anisotropy, $\Delta\tilde{\varepsilon}$, for each sample was also measured. The results will be used later for the determination of K_2 and γ_1 from the dynamic light scattering

measurement. $\Delta\tilde{\varepsilon}$ of a polar nematogen measured at a low frequency such as 1 kHz (which is essentially the static measurement) contains contributions from the polarisability anisotropy for a single molecule, $\Delta\alpha$, the permanent dipole moment, μ, and the second rank orientational order parameter, $\overline{P}_2$, by [20]

$$\Delta\tilde{\varepsilon} = \frac{NhF}{\varepsilon_0}\left[\Delta\alpha - \frac{F\mu^2}{2k_BT}\left(1-3\cos^2\beta\right)\right]\overline{P}_2, \tag{19}$$

where N is the number of the molecules per unit volume, k_B is the Boltzmann constant, T is the absolute temperature, β is the angle between the long axis of the molecule and the dipole moment, and h and F are given by

$$h = \frac{3\bar{\varepsilon}}{2\bar{\varepsilon}+1}, \tag{20}$$

and

$$F = \left[1-\bar{\alpha}\left(\frac{\bar{\varepsilon}-1}{2\pi\varepsilon_0 a^3\left(2\bar{\varepsilon}+1\right)}\right)\right]^{-1}, \tag{21}$$

in which $\bar{\varepsilon}$ is the average of the dielectric constants, $\bar{\alpha}$ is the average of the polarisability, a is the radius of the spherical cavity. Because $\Delta\tilde{\varepsilon}$ is essentially proportional to $\overline{P}_2$ as equation (19) shows and $\overline{P}_2$ is predicted to be a universal function of the reduced temperature, T/T_{NI} [21], the effect of the dopants on $\Delta\tilde{\varepsilon}$ should be compared at the same reduced temperature. Although this is theoretically correct only for a single component system, we assume it is also appropriate for our more complicated mixture. Fig.8 shows the dependence of $\Delta\tilde{\varepsilon}$ on the reduced temperature for ZLI-4792 together with 5(O)CB and 5(O)PCP dissolved in ZLI-4792, the concentration of these dopants is approximately 10wt%. The lines are shown as a guide to the eye as are those in the other graphs. As the results in Fig.8 show, the dopants increase $\Delta\tilde{\varepsilon}$ of ZLI-4792 significantly since they have a strong polarity and the components of ZLI-4792 are mainly fluorinated molecules and so have a weaker polarity than the dopants. From Fig.8, the increasing order of the effect of the polar groups is 5OCB, 5CB, 5OPCP and 5PCP, and

the alkoxy group of these compounds makes $\Delta\tilde{\varepsilon}$ larger than for those with an alkyl group. Figs.9 (a) and (b) shows the dependence of $\Delta\tilde{\varepsilon}$ on the reduced temperature for 5CBC and 5CB dissolved in ZLI-4792. Because these dopants are also cyano compounds which have a higher polarity than the components of ZLI-4792 (see Chapter 3), they increases $\Delta\tilde{\varepsilon}$ significantly as the amount of the dopants increases.

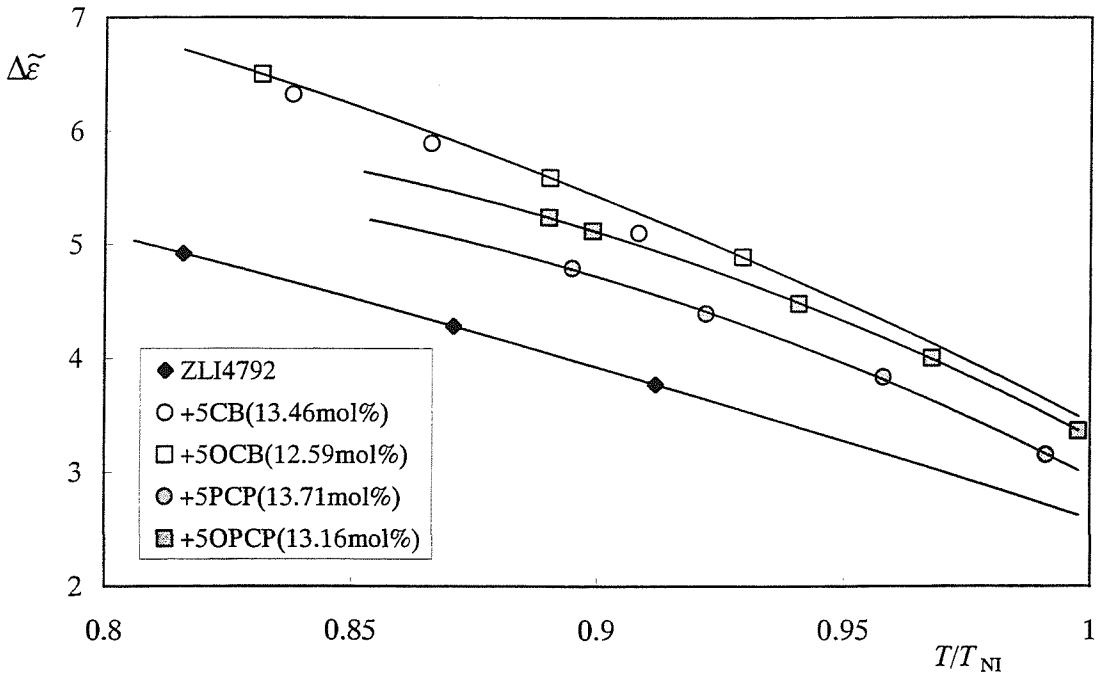

Fig.8 The dependence of the dielectric anisotropy on the reduced temperature for 5(O)CB and 5(O)PCP dissolved in ZLI-4792

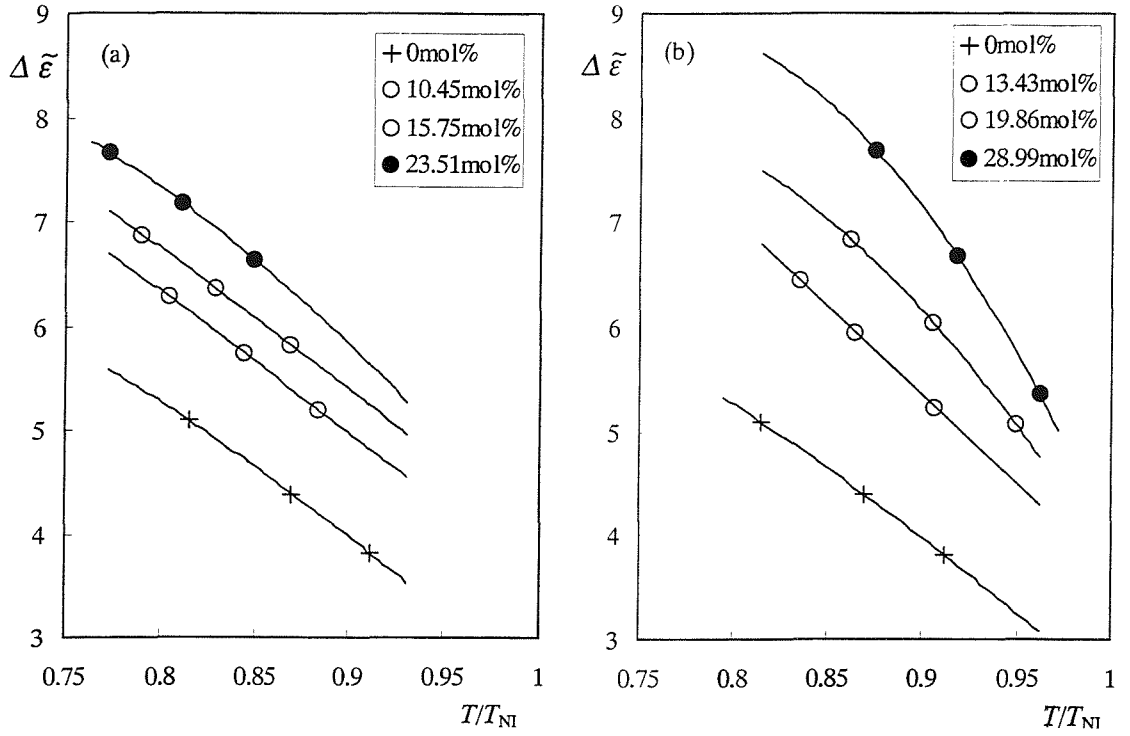

Fig.9 The dependence of the dielectric anisotropy on the reduced temperature; for (a)5CBC and (b)5CB dissolved in ZLI-4792

To compare the effect of adding dopants, the dependence of $\Delta\tilde{\varepsilon}$ on the concentration of the dopants for three values of the reduced temperature are shown in Fig.10. Here we can see that the effect of dopants is clearly different between 5CBC and 5CB. The effect of adding 5CB is essentially linear, while that of 5CBC shows a negative deviation from linearity. To try to explain this difference in behaviour, we will discuss the expected dependence on the mole fraction of a dopant on $\Delta\tilde{\varepsilon}$. Because $\Delta\tilde{\varepsilon}$ is proportional to the order parameter, $\overline{P}_2$, as predicted from equation (19), $\Delta\tilde{\varepsilon}$ of the mixture system might be expected to be given by

$$\Delta\tilde{\varepsilon} = x\Delta\varepsilon_A\overline{P}_2^A + (1-x)\Delta\varepsilon_B\overline{P}_2^B, \tag{22}$$

where $\Delta\varepsilon_A$ and $\Delta\varepsilon_B$ are the effective dielectric anisotropies of a single molecule for component A and component B, respectively, $\overline{P}_2^A$ and $\overline{P}_2^B$ are the second rank order parameters for component A and component B, respectively, and x is the mole fraction of

component A. In this experiment, component A corresponds to the dopant (5CB or 5CBC) and component B corresponds to the base mixture, ZLI-4792. Here, we assume equation (22) is valid for this complicated system even though component B is already a mixture. Because the plots in Fig.10 are obtained at the same reduced temperature, $\overline{P}_2^A$ and $\overline{P}_2^B$ are predicted to be constant since the order parameter should be a universal function of the reduced temperature. In addition, $\Delta\varepsilon_A$ and $\Delta\varepsilon_B$ are expected to be temperature independent. Therefore, $\Delta\varepsilon_A\overline{P}_2^A$ and $\Delta\varepsilon_B\overline{P}_2^B$ are expected to be individually constant and so the plots of $\Delta\tilde{\varepsilon}$ versus the mole fraction should exhibit a linear behaviour. The effect of adding 5CB to ZLI-4792 on $\Delta\tilde{\varepsilon}$ agrees with this. However, such linearity does not hold for the addition of 5CBC to ZLI-4792. It may be because $\Delta\varepsilon_A$ is not constant and $\Delta\varepsilon_A$ becomes smaller as the mole fraction of 5CBC increases. A possible explanation for this is that 5CBC is more likely to be dimerised than 5CB in the base mixture and that the number of dimers changes with.

Fig.11 shows the same plots of $\Delta\tilde{\varepsilon}$ versus the mole fraction, but for three absolute temperatures. These show the deviation for 5CB which is different from the plots in Fig.10. This may be because of the depression of the orientational order parameter from that of the base mixture. For 5CBC, the plots in Fig.11 exhibit a greater deviation than that in Fig.10.

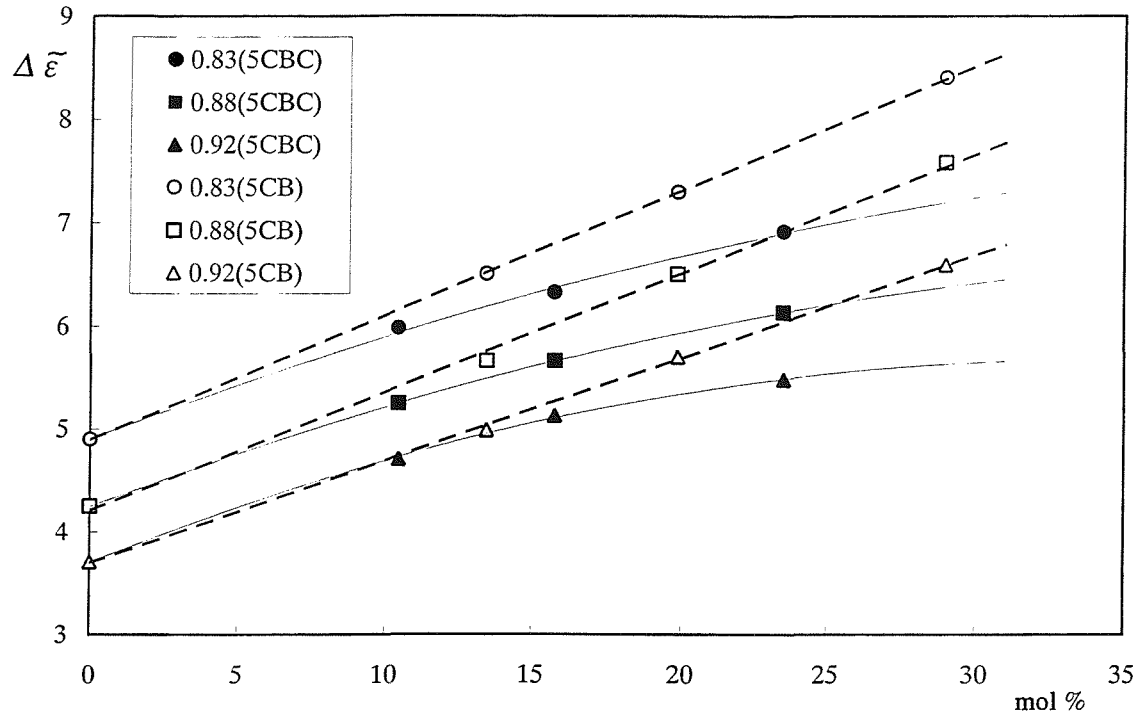

Fig.10 The dependence of $\Delta\tilde{\varepsilon}$ on the concentration of dopants, 5CBC and 5CB, for the reduced temperatures, T/T_{NI} = 0.83, 0.88 and 0.92

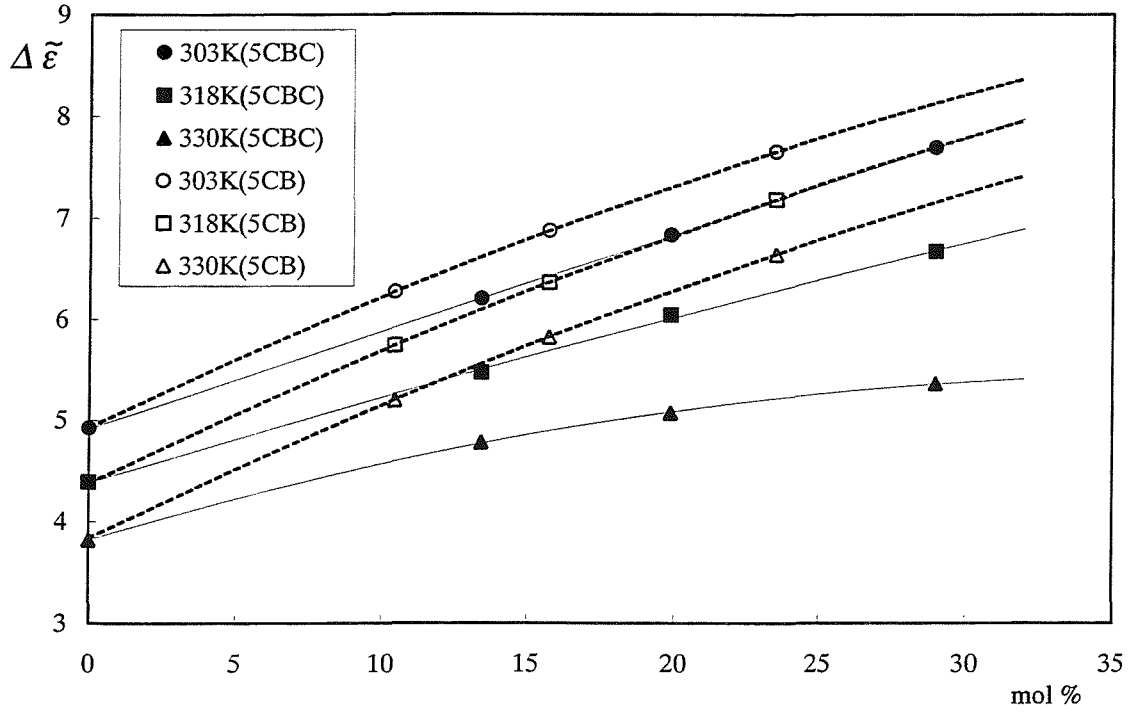

Fig.11 The dependence of $\Delta\tilde{\varepsilon}$ on the concentration of dopants, 5CBC and 5CB, for the absolute temperatures, T= 303K, 318K and 330K

5.4.3 Temperature Dependence of the Rotational Viscosity Coefficient

Next, we consider the effect of the dopants on the rotational viscosity coefficient, γ_1, together with its temperature dependence. The rotational viscosity coefficients were obtained from the slopes of the linewidth Γ_2 versus E^2 plots determined in the dynamic light scattering measurement via equation (8) and the dielectric anisotropies measured in the previous section. Fig.12 shows the dependence of γ_1 on the absolute temperature for ZLI-4792 together with about 10wt% of 5(O)CB and 5(O)PCP dissolved in it. We can see that 5(O)PCP decrease γ_1 slightly while it remains essentially unaffected by 5(O)CB although these dopants clearly decrease T_{NI} of the base mixture. We have also compared γ_1 using a reduced temperature, T/T_{NI}, scale; this is shown in Fig.13. As these plots show, 5(O)PCP are found to increase γ_1 more significantly than 5(O)CB at the same reduced temperature. These results are entirely analogous to those in Chapter 3 for a quantity proportional to γ_1 namely $\tau\overline{P}_2$ (where τ is the field-induced relaxation time).

The temperature dependence of γ_1 is predicted and found to be given by[22]

$$\gamma_1 \propto \overline{P}_2 \exp(E_a / RT), \tag{23}$$

where E_a is an activation energy and R is the gas constant. From this prediction, γ_1 has a temperature dependence given both by Arrhenius behaviour which depends on the absolute temperature, and by the orientational order which is a function of the reduced temperature. Consequently, each of the two temperature scales can only allow for one aspect of the characteristics of the rotational viscosity coefficient and so neither is sufficient to allow for the effect of the dopants which change T_{NI}. In order to investigate the effect of dopants more deeply, we need to plot the absolute temperature dependence of $\gamma_1 / \overline{P}_2$, since this gives information on the activation energy E_a; essentially the same plot was used in Chapter 3 where we considered $\gamma_1 / \Delta\tilde{\chi}$ since $\Delta\tilde{\chi}$ is essentially proportional to $\overline{P}_2$. However, we should remember that E_a may not be a constant because it could depend on the orientational order which is a function of T/T_{NI}.

We can determine E_a from the plot of $\ln\gamma_1$ versus T^{-1}:

$$\ln\gamma_1 = \ln\overline{P}_2 + C + (E_a/R)T^{-1}, \tag{24}$$

where C is a constant. Fig.14 shows this plot and that the results are indeed linear as predicted although the temperature range is somewhat small. E_a calculated from the slopes of the lines are shown in Table 2. These values show more or less the same tendency as those obtained from τ determined by ESR spectroscopy in Chapter 3 which are also shown in Table 2; 5(O)PCP increases E_a more than 5(O)CB. However the values are higher than those obtained by ESR in Chapter 3. The errors were the standard deviations for the slope values and so they are not the statistical errors.

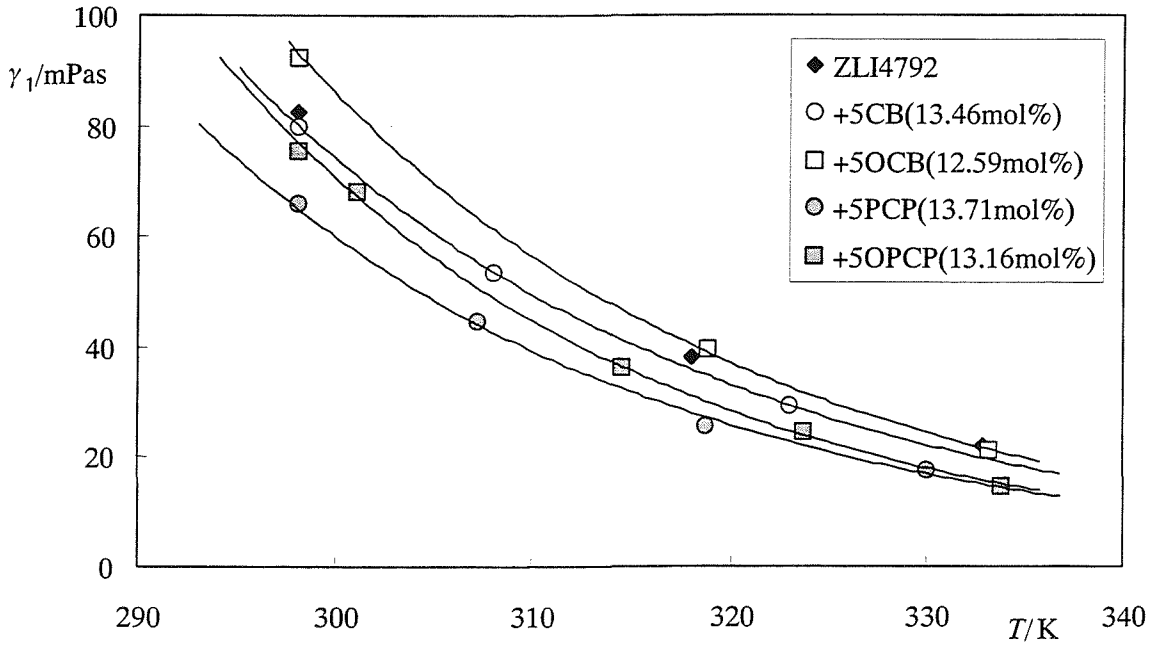

Fig.12 The dependence of the rotational viscosity coefficient on the absolute temperature

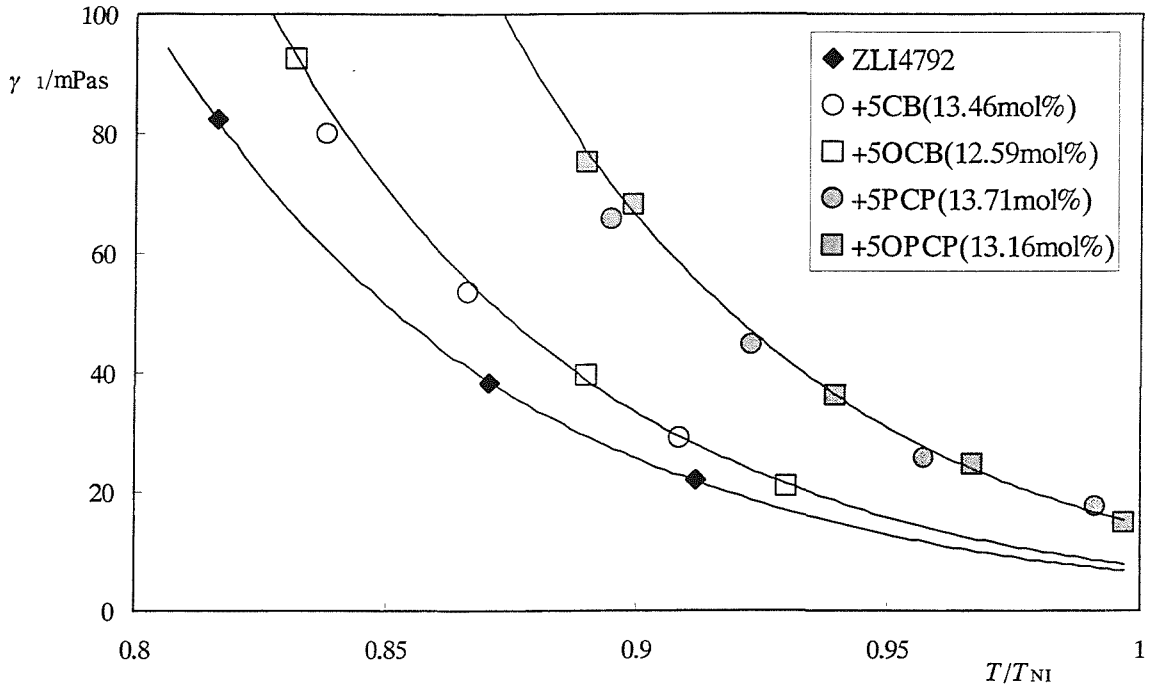

Fig.13 The dependence of the rotational viscosity coefficient on the reduced temperature.

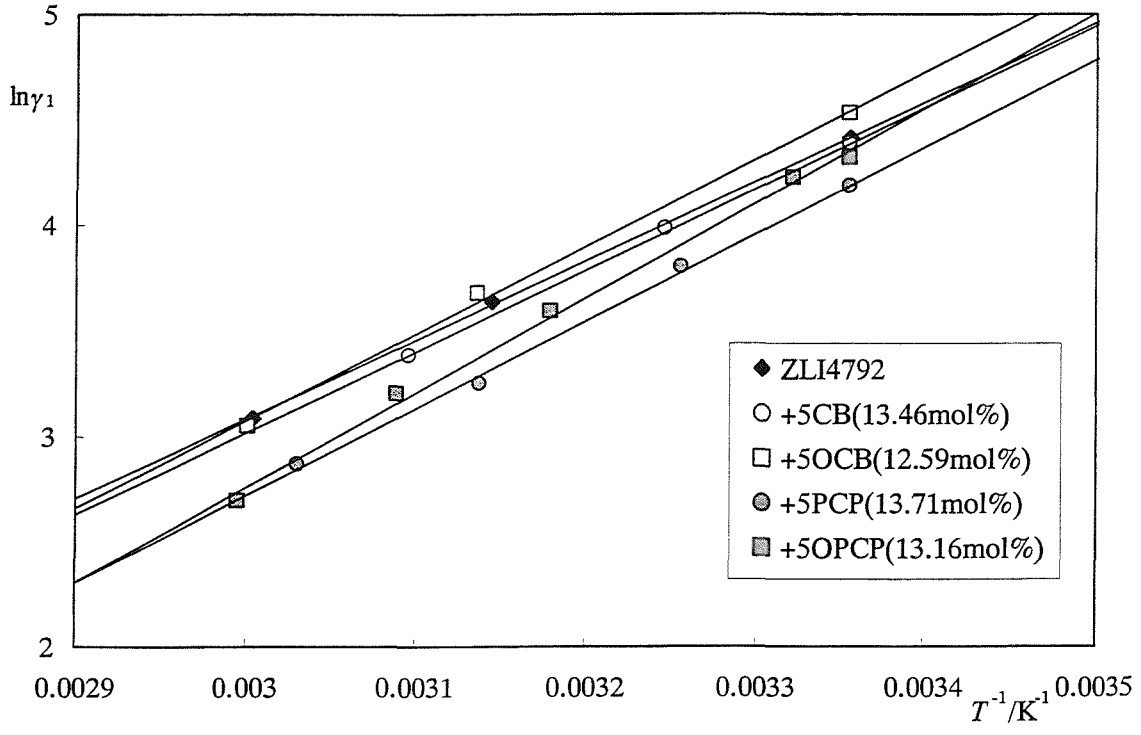

Fig.14 Logarithm of the rotational viscosity versus T^{1}

Table 2 Activation energies for the dopants dissolved in ZLI-4792

samples	wt%	mol%	E_a/kJmol^{-1} (this method)	E_a/kJmol^{-1} (ESR)
ZLI-4792	0	0	31.2±0.7	25.6±0.8
+5CB	10.09	13.46	32.2±0.8	27.0±0.3
+5OCB	9.96	12.59	34.4±1.7	27.0±1.4
+5PCP	10.02	13.71	34.5±1.3	30.2±0.5
+5OPCP	10.17	13.16	37.4±1.2	31.7±1.0

The temperature dependence of the rotational viscosity coefficients for 5CBC and 5CB for a range of concentrations dissolved in ZLI-4792 were measured, the results are shown in Figs.15 and 16. Here, the amount of the dopants is approximately 10, 15 and 23wt%, which are approximately 13mol%, 20mol% and 29mol% for 5CB, and 10mol%, 16mol% and 24mol% for 5CBC, respectively. The temperature scale used in Fig.15 is the absolute temperature scale and that in Fig.16 is the reduced temperature scale. As Fig.15 shows, γ_1 increases significantly as the amount of 5CBC increases at the same temperature whilst it remains almost the same for 5CB. The main difference between 5CBC and 5CB is that 5CBC increases T_{NI} of the host nematic whilst 5CB decreases its T_{NI} as shown in Fig.7. In addition, the magnitude of the change in T_{NI} is larger for 5CBC than 5CB because the difference between T_{NI} of the dopant and the base mixture is larger for 5CBC. Therefore, the order parameter of the host nematic is expected to increase significantly by adding 5CBC and this increases γ_1 because γ_1 is proportional to the order parameter, while the order parameter is expected to decrease slightly on addition of 5CB. For this comparison, the relationship between γ_1 and the reduced temperature, T/T_{NI}, is shown in Fig.15. As Fig.16 (b) shows, 5CB increases γ_1 with increasing concentration and this tendency is essentially the same as that in Fig.13. On the other hand, as Fig.16 (a) shows, 5CBC is found to decrease γ_1. This can be explained using equation (23) where the order parameter

is a constant on the reduced temperature scale and only the second term of the right hand side of equation (23), namely $\exp(E_a/RT)$, which is determined by E_a is effective. Because 5CBC increases T_{NI} of ZLI-4792, the corresponding temperature which gives the same T/T_{NI} is higher. This is why $\exp(E_a/RT)$ becomes smaller and consequently γ_1 becomes smaller. Moreover, E_a is possibly decreased by adding 5CBC because a small E_a also gives a small $\exp(E_a/RT)$. The opposite phenomena are expected to occur for 5CB. To calculate E_a, we plot $\ln\gamma_1$ against T^{-1} and this plot is shown in Fig.17. E_a can be calculated from the slopes of this plot and the results are shown in Table 3. The errors in Table 3 are again the standard deviations for the slope values, and not the statistical errors. Because E_a for ZLI-4792 is slightly different from that in Table 2, the statistical errors might be larger. From Table 3, we see that E_a increases as the concentration of dopants increases and 5CB increases it more than 5CBC for the same mole fraction.

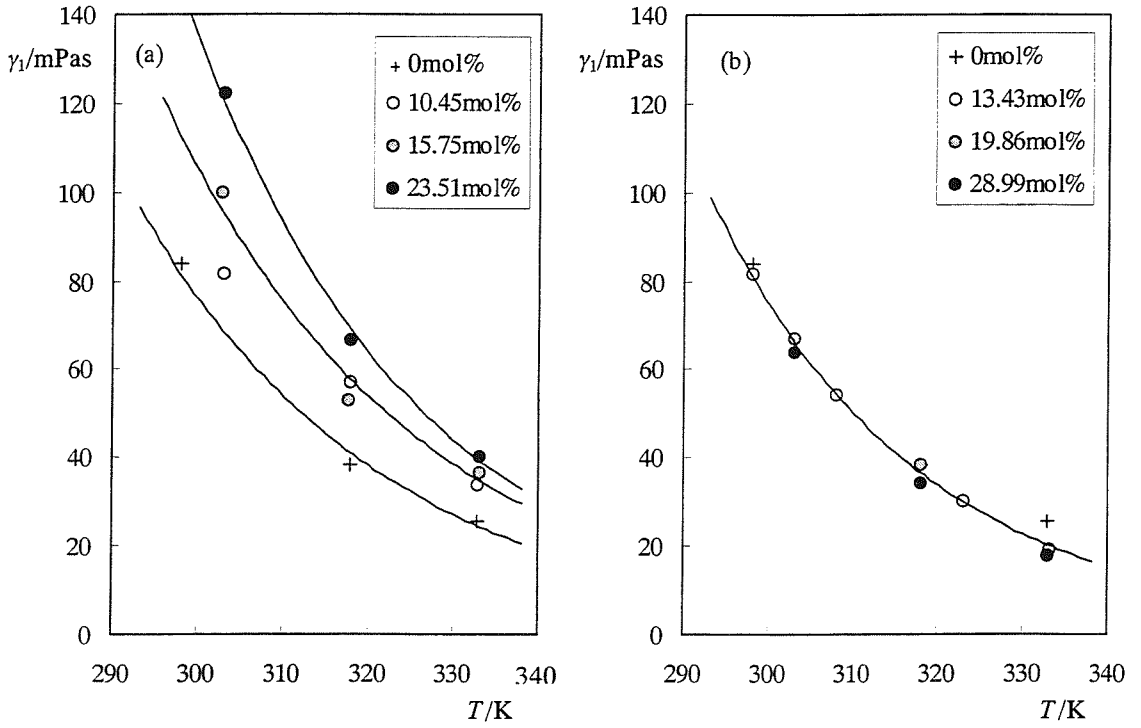

Fig.15 The dependence of the rotational viscosity coefficient on the absolute temperature; (a)5CBC in and (b)5CB dissolved in ZLI-4792

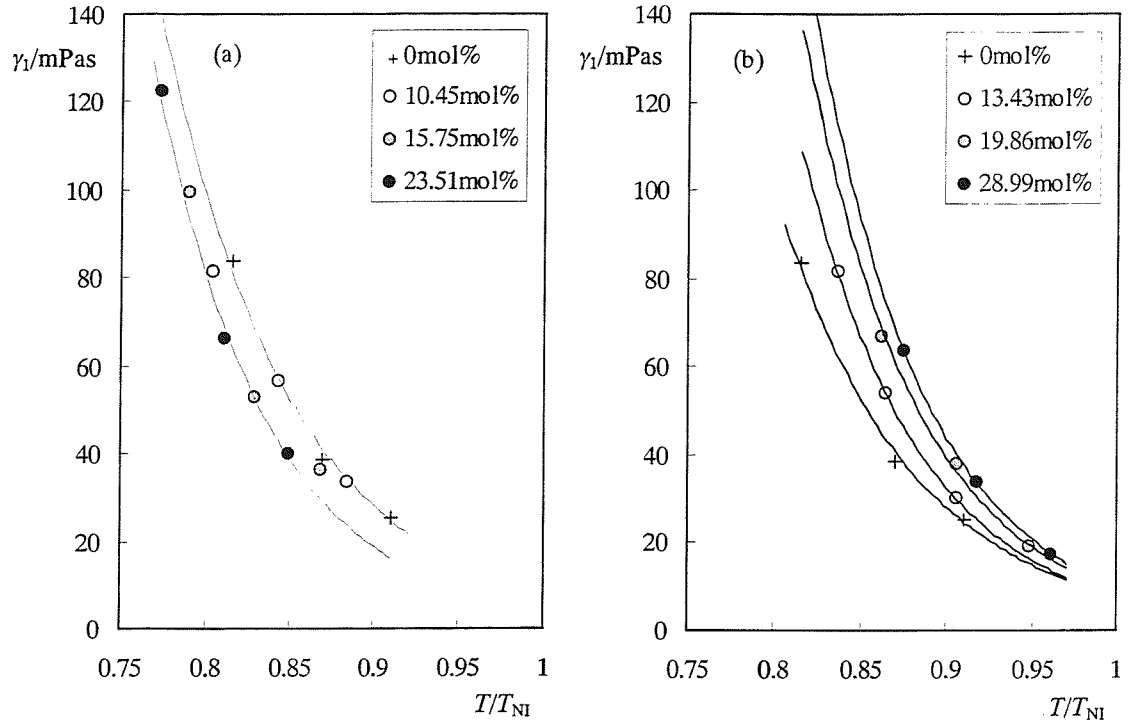

Fig.16 The dependence of the rotational viscosity coefficient on the reduced temperature; (a)5CBC and (b)5CB dissolved in ZLI-4792

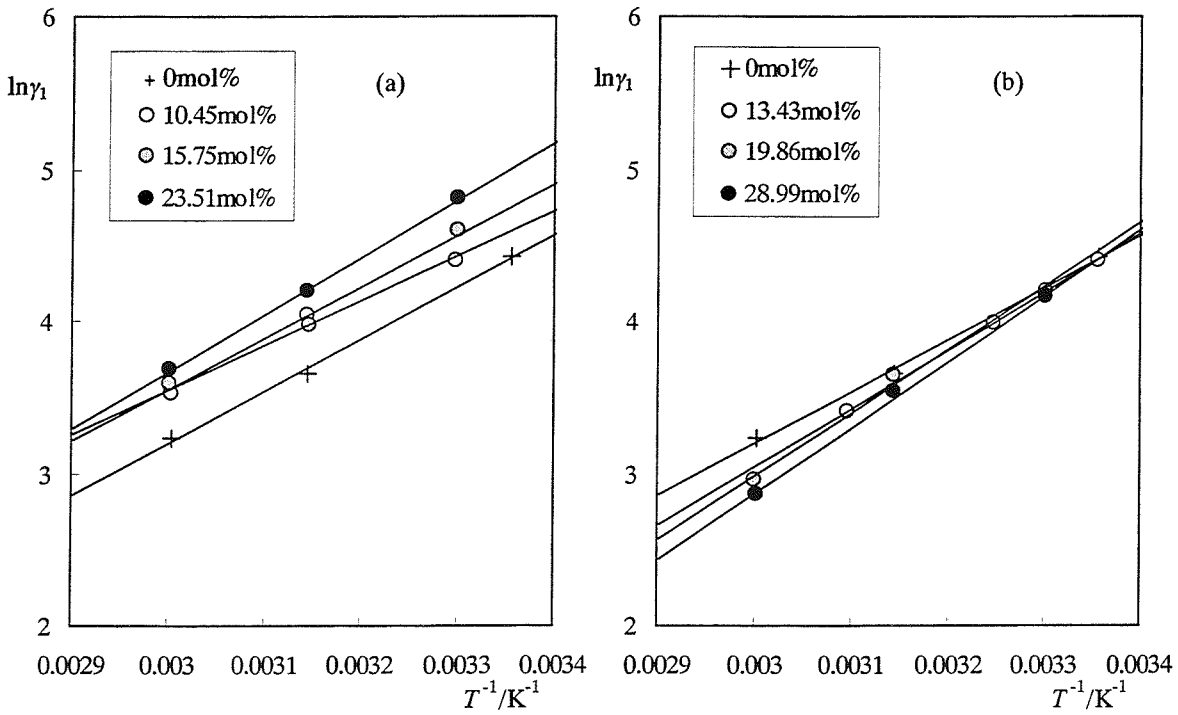

Fig.17 Logarithm of the rotational viscosity coefficient versus T^{-1}; (a)5CBC and (b)5CB dissolved in ZLI-4792

Table 3 Activation energies for 5CB and 5CBC dissolved in ZLI-4792

Sample	wt%	mol%	E_a/kJmol^{-1}
ZLI-4792	-	-	28.3±1.7
+5CB	10.06	13.43	31.9±0.3
	15.16	19.86	34.8±2.9
	22.75	28.99	36.0±1.7
+5CBC	10.05	10.45	24.6±3.1
	15.21	15.75	28.1±3.4
	22.73	23.51	31.2±0.8

5.4.4 Temperature Dependence of the Twist Elastic Constant

The twist elastic constant was obtained using the slope and the intercept values determined from the dynamic light scattering measurements and the dielectric anisotropy values measured in the previous section. Fig.18 shows the dependence of K_2 on the reduced temperature, T/T_{NI}, for ZLI-4792 together with mixtures containing about 10wt% of 5(O)CB and 5(O)PCP. This shows that the effect of the dopants is small when we compare the results at the same T/T_{NI}. Theoretically K_2 is essentially proportional to $\overline{P}_2^2$ and since $\overline{P}_2$ is expected to be a universal function of T/T_{NI}, it should also be a universal function of T/T_{NI} , that is K_2 is unchanged at the same reduced temperature. For this comparison, the dependence of K_2 on the absolute temperature, T, is shown in Fig.19. As Fig.19 shows, 5(O)PCP decrease K_2 significantly while 5(O)CB do not change it to any significant extent. This is related to the fact that 5(O)PCP decrease T_{NI} significantly since 5(O)PCP is less anisotropic than 5(O)CB. In addition, the data for 5CB and 5OCB are similar to the data for 5PCP and 5OPCP.

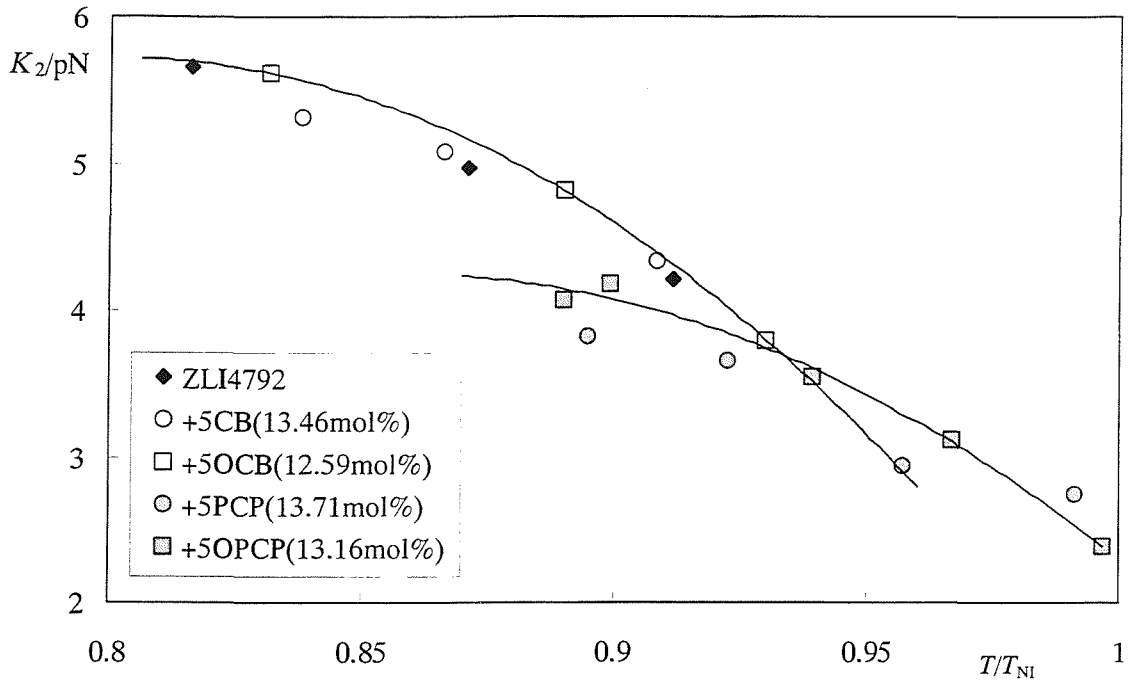

Fig.18 The dependence of the twist elastic constant on the reduced temperature for mixtures of 5(O)CB and 5(O)PCP in ZLI-4792

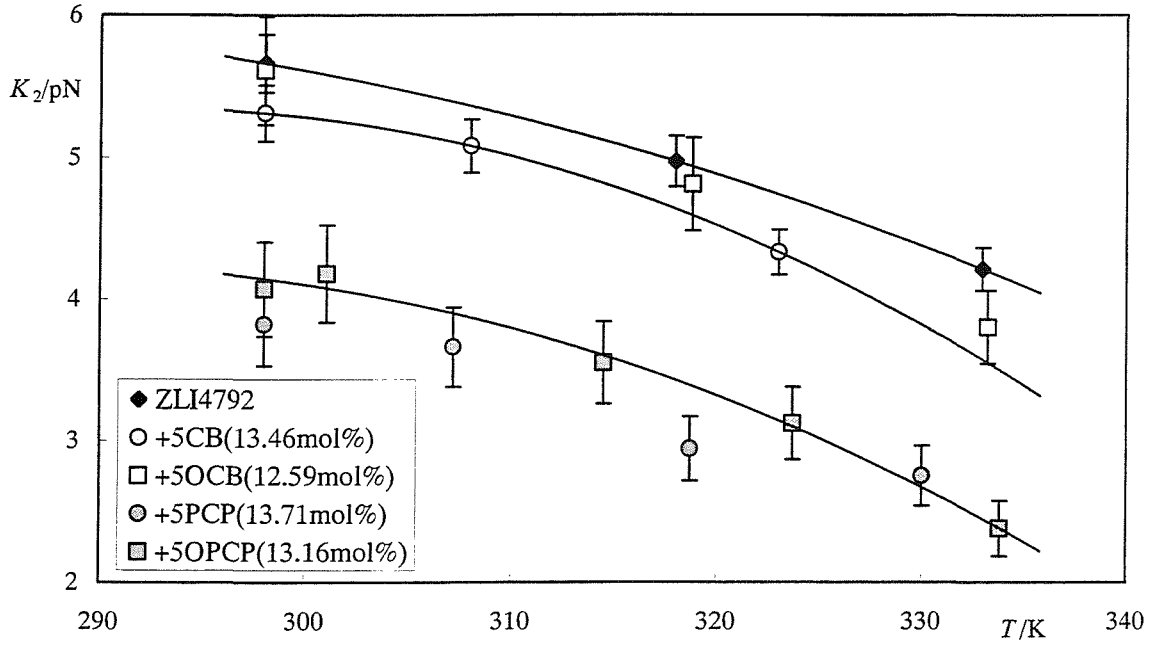

Fig.19 The dependence of the twist elastic constant on the absolute temperature for mixtures of 5(O)CB and 5(O)PCP in ZLI-4792

Next, the reduced temperature dependence of the twist elastic constant for 5CBC in ZLI-4792 and 5CB in ZLI-4792 is shown in Fig.20. This plot allows the effects of the dopants to be evaluated despite the change in T_{NI} produced by the dopant. As Fig.20 shows, adding 5CB to ZLI-4792 (Fig.20 (b)) does not change K_2 to any significant extent while adding 5CBC to ZLI-4792 (Fig.20 (a)) increases K_2 of the base mixture although the errors are large for the 5CBC solutions. Despite repeated experiments, it was not possible to obtain results exhibiting smaller errors.

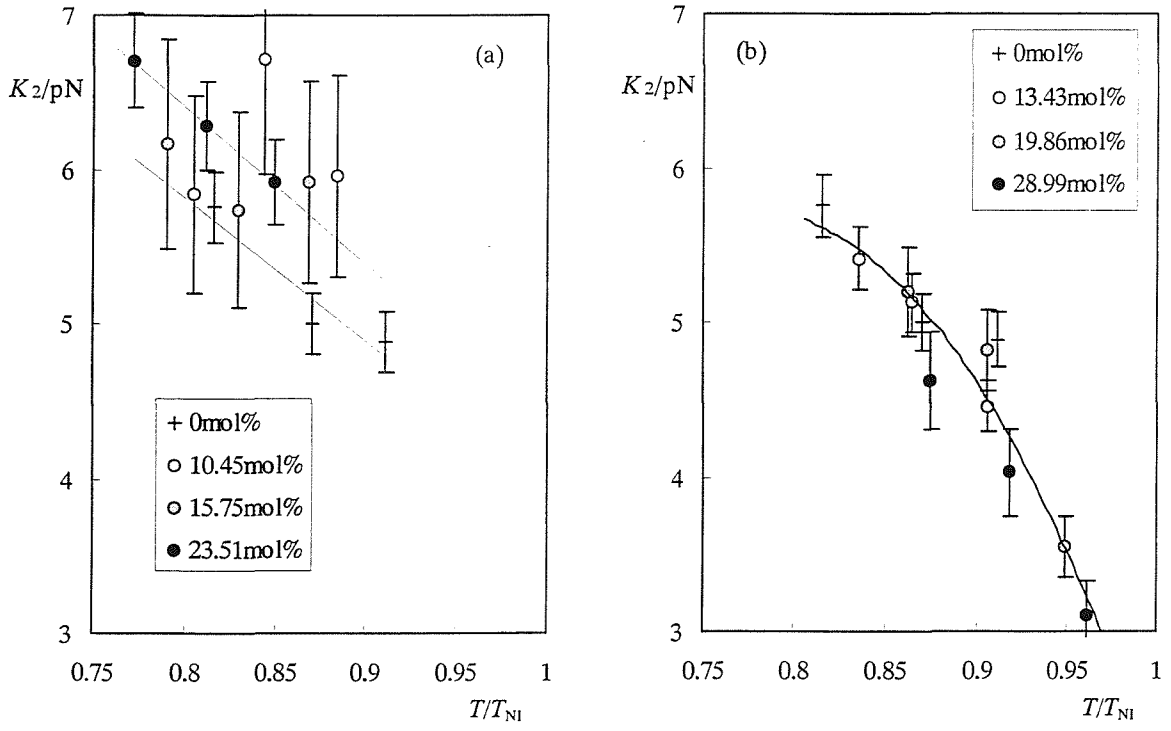

Fig.20 The dependence of the twist elastic constant on the reduced temperature; (a)5CBC and (b)5CB dissolved in ZLI-4792

5.5 Summary

The effect of dopants on the rotational viscosity coefficient, γ_1, and the twist elastic constant, K_2, together with the dielectric anisotropy, $\Delta\tilde{\varepsilon}$, were examined. The dopants used are 5(O)CB (cyanobiphenyls) and 5(O)PCP (phenylcyclopentenones) which are the

same as in Chapter 3, in addition, a range of concentrations of 5CB and 5CBC (cyanobiphenylcyclohexane) was investigated.

From the comparison between 5(O)CB and 5(O)PCP, the following results were obtained.

(1) Addition of 5(O)PCP decrease T_{NI} of the base mixture ZLI-4792 to a greater extent than 5(O)CB.

(2) The dopants increase $\Delta\tilde{\varepsilon}$ of ZLI-4792 and 5(O)CB increase it to a greater extent than 5(O)PCP, indicating that 5(O)CB have stronger polarity than 5(O)PCP and/or a higher orientational order.

(3) The effect of adding 5(O)PCP and 5(O)CB on K_2 is small if the comparison is made at the same reduced temperature, T/T_{NI}.

(4) 5(O)PCP reduce γ_1 slightly while it remains unaffected by 5(O)CB on the absolute temperature scale.

(5) The reduced temperature scale reveals a large difference in the effect of the dopants; addition of 5(O)PCP increase γ_1 more than 5(O)CB.

From the comparison between a range of concentrations of 5CB and 5CBC, the following results were obtained.

(6) 5CBC increases T_{NI} of ZLI-4792 to a greater extent than 5CB which decreases it.

(7) Both dopants increase $\Delta\tilde{\varepsilon}$ of ZLI-4792. However, the dependence of $\Delta\tilde{\varepsilon}$ on the mole fraction is different; adding 5CB exhibits a linear dependence for the same reduced temperature while 5CBC shows a negative deviation from linearity. This may suggest a greater effect for the dimerisation of 5CBC than for 5CB.

(8) The effects of adding these dopants on γ_1 are also different; 5CBC increases γ_1 while 5CB does not change it at the same absolute temperature.

(9) The reduced temperature scale reveals that 5CBC decreases γ_1 while 5CB increases it.

(10) The activation energies for these mixtures were determined from their Arrhenius behaviour and it was found that adding 5CB increases the activation energy to a greater extent than adding 5CBC.

(11) The effect of these dopants on K_2 is also different; at the same reduced temperature it remains unchanged by adding 5CB while it is increased by the addition of 5CBC although our results for this elastic constant have large errors.

5.6 References

[1] W.H. de Jeu; Physical Properties of Liquid Crystalline Materials, Chapter 6, 1980, Gordon and Breach, London.

[2] Groupe D'Etude des Cristaux Liquides (Orsay); J. Chem. Phys., **51**, 1969, 816.

[3] P.E. Cladis; Phys. Rev. Lett., **28**, 1972, 1629.

[4] P.P. Karat and N.V. Mudhusudana; Mol. Cryst. Liq. Cryst., **40**, 1977, 239.

[5] F.M. Leslie and C.M. Waters; Mol. Cryst. Liq. Cryst., **123**, 1985, 101.

[6] P.G.de Gennes and J.Prost; The Physics of Liquid Crystals, Second Edition, Chapter 3, 1993, Oxford University Press.

[7] Orsay Liquid Crystal Group; Mol. Cryst. Liq. Cryst., **13**, 1971, 187.

[8] H.J. Coles and M.S. Sefton; Mol. Cryst. Liq. Cryst. Lett., **1**, 1985, 151.

[9] M.S. Sefton, A.R. Bowdler and H.J. Coles; Mol. Cryst. Liq. Cryst., **129**, 1985, 1.

[10] H. Gruler, T.J. Scheffer and G.Maier; Z. Naturforsch, **27a**, 1972, 966.

[11] Private communication (Hitachi, Ltd.).

[12] T. Uchida and Y. Takahashi; Mol. Cryst. Liq. Cryst. Lett., **72**, 1980, 133.

[13] M.S. Sefton; Ph.D. Thesis, Manchester University, UK, 1985.

[14] P.J.R. Birtwistle; Ph.D. Thesis, Manchester University, UK, 1995.

[15] H.J. Coles; in The Optics of Thermotropic Liquid Crystals, Eds. S. Elston and R. Sambles, Chapter 4, 1998, Taylor&Francis, London.

[16] H. Kneppe, F. Schneider and N.K. Sharma; J. Chem. Phys., **77**, 1982, 3203.

[17] J.D. Bunning, T.E. Faber and P.L. Sherrell; J. Phys. (Paris), **42**, 1981, 1175.

[18] P.A. Breddles and J.C.H. Mulkens; Mol. Cryst. Liq. Cryst., **147**, 1987, 107.

[19] R.L. Humphries, P.G. James and G.R. Luckhurst; Symposia of the Faraday Society, **5**, 1971, 107.

[20] W.H. de Jeu; Physical Properties of Liquid Crystalline Materials, Chapter 5, 1980, Gordon and Breach, London.

[21] W.H. de Jeu; Physical Properties of Liquid Crystalline Materials, Chapter 1, 1980, Gordon and Breach, London.

[22] W.H. de Jeu; Physical Properties of Liquid Crystalline Materials, Chapter 7, 1980, Gordon and Breach, London.

Chapter 6

Conclusions and Future Work

1. Conclusions

This Thesis describes the results of investigations into the effect of dopants on the physical properties of nematic liquid crystals. The aim is to improve the performance of liquid crystal displays, in particular the response times and threshold voltages, especially for liquid crystal displays using the in-plane switching mode, by adding dopants to a base liquid crystal mixture. The physical properties which play important roles in determining the display's characteristics are the rotational viscosity coefficient, γ_1, the twist elastic constant, K_2, and the dielectric anisotropy, $\Delta\tilde{\varepsilon}$. The measurement technique chosen to determine γ_1 was via the field-induced relaxation time measurement using the magnetic resonance method based on ESR spectroscopy. The advantage of using this technique is that it can monitor the uniformity of the nematic director in the sample as assumed by theory. To determine the absolute value of γ_1, the diamagnetic anisotropy, $\Delta\tilde{\chi}$, should be known, and this was measured by the electric-magnetic field balance method again using ESR; the results were found to be in good agreement with the literature values. The γ_1 values obtained from this combined method were also found to be in good agreement with the literature values for γ_1. In addition the dynamic light scattering method was chosen to determine K_2 and γ_1 and the results for these properties obtained from this method were found to be in good agreement with the literature values as well as those determined by the ESR method. In order to obtain individual values of K_2 and γ_1, values of $\Delta\tilde{\varepsilon}$ are needed and the simple capacitance measurement of a cell was chosen to determine them. The investigated dopants were the 4,4'-pentyl(pentyloxy)-phenylcyclopentenones (5(O)PCP) and these were compared with the 4,4'-pentyl(pentyloxy)-cyanobiphenyls

(5(O)CB). In addition mixtures with a range of concentrations of the 4-pentyl-4"-cyanobiphenylcyclohexane (5CBC) were compared with those with similar concentrations of 5CB.

The effect of dopants on γ_1 and K_2 was examined and the temperature dependence of these properties was found to be significantly different depending on the temperature scales used for their comparison; here we have considered the absolute and the reduced temperature scales. The dopants 5(O)PCP and 5(O)CB did not change γ_1 of the base mixture on the absolute temperature scale while they exhibit different effects on the reduced temperature scale. The effect on γ_1 was different for 5CBC and 5CB. A range of concentrations of 5CB did not change γ_1 while addition of 5CBC increased it on the absolute temperature scale. However, on the reduced temperature scale, 5CB increased γ_1 while 5CBC decreased it on this scale. This complicated temperature behaviour found for γ_1 can be understood by the theoretical expression, $\gamma_1 \propto \overline{P}_2 \exp(E_a / RT)$, in which γ_1 is a function of both temperature scales since the orientational order parameter $\overline{P}_2$ is predicted to be a universal function of the reduced temperature. From this equation, the activation energies, E_a, were calculated and 5(O)PCP were found to increase E_a of the base mixture to a greater extent than 5(O)CB, and the effect of adding 5CBC on E_a was found to be smaller than that of adding 5CB.

The effect of dopants on K_2 was also examined using the reduced temperature scale since K_2 is predicted to be proportional to $\overline{P}_2^2$. 5(O)PCP decrease K_2 on this temperature scale while 5(O)CB are found to decrease it to a smaller extent. From the comparison of a range of concentrations of 5CBC and 5CB, 5CB does not change K_2 to any significant extent while 5CBC is found to increase it.

2. Future Work

There are some further measurements to be done in the future in order to make the results in this Thesis complete; they are the following.

1. The measurement of $\Delta\tilde{\chi}$ by the field balance method described in Chapter 4 for the samples used in Chapter 3 to complete the measurement of γ_1 by the ESR technique.
2. The determination of the temperature dependence of $\Delta\tilde{\varepsilon} / \Delta\tilde{\chi}$ by the field balance method to check whether the temperature dependence of both anisotropies are the same, in other words, if this ratio is temperature independent as predicted.
3. We observed a pair of side peaks in the ESR spectra obtained in the field balance experiment in zero electric field which are probably due to the flow alignment of the director on the surface of the cell. Those peaks should be elimin ated by an alternate surface alignment of the cell, e.g. by rubbing the surface in the direction parallel to the magnetic field. Such cells with surface alignment could then be used in further field balance experiments.
4. In the ESR spectra of the field balance experiment, we found powder-like patterns indicating that two director orientations coexist when the angle between the two fields was 90°. This might cause errors in this experimental determination of $\Delta\tilde{\varepsilon} / \Delta\tilde{\chi}$. To avoid this possible problem, the cell thickness should be uniform over the active area to ensure that the electric field and hence the director orientation is uniform.
5. Since the aim of this Thesis is to improve the performance of liquid crystal displays by adding dopants, the relationship between the chemical structures of the dopants and the physical properties, namely γ_1 and K_2, should be systematically examined. From this point of view, the effect of other kinds of dopants with different structures on these physical properties should be examined.